FATIGUE IN PEARLITE STRUCTURES

by

JOHN GRAHAM TAYLOR, B.Sc.

A research project carried out for the degree of Doctor of Philosophy of the Council for National Academic Awards.

Department of Metallurgy,
Sheffield City Polytechnic.

October, 1976

SYNOPSIS

The basic mechanisms of fatigue failure were studied in a eutectoid carbon steel. Three different structures were produced in the steel, these being coarse pearlite, fine pearlite and spheroidised carbide. Pearlite structures were selected because of their practical importance and also because multi-phase alloys have, until recently, received little attention from research workers.

Specimens were fatigued either in reverse plane bending or uniaxial tension-compression conditions. In the latter case, constant amplitude strain controlled tests were performed using a closed loop servo-hydraulic machine. Much of the testing was conducted under conditions giving failure beyond 10^5 cycles of stress.

Cyclic properties and changes of deformation resistance during testing were determined. The major emphasis was on the observation of the development of fatigue damage during the life of the pre-polished specimens. A number of optical and electron microscopical techniques were used to examine damage.

Fatigue damage appeared early in the life in all three structures. It existed as slip bands in the ferrite. The ferrite-cementite interface was shown to be the principal source of mobile dislocations. Damage was more localised in coarse than fine pearlite and all damage was associated with a very shallow surface topography.

Cracks appeared at slip bands and ferrite-cementite interfaces. In coarse pearlite and spheroidised carbide they were detected at up to 25% of the life whereas in fine pearlite they could not be detected until about 75% of the life. Surface crack propagation rates were greater in lamellar than spheroidised carbide structures. The proportion of the

full fracture zone occupied by the fatigue crack area was greatest in the spheroidised structure and least in the coarse pearlite.

CONTENTS

		Page
1.	INTRODUCTION	1
2.	SURVEY OF LITERATURE	4
2.1.	Scope of the review	4
2.2.	Assessment of fatigue performance	6
2.3.	Mechanisms of fatigue failure	14
2.4.	The role of plastic deformation in fatigue	16
2.5.	Stage I Crack Growth	31
2.6.	Stage II Crack Growth	50
2.7.	Summary	59
3.	EXPERIMENTAL PROCEDURE	62
3.1.	Choice of materials	62
3.2.	Preparation of material	63
3.3.	Fatigue testing	66
3.4.	Metallographic examination	70
4.	RESULTS	75
4.1.	Cyclic and monotonic properties	75
4.2.	Metallography	80
5.	DISCUSSION	94
5.1.	The dependence of cyclic properties on structure	94
5.2.	Cyclic hardening and softening phenomena	100
5.3.	The influence of orientation of surface damage	107
5.4.	Stage I Crack Growth	109
5.5.	Stage II Crack Growth	117
6.	CONCLUSIONS	125
7.	RECOMMENDATIONS FOR FURTHER WORK	127

CONTENTS

REFERENCES

STATEMENT OF POST GRADUATE STUDY

ACKNOWLEDGEMENTS

APPENDIX

TABLES and FIGURES

1. INTRODUCTION

A very large proportion of service failures in metallic materials is attributed to fatigue. The problem of fatigue has been known for almost one hundred and fifty years. During this time the volume of work carried out to study the problem has been immense. Extensive reviews [1,2,3,4,5,6] have managed to cover only a small proportion of this work.

Much of the earliest work in this field was of an empirical nature. Fatigue properties such as fatigue limit and endurance limit were determined and their dependence on such variables as material structure and surface finish was examined. The more positive approach towards improving fatigue performance based on studies of the fundamental aspects of fatigue did not follow until much later. The earliest studies into the basic mechanisms [1,2] date back to the beginning of this century. Following the development of suitable metallographic techniques and equipment, the volume of work on basic mechanisms has increased dramatically, particularly during the last twenty five years. This recent work has substantially increased our knowledge of the fatigue process. Unfortunately, this increase in knowledge has been accompanied by increasingly rigorous demands on materials in service with the result that fatigue fracture remains the most common source of service failure.

Much of the work into basic mechanisms of fatigue has been focussed on simple materials based on F.C.C. and B.C.C. structures. It is only in the last few years that the more complex materials based on multi-phase structures have received more attention. As a result the total knowledge of the more fundamental aspects of fatigue in this important group of materials is sparse. For commercial

applications where good fatigue performance is essential, it is normally this group of materials to which the engineer looks in selection. The need for a deeper understanding of the fatigue mechanisms in this group of materials is therefore great if any further improvements in fatigue performance are to be achieved.

The most widely used metallic material is steel. The range of microstructures that can be developed in steels is very wide. The most common structure associated with good strength is that based on pearlite. Pearlite is composed largely of the ductile ferrite phase containing about 13% by volume of the hard intermetallic compound, cementite. In some steels, pearlite may constitute almost the whole structure as in the case of those used for ropes and springs. Previous studies of basic mechanisms of fatigue in steels are few and where materials containing pearlite have been involved, the constituent has occupied only a small proportion of the structure. Its influence on the basic mechanisms has therefore been difficult to evaluate. This investigation was started to fill this gap in knowledge.

In the work reported here, the mechanisms of fatigue failure have been examined in three pearlitic structures; coarse pearlite, fine pearlite and spheroidised carbide. All have been developed in a steel of eutectoid carbon content. Cyclic properties and changes of deformation resistance during testing have been determined. The major emphasis has been the observation of the progress of fatigue damage during testing of pre-polished specimens in conditions giving failure at between 10^5 - 10^6 cycles. A number of metallographic techniques have been used for observation of fatigue damage. These include both optical and electron microscope techniques. Electron

microscopical techniques have included the production of two-stage replicas of selected areas on the specimen surface for examination and also the use of the scanning electron microscope. This has been extended to include the production of foils from sections of both fatigued and non-fatigued specimens for electron microscope examination.

This thesis includes a review of the available literature relating to previous work on the microscopic aspects and mechanisms of fatigue in multi-phase materials. The results of the investigations described above are presented and discussed. Finally a number of areas have been identified as a result of these investigations where further work is recommended.

2. SURVEY OF LITERATURE

2.1. SCOPE OF THE REVIEW

Fatigue failure and its importance in a wide range of materials has been recognised for almost one hundred and fifty years. During this time, a vast amount of research work has been carried out in an effort to understand the phenomenon and to prevent fatigue failure. This work can be classified in three categories:-

a) the traditional use of testing machines to determine fatigue characteristics as measured by such properties as the fatigue limit, endurance limit, etc.

b) studies of the dependence of fatigue or cyclic behaviour on such variables as the stress or strain amplitude, environmental conditions or material structure etc.

c) studies of the basic mechanisms of fatigue

The most traditional method of quantifying fatigue characteristics has been that where an S-N curve is derived from tests on a number of specimens at different loads. The curve is obtained by determining the stress amplitude (S) for each load and the number of cycles (N) of periodic load changes required to completely fracture the specimen at each stress amplitude. A disadvantage with this type of test is that the stress may alter throughout the test even though the load applied remains constant. This arises when a crack forms in the specimen. The true stress at the tip of the growing crack then increases.

In the last twenty years, rapid improvements have been made in the development of fatigue testing techniques. An important field of development has been that of machines where both stress and

strain amplitude may be measured continuously throughout a test. Furthermore, during testing the deformation may be controlled at a given value whilst the stress is measured; this is referred to in literature as strain controlled cycling. Similarly, the load may be controlled and strain measured. This advance in machine design and control has provided facilities whereby the dependence of fatigue behaviour on stress and strain can now be reliably predicted.

Evidence of studies into basic mechanisms of fatigue date back to the early years of this century.[1,2] Surface observations of iron showed slip bands appearing in some grains after a few cycles of stress.[2] This represented one of the first studies of the microscopic aspects of fatigue.

In the last twenty five years, the volume of work on the mechanisms and microscopic aspects of fatigue has been immense. Much of the work was focussed on the simple materials, mainly pure metals or single-phase alloys based on the F.C.C. structure and in either single- or poly-crystal form. A number of excellent reviews cover the work in the early stages of this period.[3,4,5,6] Studies of the more complex materials, for example, multi-phase alloys and materials having structures other than F.C.C. were much less extensive but have received more attention in the last few years.

This review concentrates on the microscopic aspects and mechanisms of fatigue in multi-phase materials. Work relating to existing knowledge on the simple materials, as defined earlier, has not been neglected and is discussed where appropriate. As an introduction to the review, current methods of assessing fatigue

performance are described. A number of parameters determined from such testing methods can be used with reasonable accuracy to quantify the fatigue behaviour of materials. These parameters are explained and current views on linking them with microstructural features are discussed.

2.2. ASSESSMENT OF FATIGUE PERFORMANCE

The stress-strain relationship of a material as measured in a monotonic tension test is not applicable to situations where cyclic loading occurs because this stress-strain relationship varies with the cyclic history. The magnitude and rate of variation in this relationship are influenced by several variables, the most important of which are the material, its initial condition (that is annealed or cold worked) and the level of plastic strain in each cycle. If a material is subjected to cyclic deformation of constant amplitude, such variation is manifested in a change of stress required to maintain this amplitude. An increase of stress indicates cyclic hardening whilst a decrease indicates softening. Cyclic stability is characterised by the stress remaining constant. These hardening or softening responses are represented schematically in fig.1 and examples exist elsewhere.[7,8] Where such property changes occur, they are usually completed early on in the fatigue life of most metals such that the relationship remains stable through most of the life.

In the traditional S-N curve, quoted earlier, fatigue performance has been assessed in terms of the fatigue limit or, in the case of most non-ferrous metals, the endurance limit which is the stress level that produces fracture after N stress cycles where N is generally 10^7. Improvements of fatigue performance have in the

past been associated with methods of raising the stress corresponding to the fatigue limit or, for those appropriate materials, the endurance limit. This concentration on the fatigue limit was justified by the predominance in design of the concept of infinite life. In many situations however, it has become both necessary and desirable to design for a finite fatigue life which could range from a few cycles to about 10^6 cycles. Examples of these situations include thermal or mechanical strain cycling as encountered in nuclear plants, steam turbines and aircraft structures. Under these conditions, values for the fatigue or endurance limit often give no reliable prediction of material behaviour. Extensive low cycle and high cycle fatigue studies in recent years have considerably improved the understanding of the fatigue phenomenon. Fatigue performance under either low or high cycle conditions can now be assessed in terms of a number of parameters which will be described in the following sections. If these parameters can be linked with microstructural characteristics then the opportunity arises for design of materials with specific fatigue performance. This aspect is also discussed later.

In order to identify these parameters it is first necessary to examine the ways in which fatigue behaviour can be quantified. In addition to the S-N curve, two important forms of fatigue behaviour presentation are the cyclic stress-strain and strain-life curves.

2.2.1. The Cyclic Stress-Strain Curve

This represents the steady state cyclic deformation resistance of a material. The curve is produced by cyclically deforming several samples of a material at a range of strain

amplitudes and joining the tips of each of the stable hysteresis loops obtained. An alternative procedure is the incremental step test [7] where a single sample is used. Here the sample is subjected to a programme of continually increasing and then decreasing strain levels. A continuous plot of stress and strain gives a series of superimposed hysteresis loops, each overall loop block corresponding to one programme. After several repetitions of the programme, the material stabilizes and the locus of loop tips is the cyclic stress-strain curve.

Figs. 2 and 3 show cyclic and monotonic stress-strain curves for a number of materials.[7,8] In the elastic region, the curves are similar but at the onset of plasticity the cyclic and static curves diverge. The values of flow stress and strain hardening coefficients for each material as determined from the monotonic curve are not the same as those determined from the cyclic curve. A comparison of the curves demonstrates the nature and extent of the cyclic changes. Fig. 2 shows cyclic softening of a steel, fig. 3 shows softening at small strains but hardening at high strains in an alloy steel and the nickel-based Waspalloy cyclically hardens at all strain levels.

An indication of the likely response to cycling can be obtained from the monotonic strain hardening exponent. A high exponent of above 0.1 indicates a material which will probably cyclically harden whilst if the value is below 0.1, cyclic softening is likely. A value of about 0.1 is indicative of a cyclically stable material.[9] The ratio of $\frac{\text{tensile strength}}{\text{yield strength}}$ has also been used to indicate similar trends. If this ratio

is greater than 1.4, cyclic hardening is likely whilst if less than 1.2, cyclic softening occurs.[8]

The relationship between stress amplitude σ_a and the plastic strain amplitude $\frac{\Delta \epsilon_p}{2}$ in the cyclic stress-strain curve can be expressed in the following form[10]:-

$$\sigma_a = K' \left[\frac{\Delta \epsilon_p}{2} \right]^{n'} \qquad \text{——————} 1$$

where K' = cyclic strength coefficient

n' = cyclic strain hardening exponent

Both K' and n' are constants which are influenced by material characteristics.[9] In addition, n' is probably the most important parameter identified so far as an indicator of fatigue behaviour. The relationship between n' and microstructure has been extensively studied.[11] High values of n' are associated with structures which allow extensive cross slip and dislocation motion. Low values are associated with those structures which restrict dislocation motion and have a limited number of slip systems. Typical values of n' for a number of materials have been shown to lie within the range 0.10 to 0.25.[12] A study[13] of various materials in low cycle fatigue tests has shown that increased fatigue life for a given strain amplitude can be correlated with an increase in the value of n'. This linking of n' with the microstructure and other material parameters is discussed in later sections.

2.2.2. Fatigue Life Data

In assessing the fatigue resistance of a metallic material, it is useful to know whether this resistance can best be quantified in terms of cyclic stress or cyclic strain. Take for

example, low cycle fatigue conditions where a life of say 10^3 cycles may be sufficient for a material in certain applications. Here the capacity for accommodating cyclic strain is more important than if the same material is expected to give a longer life of say 10^6 cycles. In the latter situation, a stress based analysis may be more relevant.

As mentioned earlier, the S-N curve was at one time the most common form of presenting fatigue performance data. Nowadays, a number of different presentations exist. Three important ones are those which show a relationship between fatigue life and:

(i) stress(similar to the S-N curve)

(ii) plastic strain

(iii) total strain

Fig. 4 shows a schematic stress-life curve which has been produced from a number of load controlled cyclic tests. It is basically an S-N curve with stress and life plotted on logarithmic scales. The relationship between stress and life is given by[14]:-

$$\sigma_a = \sigma_f' (2N_f)^b \qquad \text{——————————} \quad 2$$

where σ_a = true stress amplitude

N_f = number of cycles to failure

σ_f' = fatigue strength coefficient which is given by the intercept on the stress axis corresponding to one stress reversal (i.e. $2N_f = 1$)

b = fatigue strength exponent which is given by the slope of the curve.

Both b and σ_f' characterize the cyclic stress resistance of a material. Since b is the slope of the line, it has a negative

value because life increases as the stress is reduced. For high cyclic stress resistance, the intercept on the stress axis giving σ_f' should be at a high level whilst the line should have a shallow slope. Reported values of b range from about -0.05 to -0.20 [8,10] and the most shallow slope in this range is given by -0.05. Its value has been shown[10] to be related to the cyclic strain hardening exponent n' in the following way:-

$$b \simeq \frac{-n'}{1+5n'} \qquad \text{——————————} \quad 3$$

A decrease of n' therefore produces a more shallow slope and thus an increase in fatigue life at low stress levels. The value of the fatigue strength coefficient σ_f' has been shown to be approximately equal to the monotonic true fracture strain.[9,10] Hence the material conditions which are likely to result in high cyclic stress are the combination of a high monotonic true fracture strength and a low cyclic strain hardening exponent.

The plastic strain-life relationship is given by [15,16]:-

$$\frac{\Delta\epsilon_p}{2} = \epsilon_f'(2N_f)^c \qquad \text{——————————} \quad 4$$

where $\frac{\Delta\epsilon_p}{2}$ = plastic strain amplitude

N_f = number of cycles to failure

ϵ_f' = fatigue ductility coefficient

and c = fatigue ductility exponent

A schematic plastic strain-life curve is shown as part of fig.5 where both strain and life are plotted on logarithmic scales. It has been produced from a number of deformation controlled tests. The values of c and ϵ_f' characterize the cyclic strain resistance

of a material. The fatigue ductility exponent c is given by the slope of the line and has a negative value, which can range from -0.5 to -0.7[10]. Its value has also been shown to be related to n' in the following way [10]:-

$$c = \frac{-1}{(1 + 5n')} \qquad \text{——— 5}$$

An increase in value of the cyclic strain hardening exponent hence produces a flatter plastic strain-life line.

The value of ϵ_f' is given by the intercept of the line on the strain axis corresponding to one stress reversal (i.e. $2N_f = 1$). Its value has been shown to be approximately equal to the monotonic true fracture ductility.[9,11] High cyclic strain resistance is thus achieved with a combination of a high value of ϵ_f' with a shallow slope c, in other words, a high monotonic fracture ductility and a high value for the cyclic strain hardening exponent.

The final relationship considered in this section is that of total strain and life. The resistance of a material to total strain cycling is made up of two parts, the elastic and the plastic strain resistance.[17] Morrow[10] has expressed the relationship in the following way:-

$$\frac{\Delta\epsilon_t}{2} = \frac{\Delta\epsilon_e}{2} + \frac{\Delta\epsilon_p}{2} \qquad \text{——— 6}$$

where $\Delta\epsilon_t/_2$ = total strain amplitude

$\frac{\Delta\epsilon_e}{2}$ is the elastic strain amplitude and can be derived from equation 2 by dividing by the elastic modulus. Hence:

$$\frac{\Delta \epsilon_e}{2} = \frac{\sigma_a}{E} = \frac{\sigma_f'}{E} (2N_f)^b$$

$\frac{\Delta \epsilon_p}{2}$ is the plastic strain amplitude and is given in equation 4. Equation 6 therefore becomes:

$$\frac{\Delta \epsilon_t}{2} = \frac{\sigma_f'}{E} (2N_f)^b + \epsilon_f' (2N_f)^c \qquad \text{——————} \quad 7$$

Figure 5 shows a schematic presentation of a total strain amplitude-life curve. Also included are the elastic and plastic strain amplitude life curves which make up the total. It can be seen that as the number of cycles to failure increases, the contribution of the elastic portion to the total value increases. At long lives, the elastic strain component predominates. Hence, as shown, in equations 2 and 3, a high fatigue strength coefficient σ_f' and a low value of the cyclic strain hardening exponent n' are essential for good fatigue resistance at long lives.

In the low cycle region, the plastic strain component predominates. Equations 4 and 5 show that ductility is important for good fatigue resistance in this life range and this means high values for both the fatigue ductility coefficient ϵ_f' and n'. Figure 6 shows the influence of n' on the various parameters identified in stress-life and strain-life relationships. High plastic strain fatigue resistance and high stress fatigue resistance are achieved by opposing changes in the cyclic strain hardening exponent, n'. Hence, in the design or selection of alloys for good fatigue resistance based on existing knowledge, there are two possibilities. Firstly, one aims for maximum improvement possible in either the plastic strain or cyclic

stress resistance regimes. Alternatively, one aims for a balance of fatigue strength and ductility with improvement spread over both the plastic strain and cyclic stress resistance regimes but less than the maximum possible with the first option.

The key to further improvements in fatigue performance may lie in several areas. An important one is that of the design of alloys to have cyclic strain hardening exponents which lie beyond the narrow range of values[12] which exist to date (0.10 - 0.25). From the existing knowledge a much lower value for the exponent would give excellent fatigue resistance at long lives, provided a high fatigue strength coefficient was maintained.

2.3. MECHANISMS OF FATIGUE FAILURE

The fatigue failure process of a metallic material comprises of more than one stage. This fact has been known for a long while and a number of theories have been proposed for these divisions of life. A widely accepted view is that three distinct stages exist, these being:-

a) the initiation of a crack

b) propogation of a crack into the material

c) the attainment of a critical crack size at which the material then completely fractures in a rapid manner.

On this basis, good fatigue resistance is achieved by restricting crack initiation, reducing the crack propogation rate and increasing the critical crack size for rapid fracture.

A similar approach is that due to Forsyth.[18] Here fatigue failure takes place by two stages of cracking. Stage I involves crack growth from an initiation site and growth is along planes of maximum resolved shear stress. Stage II follows and involves

growth along planes at 90° to the tensile axis. Rapid fracture occurs when a critical crack size is reached. Fig. 7 shows a sequence of the crack stages.

An underlying feature of both stages is their dependence on plastic deformation. For example, cyclic slip dominates the direction of Stage I crack growth. Furthermore, cyclic slip and a tensile stress are necessary for Stage II. In the remaining part of this survey dealing with fatigue failure mechanisms, the approach of Forsyth[18] has been adopted. Failure is considered in terms of two stages of crack growth and the dependence of each stage on microstructural characteristics is discussed. Because of its importance, a section on plastic deformation precedes those on the crack growth stages.

In the following sections, mention will often be made of low and high cycle fatigue. A number of definitions of these two conditions have been encountered. The most widely used term is the transition fatigue life[19] and this value identifies the boundary between the two conditions. Its value can be defined by reference to the lines shown in fig.5. The point of intersection of the elastic and plastic strain lines identifies the transition and the corresponding value on the horizontal axis gives the transition fatigue life. Low cycle fatigue refers to those conditions of stress or strain amplitude which give failure in lives less than the transition fatigue life. Here the plastic strain component predominates. High cycle fatigue gives failure beyond the transition fatigue life and under these conditions, the elastic strain component becomes predominant. Studies of a number of materials including steels[20] have shown that Stage II occupies most of the

life in low cycle fatigue but for high cycle fatigue, Stage I dominates the life.

2.4. THE ROLE OF PLASTIC DEFORMATION IN FATIGUE

Plastic deformation plays an important role in all the stages which lead up to fatigue failure. In order that fatigue damage may accumulate and subsequent failure occur, plastic deformation must take place. For such deformation to occur, the stress applied must exceed a certain value which is characteristic of that material under the cyclic conditions. This value is called the micro-cyclic yield stress[13] and for most materials it is well below the stress at which yielding occurs in a tension test under similar conditions, i.e. temperature, strain rate. An exception is that of germanium whose micro-cyclic yield stress equals that of its fracture stress.[21] If germanium is tested at a cyclic stress amplitude such that plastic deformation can occur, fracture occurs within the first reversal. A lowering of stress amplitude to prevent immediate fracture and so enable stress cycling, does not then produce fatigue failure and this is attributed to the absence of plastic deformation.[21]

The dependence of plastic deformation in fatigue on such factors as strain amplitude, strain rate, temperature and material condition has been widely studied. Similarities have been shown to exist in deformation processes between cyclic and unidirectional testing for many single phase materials.[10] For this survey, attention has been focussed on the effect of material condition.

The results of past work can be broadly classified into two areas. Firstly, those relating to examination of the micro-structures produced by fatigue and the mechanisms leading to their

formation. Secondly, measurements of change in deformation resistance and their dependence on and association with changes of microstructure.

2.4.1. Mechanisms of Deformation in Fatigue

The two most important mechanisms of plastic deformation in crystalline materials are slip and mechanical twinning. The operative mechanisms in cyclic deformation are similar to those in unidirectional deformation for a wide number of materials. In F.C.C. and most B.C.C. materials studied, slip is nearly always the operative mechanism. For example, in the early work of Forsyth on a F.C.C. silver-aluminium alloy[22] slip was dominant at low stress amplitudes just above the fatigue limit, but at higher stress amplitudes, kink-type deformation bands were observed. Both slipping and mechanical twinning have been observed in several C.P.H. materials such as magnesium[23] and α-titanium[24], during cyclic testing. Iron-silicon alloys normally cyclically deform by slip but at certain silicon contents, mechanical twinning was also observed.[25] In the work of Modlen and Smith[26], slip was observed during cyclic deformation of ferrite-cementite structures.

2.4.2. Effect of Cyclic Deformation on Microstructure

Studies of microstructural changes during cyclic deformation have consisted of:-

a) surface observations by optical and electron microscopy using taper sections, replicas and interferometric techniques

b) transmission electron microscopy to examine dislocation structures both near the surface and within the sample.

A number of variables such as strain amplitude and tempera-

ture influence the changes but the most important variable is the material condition. Three features associated with a material condition, have been identified as having an important effect on the microstructural changes and fatigue behaviour. These are:-

(i) mode of slip which is related to stacking fault energy[27]

(ii) homogeneity of slip[28,29]

(iii) reversibility of slip[11]

All three are dependent on the composition of a material and its microstructure. The mode or character of slip has been described[27] in terms of either planar or wavy glide. Planar glide is largely two-dimensional whereas wavy glide describes the spreading of glide to a three dimensional form. This spread is influenced by the ease of cross-slip of screw dislocations which in turn is related to the stacking fault energy. Aluminium and iron are examples of high stacking fault energy (S.F.E.) materials and readily cross slip during plastic deformation. Alloying can alter the S.F.E. value as in the case of copper (40 ergs/cm^2) whose value is lowered to 1.5 ergs/cm^2 when alloyed with 7.5 wt% of aluminium.[30]

Homogeneity of plastic deformation is influenced when a microstructure is altered from single to multi-phase. A single phase material is homogeneous in composition under properly controlled conditions and some degree of homogeneity of plastic deformation can be expected. In a material containing phases whose plastic deformation properties differ, homogeneity cannot be expected. This situation is discussed in the following sections.

Gough[31] has shown that slip in fatigue occurs on the same slip systems as under static loading for many materials having F.C.C., B.C.C. and C.P.H. structures. In α-iron, the operative planes are (110), (112) and (123) with a $\langle 111 \rangle$ direction. In static loading, the slip bands formed at the surface have a step contour whereas those in fatigue do not. Instead, a surface develops which is a series of grooves and ridges, the features of which are very dependent on the ease of cross slip and reversibility of slip. If slip occurs on many planes as a result of easy cross slip then the surface topography shows shallow grooves and ridges. If slip is restricted to only a few planes, a sharply defined notch peak topography can develop. In the work of Forsyth[32] on partially age-hardened aluminium -4% copper alloy, the surface topography after fatigue showed fine tongues of metal extruded from slip bands. These were called extrusions. In this alloy they were shown to be very thin and about 10μmetres high. This phenomenon has since been observed in annealed copper,[33] α-brass,[34] iron and silicon-iron.[35]

The reverse process to extrusion formation, namely intrusions have also been observed at the surface after fatigue[36,37]. These are crevices and can grow into cracks.[34]

The importance of the surface in fatigue has long been realised, even before slip bands were observed. Several experiments have been conducted where periodic removal of the damaged surface by polishing has shown to increase the fatigue life.[33] The increase is attributed to the removal of many of the slip bands although some do remain and these are called persistent

slip bands. The structure of the slip bands has been studied in order to understand the fatigue mechanism. Much of this work has involved an examination of the dislocation structures associated with the slip bands.

2.4.2.1. The Development of Surface Slip Bands

The onset of fatigue damage at room temperature in a variety of single phase materials is characterized by the development of fine slip bands on the surface. Further cycling leads to a concentration of slip in certain bands and eventually cracks may develop in these bands. It is within these areas that extrusions and intrusions have been observed in many materials. In the case of annealed copper, the fine slip develops during an initial stage in which rapid hardening occurs.[38] Fig.8 is a schematic representation of the change in stress required to maintain a constant strain amplitude and shows this hardening followed by a saturation stage where the stress remains constant. As mentioned earlier, not all materials show this hardening stage. Some may show softening and others show no change at all.

Slip concentration occurs within the saturation stage. The bands showing intensified slip are called persistent slip bands and may extend within the specimen for several microns. Light electropolishing removes the fine homogeneous slip bands but these intensified slip bands persist, hence their name.[33] Extensive studies of these bands[39,40,41] have shown that they possess characteristics which may differ from the matrix, for example,

a) they are softer

b) their strain hardening rate is lower and

c) they have a higher capacity for slip reversibility

In addition they have a characteristic dislocation structure in which the dislocations are arranged in cellular form typical of high stress amplitude. This aspect is discussed further in the following section. Their formation in single phase materials is explained in terms of a mechanism based on debris hardening.[42] Initially the material hardens uniformly and once filled with debris the local stress builds up such that the debris structure becomes unstable. This localised softening due to debris breakdown leads to strain concentration which is an undesirable feature where crack initiation resistance is required.

In single phase materials, a reduction in S.F.E. produces a more homogeneous distribution of slip and hence the formation of P.S.B's is delayed.[43] Lower temperatures generally produce a similar effect.[19] Testing in a vacuum[44] and also high frequency cycling[45] encourage a more homogeneous distribution of slip.

In those multi-phase materials studied, fatigue produces fine slip in ductile phases which then becomes localised in a few isolated regions resulting in persistent slip bands. These become sites for local strain as described above. However, additional soft zones may form due to cyclic induced microstructure changes and these produce inhomogeneous strain. For example, second phase particles may be located in the matrix such that dislocations penetrate them during cyclic stressing. The shearing action reduces the particle size and

the situation can arise where the particle dissolves in the matrix. The strengthening effect of that particle in the localised area is therefore lost and the resultant soft zone acts as a strain concentration. This has been observed in a number of alloys including low carbon steel[46] and nickel-base superalloys.[47] The operative mechanisms have been studied in a range of solution treated and aged aluminium-copper alloys.[48] To promote homogeneous slip, one must therefore develop a structure where the second and other phases are stable against moving dislocations and yet there are numerous dislocation sources within. This was the basis of the recommendations made from studies of iron-carbon alloys.[46] Thermomechanical treatments of aluminium alloys[49,50] have shown that structural developments for promoting homogeneous slip have improved fatigue properties in both high and low amplitude conditions.

2.4.2.2. Characteristics of Dislocation Structures

The dislocation arrangements produced by cyclic stressing of a number of single phase materials may be classified into two groups, these being:-

a) a cell or sub-grain boundary structure (fig.9A)

b) a banded structure containing loops and tangles of dislocations (fig.9B)

The structure develops within the initial stage of the curve shown in fig.8 which as mentioned earlier, corresponds to rapid hardening for many materials. The type of arrangement depends on the ease of cross-slip. A high stress amplitude or S.F.E. promote easy cross-slip of screw dislocations and favours the cell type structure.[51] An increase of temperature

increases the cell size and alters the types of dislocations found within the cell walls. Difficulty in cross-slip results in a banded structure of dislocations and this is found generally at low stress amplitudes and in materials with low S.F.E. values.

Almost all the early work on dislocation studies was carried out on copper and aluminium together with their respective simple alloys. Much of this has been covered in reviews, published in recent years.[3,5,6] Studies of α-iron have however shown that similar dislocation arrangements exist[52,53]. In the stage corresponding to rapid hardening, a low stress amplitude produces an inner substructure of dislocation tangles whereas a cell structure develops at high amplitude. The banded structure found in α-iron[54] shows similarities with that found in F.C.C. materials of high S.F.E., e.g. copper, which are tested at low amplitudes. Both show bands containing dislocation jogs and loops; the band dimensions are approximately equal. In α-iron, the band dislocations are mainly screw character whilst those in copper are predominantly edge dislocations.

In the region shown in fig.8, corresponding to saturation hardening, single phase materials show no major change of arrangement in the inner dislocation structure at low stress amplitudes and no increase of dislocation density. This may not always be the case with high amplitudes; for example, the cell walls in polycrystalline copper can become more sharply defined in this stage.[51] Differences between surface and interior structures have been observed in both F.C.C. and B.C.C.

materials. In zone refined iron[55], low amplitude cycling conditions give rise to isolated clusters of dislocations and scattered loops in the central portion of the specimen but not so in regions within 25μ metres of the surface. Here the structure contains bands of intense dislocation tangles and arrays of parallel rows of dislocation loops. Such arrays are often associated with the intense surface slip bands. These observations do not however correspond with those associated with the persistent slip bands (P.S.B.) found at the surface of so many fatigued materials in the saturation stage. The dislocation structure within these bands is composed of cells irrespective of whether the matrix is banded or cellular. Such a structure is characteristic of high strain fatigue and extensive cross slip. A number of theories have been proposed to explain the cell structure association with P.S.B's[40,6] but as yet no complete explanation is available. The importance of the role of P.S.B's in the fatigue failure mechanism is well established and further work is needed in this area to obtain a more concise explanation of the associated dislocation structure.

In multi-phase materials, the limited amount of work does show that on cyclic stressing, the resulting arrangement of dislocations is influenced by additional phases. The precise nature of the arrangement is influenced by the amount of these additional phases and their size and shape. In an iron-carbon alloy (0.08%C) containing only a minute amount of pearlite, high amplitude cycling produces a similar arrangement to that of pure iron[56] under the same cycling conditions.

With a higher amount of pearlite, as in a normalised iron -0.25% carbon alloy, the extent of dislocation jogs and loop formation is far less than in the lower carbon alloys. At intermediate and high amplitudes, sub-grain boundaries are observed but no continuous cell structure is formed. Similar observations have been obtained in the same alloy during cyclic testing after heat treatment which transforms the lamellar cementite to spheroidal form. These findings confirm the influence of cementite as restricting dislocation mobility in the ferrite matrix. If the alloy is quenched and aged at room temperature to give a fine distribution of small carbide particles in ferrite, the effect of cyclic testing on the dislocation arrangement is quite different. In the first case, there is an almost complete removal of the carbide particles; this is attributed to their shearing by moving dislocations and eventual resolution in the ferrite. Secondly, the structure shows dense clusters of dislocation jogs and prismatic loops which suggests considerable dislocation mobility. The supply of dislocations is attributed to two sources:-

i) quenching stresses during heat treatment which increase the dislocation density and,

ii) resolution of carbide particles in the ferrite.

Dislocation mobility therefore appears to be increased in this alloy when the additional phase is finely distributed.

Work[48] on an aluminium -4% copper alloy has shown that the nature of the additionalphase and its size influence the arrangement of dislocations after cycling. Where the structure contains a phase which is penetrable by moving

dislocations, both high and low amplitude have a similar effect. A homogeneous dispersion of fragmented dislocations with dense bands of dislocations is produced. In addition, where the phase has an ordered structure, dislocation motion disturbs the atomic arrangement within the phase and consequently destroys the ordering.

If the additional phase in the aluminium-copper alloy is not penetrated by dislocations, a different arrangement is produced by cyclic testing. It is dependent on the spacing of the phase in the matrix and the stress amplitude. At low amplitudes, dislocations are stored at the interfaces of the particles in both the fine and coarse structure. With a fine structure, single dislocations extend within the matrix between the particles but are absent in the coarse structure. At high amplitudes, dislocations may accumulate at the particle interface in both coarse and fine structures. Where the particle spacing is wide (i.e. $\simeq 1 \mu m$) dislocation cell walls are formed in the matrix.

All the observations of dislocation arrangements mentioned so far have referred to the early stages of the fatigue life. A few studies have been conducted of the structures produced in the vicinity of a fatigue crack as it grows through the material. These suggest that in the few materials studied, extremely high plastic strains exist in the region immediately ahead of the crack. A fine sub-cell structure is observed in copper[57], aluminium -4% copper and a titanium-aluminium vanadium alloy[58] all having high S.F.E. values. In copper, the cell diameter decreased as the crack tip was approached,

and a diameter of 0.1 μm has been measured.[59] This is much smaller than ever observed in bulk deformation where a cell structure is produced. In an 18-8 stainless steel (low S.F.E.) a cell structure is formed but α-martensite has also been detected at the crack tip.[60]

2.4.3. Changes in Deformation Resistance during Cyclic Testing

Cyclic testing produces a change of mechanical properties in the early stages of the fatigue life for all metallic materials studied to date. This phenomenon has been known for a long time and was first detected by interrupting the test and subjecting the cycled specimen to either a hardness, tensile or some other suitable test. Nowadays such changes can be measured without interruption to the cyclic test using modern closed-loop fatigue machines. Whilst such changes have generally been studied during the early stages of fatigue, they are also known to occur on a highly localised scale at the tip of a crack as it grows through the material.

Cyclic testing of single phase metallic materials produces hardening or softening in the early stages which then leads on to a saturation stage. Fig.8 is a schematic representation of cyclic hardening followed by saturation. Annealed materials usually show hardening and the saturation stage is reached within 10 - 20% of the fatigue life.[10] Cold worked materials usually soften although they can harden when the strain amplitude is equal to or greater than the plastic strain required initially to cold work the material.[61] Where softening occurs, a saturation stage is reached within 40 - 50% of the life.[10]

Material condition is not the only factor influencing the

changes of deformation resistance during cyclic testing. Temperature, frequency of testing, number of cycles and stress or strain amplitude have also been shown to be important.[10,62]

The major causes of cyclic hardening in single phase materials is attributed to an increase of dislocations and their interaction with each other and with point defects. In F.C.C. materials, a model of hardening has been derived from transmission electron microscopy studies.[42] This work has shown that large numbers of dislocation loops or debris are produced on cyclic testing. The characteristic features of this debris hardening model are that higher hardening rates are produced in the rapid hardening stage when conditions favour easy cross-slip. Softening of cold worked materials is attributed to release of dislocations from tangled networks and to dislocation annihilation. Where good overall fatigue performance is required cyclic hardening is often preferable to softening particularly where load carrying ability is important.[12]

In recent years there has been considerable study of changes in deformation resistance in multi-phase materials. The changes are influenced by those structural characteristics which control the availability of mobile dislocations under the plastic strain and also by the barriers which obstruct their movement.[63] Such characteristics include grain size and the nature and distribution of phases. A recent study[48] has confirmed some of these findings in the case of an aluminium-4% copper alloy. After treatment to produce a finely spaced ordered precipitate in a ductile matrix, the precipitate distribution was such that dislocations penetrated them during cyclic testing. With a strain

amplitude giving failure in about 10^3 cycles, cyclic hardening initially occurred due to accumulation of dislocations and the friction stress exerted by the precipitates. Beyond about 15% of the life, hardening was replaced by softening until fracture. A similar effect occurs in a nickel-base alloy containing a finely dispersed ordered precipitate.[47] The softening is attributed to a disordering effect on the precipitate by the movement of dislocations. It does not however occur in aged iron-1.5% copper alloys which have been treated to give stable non-coherent precipitates of copper[64]. On cycling this material in the low cycle region, hardening initially occurs and is followed by saturation. Maximum hardening is obtained with a fine distribution of particles. The particles obstruct dislocation movement and no reversion of copper is observed in the ferrite. This alloy shows typical features of an annealed single phase material. It has been concluded[48] that where precipitates are not ordered, bulk softening does not occur on cyclic testing. This may not always be the case since precipitates can be sheared and reach a size where resolution in the matrix occurs. This has been observed in a number of alloys[46, 47, 65] and has already been discussed in relation to surface slip band development and the associated localised softening.

In the case of aluminium -4% copper, altering the type and distribution of precipitate produces a change in the response to cyclic deformation.[48] Where the precipitate size and distribution allow movement of dislocations between them without penetration, cyclic hardening and saturation are observed at amplitudes giving failure within 10^3 to 10^5 cycles. Hardening is due to

an accumulation of dislocations and their mutual interaction.

A number of plain carbon and alloy steels have been studied under cyclic conditions[20,66,67,68]. Some show softening at low strain amplitudes but hardening at high amplitudes. Others show softening over a wide range of amplitudes. In plain carbon steels, the range of carbon contents studied extends up to 0.55%. With a carbon content of about 0.1%, a normalised steel shows softening followed by hardening and then saturation under amplitudes giving lives greater than 10^5 cycles.[63,67] The initial softening is due to the unpinning of dislocations which are then free to move within the structure. The rate of unpinning and movement of dislocations increases with stress amplitude and hence softening is completed within a lower number of cycles. The hardening which follows, arises from the obstructions to dislocation motion which take the form of vacancies and dislocation loops.

Grain size and carbon content influence the deformation resistance of those plain carbon steels mentioned above.[66,67] Grain size has been studied in annealed samples of a 0.11% carbon steel having 0.0011% nitrogen. Cycling at amplitudes giving failure between 10^5 - 10^7 cycles, produces softening in fine grained but hardening in coarse grained steels. Similar cycling conditions produce initial softening then some hardening and subsequent saturation in a normalised 0.55% carbon steel. The extent of hardening is far less than observed in lower carbon steels. Furthermore, saturation is reached earlier in the life with the higher carbon steels. No explanation or metallographic evidence have been presented to explain these observations.[67]

They can however be explained using a theory proposed from the results of research work described in this thesis. This involves the role of an interface within the structure. In the steels mentioned above, interfaces exist at boundaries between grains and phases. The major phases are ferrite and cementite, the proportion being influenced by carbon content. These interfaces are sources of mobile dislocations and sinks for many of the point defects produced by moving dislocations. In both the fine grained and high carbon steels, there is a greater extent of interface area than the coarse grained and low carbon steels respectively. Hence there is an increased availability of mobile dislocations for plastic strain. Furthermore, the build up of point defects to oppose dislocation movement is less extensive. Both factors discourage any hardening during cycling and hence may account for the observations obtained.

Several high strength steels have been shown to cyclically soften.[68] These include an 18% nickel maraging steel and a plain carbon steel in the quenched and tempered condition. An ausformed alloy steel cyclically softens in compression but cyclically hardens in tension. These deformation resistance changes can be predicted using the monotonic behaviour as outlined previously.[11] A value above 0.10 for the strain hardening coefficient indicates cyclic hardening whilst below this value, softening is expected. The ausformed steel has a lower monotonic strain hardening coefficient in compression than in tension and this accounts for the difference in cyclic response.

2.5. STAGE I CRACK GROWTH

For this review, the above term describes the period from the

first application of load up to the point at which a crack begins its growth on a plane approximately normal to the direction of the maximum tensile stress. This is shown in Fig.7. It includes the period of crack initiation and also that where the crack grows along a plane of high shear stress. In addition, it incorporates changes in deformation resistance which have been discussed in section 2.4.3. Crack initiation sites and shear mode crack growth characteristics are separately discussed but no attempt has been made to separate crack initiation and shear mode crack growth. In one review[3] this separation is justified on the grounds that crack growth along planes of high shear stress into the material requires a higher stress than crack initiation at the surface. However, the region on a fracture surface corresponding to Stage I crack growth is very small; in most cases, it occupies only a few microns or grain diameters and is hence difficult to observe. Furthermore, the shear mode crack can be considered as an enlarged initiation site. Separation of the two is therefore very difficult from metallographic observations.

In high cycle fatigue, as defined earlier, where the elastic strain component is predominant, a large amount of the life can be spent in Stage I crack growth. For an un-notched and laboratory sized specimen it can be as high as 90% of the total life.[3] For an extremely large sized component in the un-notched state, the number of cycles required for Stage II crack growth can be high and the proportion of life spent in Stage I growth is then not as high as 90%.

In low cycle fatigue, only a small amount of the life is spent in Stage I, the majority being spent in Stage II, i.e.

tensile mode crack growth. In sharply notched specimens, Stage II crack growth may begin immediately on the first application of load.

2.5.1. Initiation Sites for Fatigue Cracks

In the absence of sub-surface defects, a fatigue crack initiates at a free surface. Furthermore, it initiates at regions of plastic strain concentration. Such sites include slip bands, grain boundaries, twins, microstructural defects and, in the case of multi-phase materials, inter-phase boundaries and precipitate free zones. The sites at which fatigue cracks initiate are dependent on microstructural features and testing conditions. For example, grain boundaries [69,70] are preferred sites at high strain amplitudes (above 0.01) or high temperatures.[71] Some alloys have shown an initiation site dependence on the testing frequency.[72,73] Second phase particles in the form of inclusions can influence the crack initiation characteristics. This has been shown in a commercial high strength aluminium copper magnesium alloy.[74] Here the presence of a uniform distribution of small inclusions encouraged homogeneous slip and the formation of a sufficiently high stress concentration for crack initiation required a larger number of stress cycles than in the same alloy containing a non-homogeneous dispersion of inclusions.

Over the years, much attention has been given to slip band initiation sites as a result of the early work being focussed on single phase materials in either single- or poly-crystal form. In recent years where more attention has been directed to multi-phase materials, slip bands have remained an important site.

The following section considers each of the above mentioned sites for crack initiation at room temperature and outlines the possible mechanisms.

2.5.1.1. Slip Bands

Crack initiation at slip bands is a common occurrence in many single phase metallic materials under high cycle fatigue and room temperature conditions. This has been widely reported in reviews.[3,4,5] Several multi-phase materials show similar crack initiation characteristics under the same type of testing conditions and examples include low carbon steels,[26,52,66,75,76] high alloy steels,[77] aluminium alloys[74] and titanium alloys.[78]

As mentioned earlier in 2.4.2. the surface disturbance associated with slip band formation in cyclic loaded specimens differs from that found in static loading. On cyclic testing, the surface topography develops to show a series of grooves and ridges. Some materials show thin folds of material which are pushed out of the surface at slip bands and these are called extrusions.[32] They are generally associated with small crevices called intrusions[36,37] which penetrate slip bands. This surface disturbance creates a redistribution of stress and the grooves and intrusions become sites of stress concentration. Cracks develop within them. If, therefore, the extent of the surface disturbance can be minimised, the resistance to crack initiation can be increased. The severity of the surface disturbance depends on several factors but the most important ones relate to slip character. The ease of cross-slip, reversibility and homogeneity of slip each influence the surface disturbance on cyclic loading. In the

extreme, if slip in alternate cycles could be exactly reversed in the same atomic planes, there would be no surface disturbance and the crack initiation resistance would be infinite. An increase in the degree of slip reversibility in a copper-aluminium alloy has been shown to reduce the severity of surface notching and increase crack initiation resistance.[79]

Materials having high S.F.E. values readily cross slip and promote slip band formation. The resulting surface notching is far more severe than in those materials which show difficult cross slip. In the latter, dislocations are constrained to move in a more planar manner and this results in more homogeneous slip.[27] Hence plastic strain is distributed more uniformly throughout the structure and the formation of regions having plastic strain concentration levels sufficient for crack initiation is delayed. This is further discussed in a section dealing with multi-phase materials.

A number of dislocation mechanisms have been proposed to account for the surface disturbances produced by cyclic loading. However, there is not one mechanism which alone satisfies all the experimental observations. Several of these mechanisms are considered in the literature reviews referred to earlier[3, 4, 5]. For this review, two mechanisms are considered, these being by Mott[80] and May.[81] That proposed by Mott involves the cross-slip of screw dislocations where an extrusion forms by the motion of screw dislocations in one direction along a plane and their return in another plane to complete a closed circuit. The mechanism assumes that dislocation motion is not reversible.

It does not account however for intrusion formation and the appearance of extrusions within the very early stages of fatigue. The mechanism has been subsequently modified[82] and now involves the generation of both edge and screw dislocations. In a single stress cycle, hundreds or thousands of screw dislocations can be generated and this can account for the very early appearance of extrusions and intrusions. Whilst dislocations may move along a closed circuit as in the early model, it is not essential in the modified one. It is however necessary that there exists a path discrimination between positive and negative dislocations. The passage of screw dislocations leaves a concentration of positive and negative edge dislocations and this is sufficient to produce extrusions and intrusions.

May[81] proposed that the surface disturbance is attributed to a process of random reversed slip. Dislocations move on paths under one half cycle of stress but return along paths which are shifted in a random fashion with respect to previous paths. This random distribution of slip roughens the surface and redistributes stress so that the slip tends to concentrate in the valleys and thus they are deepened. The mechanism could occur equally well in materials where cross slip is easy or difficult. It does not explain how the random slipping is initiated nor does it explain how extrusions can develop in relatively few cycles. On the other hand mathematical development of the model, with certain assumptions, has led to values for cycles to failure with the right order of magnitude.

2.5.1.2. Grain Boundaries

Crack initiation at grain boundaries has been observed in many metallic materials under conditions of high cyclic strain.[6] Studies[69,83,70] of aluminium, copper and nickel showed that for lives above 10^5 cycles, cracks initiated at slip bands but for lives less than 10^3 cycles, they initiated at grain boundaries. Other materials including 70:30 brass, copper-aluminium alloys and steels showed a similar trend.[84]

In high strain fatigue, localised surface rumpling occurs and produces grooves at grain boundaries. The stress concentrating effect of the grooves produces further deepening and the crevices become the nucleii for fatigue crack growth. Surface rumpling is attributed to the strain discontinuity at grain boundaries and the localized increases in surface area during one half cycle which are not recovered during the other half cycle. A model, developed to explain this behaviour, and based on the plastic instability,[85] gives a relationship between the number of cycles required to initiate a crack and the plastic strain range. This relationship has been shown to satisfy results obtained from tests on copper, aluminium and nickel.

Grain boundary crack initiation occurs in materials at high temperatures. Cyclic testing at a temperature T leads to cracking in these sites in materials of melting point T_m, where the relationship T/T_m is greater than 0.5.[6] (T and T_m measured in ^oK) At room temperature, this relationship is exceeded in such low melting point materials as lead and tin. Lead was shown[86] to develop serrated grain boundaries during

the early stages of cyclic testing. The formation of cracks within the grain boundaries was attributed to grain boundary sliding. In tests at high temperatures, two additional material characteristics, namely creep and environmental attack, are superimposed on the fatigue behaviour and in some cases may entirely dominate the material behaviour. It then becomes difficult to isolate the true effects of temperature on fatigue behaviour. A discussion of these other characteristics is beyond the scope of this review. They are however discussed in several reviews, in particular a comparatively recent one[19] which discusses the significant developments in fatigue at high temperature and the prediction of life in service.

Grain boundary crack initiation is also observed in some materials at room temperature and at cyclic stresses giving long fatigue lives (above 10^5 cycles). It has been reported in iron containing 0.1% phosphorus[87] and irons containing 0.027% and 0.0005% of oxygen.[88] The principal cause in these materials is impurities at grain boundaries which lead to decohesion. In the latter two materials, oxygen segregation in the form of iron oxide particles was revealed at grain boundaries, the volume fraction being greater in the higher oxygen alloy. The embrittling effect of the particles was accentuated by cyclic stress. For example, the alloy containing 0.0005% oxygen showed grain boundary embrittlement under cyclic testing but not under tensile testing.

An additional factor considered responsible for grain boundary crack initiation in the above alloys has been that of elastic anisotropy of the B.C.C. structure of iron. Its

contribution in iron however is thought to be far less than in the case of β-brass which is also B.C.C., where the factor is considered to be the principal cause of crack initiation at grain boundaries at room temperature. Studies of fatigue of β-brass[89,90] have shown grain boundaries to be the principal sites for crack initiation. Intergranular films were not detected and initiation sites could not be correlated with inclusions in the work. Instead the material shows a marked anisotropy, far greater than that of iron. The figures below show this in the variations of elastic moduli with crystallographic direction.

β-brass: $E\langle 111\rangle / E\langle 100\rangle = 8.94$

α-iron: $E\langle 111\rangle / E\langle 100\rangle = 2.16$

During cyclic stressing, it is suggested[89,90] that high stress concentrations develop at grain boundaries resulting from this high elastic anisotropy. The high stress is then relieved by crack formation at the boundary and this forms the nucleus of the initiating crack. At 78°K, work[89] showed fatigue crack initiation mostly at slip bands instead of grain boundaries in spite of the increased elastic anisotropy and grain boundary weakness at this temperature. This was attributed in one case to the formation of a martensitic structure in localised areas within the matrix at this temperature and that cracks initiated at the interface between the two products[89]. In the other case, cracking was attributed to a low cleavage strength[90] of the material at 78°K since no martensitic product could be detected with the cracks. These findings clearly demonstrate the interaction of a number of possible factors in

determining the sites for fatigue crack initiation.

Grain boundaries have also been shown to be principal sites for crack initiation in molybdenum,[91] another B.C.C. material, on cyclic testing at stress levels giving fatigue lives in the range 10^2 - 10^6 cycles. Other sites included slip bands and regions of impingement of grain boundaries by slip bands. At the higher stresses, the predominance of grain boundary cracking increased. No mechanism was proposed for the observations in the work. It was however shown that on tensile testing, there was no grain boundary embrittlement; instead, a characteristic yield drop and uniform deformation were observed giving a ductile fracture. A possible reason for the behaviour of molybdenum may be that of grain boundary impurities based on oxides or nitrides. These would then cause decohesion similar to that in the iron alloys[88] where, in the case of the lowest oxygen content, the embrittling effect is accentuated by cyclic stress. Analysis showed the molybdenum to contain oxygen and nitrogen but at extremely low levels, these being 40 and 10 parts per million respectively.

The incidence of crack initiation at grain boundaries in single phase F.C.C. materials is rare at room temperature and low cyclic stresses. It has been observed in polycrystalline aluminium[92] and α-brass.[34] The effect of boundary mis-orientation on grain boundary crack initiation has been studied by several workers[34,93,94] and the results obtained are not consistent. In copper tri-crystals,[93] small misorientation across a grain boundary was associated with crack initiation at the boundary. Under these conditions, slip bands crossed

grain boundaries whereas at high misorientations, slip bands terminated at some distance from the boundary. The interaction of slip bands with grain boundaries at small misorientations was thought to create a sufficient number of vacancies to initiate a crack in the boundary. In another study[94] of bi-crystals of copper and α-copper-aluminium alloys, a different effect was observed. Cracks initiated at grain boundaries where misorientation was high. This contradiction of results has been difficult to explain. The principal cause proposed has been that of the more complex situation regarding misorientation between grains that exists in the poly- and tri-crystal specimens than in the bi-crystalline specimens.

2.5.1.3. Twin Boundaries

Mechanical twinning is a principal mode of plastic deformation in C.P.H. materials. Studies of pre-twinned metals such as cadmium, zinc, magnesium and α-titanium have shown crack initiation at interfaces between mechanical twins and the matrix, on cyclic testing at stress levels giving lives of 10^4 - 10^5 cycles and at room temperature.[23] In this work cyclic stressing was shown to produce serrations at twin interfaces and also fragment suitably oriented twins into smaller twins. Cracks initiated from these interfaces before 25% of the fatigue life had elapsed. Studies of fatigue behaviour[24,95] in α-titanium have shown that whilst mechanical twinning has an important effect on it, the types of twins observed are not always the same. In one study, $\{10\bar{1}2\}$ type twins were observed to predominate.[95] In another,[24] cracking

was almost exclusively associated with $\{11\bar{2}1\}$ type twins although not all such mechanical twins showed damage. The damage occurred at discrete regions along the twin matrix interface and was found to occur when twins were subjected to a shear stress greater than a critical value. The twins were considered as barriers to dislocation movement so that where slip bands in the matrix intersected twin boundaries, the localised dislocation build-up produced decohesion.

Crack initiation at twin boundaries has been found to occur in B.C.C. materials under certain conditions. Hempel[75] showed this in Armco iron on testing at 93°K and stress levels giving lives of under 10^5 cycles. An iron -4% silicon alloy[25] showed similar characteristics at room temperature and low cyclic stresses but only when in the pre-twinned condition. When fully annealed and untwinned, slip band cracking occurred and some mechanical twinning was subsequently observed close to existing slip band cracks. It was concluded from this work that a high level of stress was required to produce mechanical twinning. Such a high level was possible arising from the local stress concentrations around slip band cracks.

Studies of single phase F.C.C. materials include work on copper where the role of annealing twins as cracking sites have been studied under a range of conditions.[96] The cracking tendency at such sites was shown to be dependent on the twin/matrix interface orientation with respect to the applied stress. Cracks appeared at the interface when it was parallel to the primary slip plane. Where the plane and interface were not parallel, there was only occasional cracking. Under

conditions of parallelism, the interface showed intense deformation and the surface developed extrusions. This intense deformation was attributed to the presence of steps or ledges in the twin interface which acted as dislocation sources and stress concentration points.

Twin boundary crack initiation has been shown to occur in multi-phase titanium alloys and nickel-chromium-cobalt alloys.[97] Slip band initiation was also found in the titanium alloy. In the case of the nickel alloy, the studies applied only to cyclic testing under low cycle fatigue conditions where the plastic strain amplitude was high. The reasons for such cracking were not explained.

2.5.1.4. Inter-phase Boundaries

Much of the work done so far on such sites has been based on inclusions in such materials as steels and aluminium alloys. The importance of non-metallic inclusions as fatigue crack initiation sites has been known for a long while and extensively documented.[98,99,100] It is only in recent years that the mechanisms responsible for crack initiation have been understood.

Studies of aluminium alloys in high cycle fatigue[99] showed crack initiation at the inclusion-matrix interface. There was no visible sign of slip in the region. Continuous examination of the surface during fatigue showed the appearance of tiny voids at the interface. These opened up during further cycling to become propagating fatigue cracks. Similar results were obtained in high strength steels[100] and a modelof crack initiation has been proposed based upon experimental

observations and theoretical stress analysis. This model predicts debonding at the inclusion-matrix interface in those regions lying about 90° to the principal stress axis. Debonding proceeds along the interface and microcracks grow into the matrix as a result of a build-up of point defects.

Fatigue crack initiation at boundaries other than those between a matrix and inclusions have been studied in only a few materials. These include titanium alloys containing the α(H.C.P.) and β(B.C.C.) phases,[78] a commercial zirconium alloy containing zirconium hydrides in the matrix[101] and a number of composite materials.[102] In the titanium alloy[78] cracks initiated at the interfaces between the α and β phases on cyclic testing at room temperature and stresses giving high cycle failure. Slip bands could not be detected. If the stress or temperature was raised, cracks initiated at slip bands within the α-phase very early in the life. Cracking at the interface was attributed to debonding but no damage mechanism was proposed to account for the phenomenon. In the zirconium alloy,[101] a low interface coherency between the zirconium hydrides and the matrix accounted for crack initiation at such interfaces. However, either fracture of hydride plates or void formation at the hydride/matrix interface were also responsible for cracking at these sites.

The effect of interface strength on crack initiation has been studied in two composite materials,[102] these being an "in-situ" variety formed by unidirectional solidification of the eutectic alloy Al - Al_3 Ni, and a manufactured variety based on Al - B. The interface is much stronger in the

eutectic alloy than in the composite of aluminium and boron. Cyclic testing at levels giving failures in about 10^5 cycles showed a difference of behaviour between the two composites. In the Al - Al_3Ni composite, slip bands developed in the matrix away from fibres and both extrusions and cracks formed within the first 10% of the life. The interface between fibre and matrix showed no break up until the final stages of the fatigue life. In the Al - B system, the weaker interface showed the development of cracks from the very early stages of cyclic testing. The cyclic stress required to maintain a pre-set strain amplitude decreased throughout the test whereas for the Al - Al_3Ni material there was an increase of stress up to the final stages of failure. From the results of this work, any method promoting interfacial strength between phases should reduce the propensity of crack initiation from such interfaces.

2.5.1.5. Precipitate Free Zones

Such zones may exist in those multi-phase materials strengthened by precipitation of additional phases. They are regions at which strain concentrates and promotes early crack initiation at slip bands. The mechanism of cracking is similar to that described for slip bands, in 2.5.1.1.

There are two reasons for the formation of such zones. Firstly, they may develop during a heat treatment process. Secondly, they can develop during cyclic testing where dislocations repeatedly shear a particle down to a size at which it can revert into solid solution. This precipitate reversion then leads to precipitate free zones. The reversion behaviour has been observed in a number of materials including steels[46] and various aluminium alloys.[72,103,104] but in materials containing

precipitates which obstruct the dislocation motion, this reversion does not occur.

2.5.1.6. Microstructural Defects

Typical defects in commercial materials include non-metallic inclusions, holes and soft spots arising from improper heat treatment. All promote the concentration of strain in localised areas which then accelerates crack initiation. In general the mechanism of crack initiation is based on slip bands or debonding at inter-phase boundaries. Such defects can be very important and it is well known that they impair fatigue performance.

2.5.2. Shear Mode Crack Growth

Following initiation from any of the sites mentioned above, almost all the materials studied so far in fatigue show crack growth along planes of maximum shear stress. This continues until a critical crack depth is reached where the crack characteristics alter to a tensile mode. An exception to this has been shown to be molybdenum[91] which showed crack initiation but no shear mode growth. It did however show the tensile mode of crack growth.

The rate of growth of the shear mode crack is usually very low (about 50 A^{o}/cycle) and the area occupied on the total fracture surface is very small. In the past, this limited size has made the examination difficult. Even then, metallographic examination has showed these areas to be almost featureless. In contrast, the tensile mode of crack growth (Stage II) extends over a large area of the fracture surface and contains much interesting microscopic detail.

Much of the existing knowledge about shear mode crack growth has been gained from only a few studies. In one such study, the mechanism was examined in copper single crystals.[105] It was shown that the initiation and growth of Stage I cracks were dependent on repeated and reversed plastic deformation rather than intermittent unidirectional deformation. Under cyclic compression stresses, cracks were not observed to initiate or grow in single crystals even when the stresses were several times the monotonic yield stress. In contrast, a poly-crystalline sample showed crack initiation and growth under compression cycling. This was attributed to either residual stresses or localised tensile stresses created by the interaction of grains. In a further study of aluminium,[106] cyclic tension stresses gave dislocation structures typical of monotonic deformation rather than of cyclic deformation.

In the work on copper,[105] two mechanisms were suggested for shear mode crack growth. The first is the "plastic blunting process"[107] within a single slip band. This takes place by a repetitive plastic rounding and closing of the crack tip through plastic flow within a single slip band. The mechanism is a slight modification of the one which accounts for the tensile mode crack growth and which is described fully in section 2.6.2. The second mechanism is based on an "unslipping model". Here the material on one side of the crack is displaced by shear on the tension cycle. On the compression cycle, the specimen surface geometry is restored but the crack length is increased. Both models are schematically presented in fig.10. The difference between the mechanisms arises from the types of associated

plastic deformation and hence slip character. The unslipping model is applicable to materials of low S.F.E. having a planar slip mode. The plastic blunting model is appropriate to materials of high S.F.E. where cross slip is easy and hence crack tip blunting possible.

Examination of shear mode fracture surfaces has not been extensively carried out. The most detailed appears to be that for a nickel-base superalloy having a two-phase structure and in single crystal form.[108] On cyclic testing to give failure in about 10^5 cycles, crack initiation occurred at surface pores and the crack grew along several $\{111\}$ planes. The fracture surface was highly reflective and showed crystallographic fracture steps and river lines when tested in air but under vacuum testing, there were fewer steps and lines. There was a very high dislocation density within a band extending approximately 25μm from the fracture surface and confined mainly to the matrix. It was difficult to determine the nature of the dislocations but diffraction contrast experiments suggested that they were dipoles.

In a more recent study of a multi-phase aluminium alloy,[109] shear mode cracks propogated by the development and linking up of holes within precipitate free zones and persistent slip bands. Well defined striations were observed on the fracture surface. Such striations have also been observed in β-brass[89], thoriated nickel[110] and an aluminium alloy[111] and are similar to those found in the tensile mode crack, stage II. The presence of striations and the need for reversed plastic deformation have led to a generally accepted conclusion that a repetitive mechanism of plastic deformation operates in both the shear mode

crack growth stage and the tensile mode growth, namely stage II.

2.5.2.1. Influence of Microstructure

Extensive shear mode crack growth is encouraged at low cyclic stresses and in corrosive environments. These facts are well known but there is little work relating microstructural characteristics and shear mode crack growth.

Some materials such as α-brass show a fatigue life dependence on grain size under cyclic stressing giving long life.[112] This material has a low S.F.E. and cross slip of dislocationsis difficult. In aluminium, which has a high S.F.E. value there is no dependence of life on grain size under similar cyclic testing conditions. A similar effect is observed in copper, whose S.F.E. value is high but less than that of aluminium. The difference of behaviour is attributed to the stage I crack growth in both copper and aluminium being insensitive to grain size whereas in brass it is not.

Under cyclic testing, the dislocation structure developed in copper and aluminium is cellular whereas in brass it is planar. The cell walls behave as grain boundaries and are not penetrable by moving dislocations. Hence the dislocations move within the cells and few interact with grain boundaries. The cracking rate is therefore determined by the cell size which in turn is dependent on the stress amplitude as previously mentioned in 2.4.2.2. In brass there are no cell walls formed so that dislocation motion is inhibited only by grain boundaries. Dislocations therefore move within the plastic zone at the crack tip but on reaching a grain boundary they are restrained by boundary pile ups. Crack growth is thus

retarded. As the grain size is increased, boundary interference is less frequent and this stage of crack growth is accelerated.

The work above[112] represents the most detailed study of microstructural effects on stage I crack growth so far. Some of its findings are in conflict with the results of earlier work. For example, in earlier work on brass[113] it was shown that grain boundaries obstructed dislocation movement to such an extent that once a crack penetrated a boundary, it entered the stage II growth. This is of course not the case. Recent work[112] has shown that stage I cracks can cross grain boundaries and continue in this stage of growth into other grains. The effect is shown schematically in fig. 7.

2.6. STAGE II CRACK GROWTH

A stage II crack follows the stage I crack growth period as shown in fig.7. It involves growth of a crack in a plane of maximum tensile stress. A small plastically deformed zone is created at the crack tip and the zone size increases as the crack becomes longer. Growth of the crack continues until a critical depth is reached where catastrophic failure occurs.

The relationship of plastic zone size with specimen thickness significantly influences the crack growth characteristics. Consider, for example, a thick specimen under test at low cyclic stresses. At the beginning of stage II, the plastic zone size is relatively small compared with the sample thickness and hence plane strain conditions exist at the crack tip. As the zone size increases with crack extension, its ratio to sample thickness also changes and produces a change in both the stress and strain

conditions at the crack tip. A transition from plane strain to plane stress conditions occurs and the crack growth rate accelerates until catastrophic failure conditions are achieved. In thin specimens this transition from plane strain to plane stress can occur almost immediately if the conditions are right.

The plastic zone size is a controlling factor for the propogation of fatigue cracks and studies[114] have shown that the zone size is dependent on the stress intensity factor and material properties[115] at the crack tip. This is discussed in the later section on studies of crack growth rates.

Studies of this stage of crack growth fall into two categories, those involving metallographic examination and the more quantitative investigations involving measurements of crack growth rate and its dependence on testing conditions and material properties. The material scientists are mainly responsible for metallographic studies and the subsequent proposed mechanisms for crack growth. The more quantitative aspects have been studied in order to facilitate prediction of growth rates and fatigue lives. Each of these groups of studies are considered in the following sections.

2.6.1. Metallographic Features of Stage II Crack Growth

Metallographic examination of stage II fatigue crack growth has been extensive. The techniques used have included optical, electron and scanning electron microscopy. In general this crack follows a transgranular non-crystallographic route. It can follow grain boundaries as for example in the case of three B.C.C. materials, iron alloys,[88] β-brass[89] and molybdenum.[91]

The dislocation arrangement in the crack tip and in regions close to the crack surface has been examined by transmission

electron microscopy. The first studies of this type were on pure single phase materials such as copper[116] and aluminium.[117] Multi-phase materials including aluminium[72] and titanium[58] alloys have also been studied and the results appear consistent with those for the single phase materials. A highly mis-oriented sub-grain structure is formed adjacent to a fatigue crack and in the multi-phase materials the size of the region containing these sub-grains is smaller than in the single phase materials. The sub-grain formation in different microstructures is attributed to the high strain at the tip of a growing fatigue crack which is considered to activate recovery of the structure in a localised region.

The dislocation structures in regions adjacent to a growing crack are characteristic of high strain amplitude cycling of bulk specimens. In the case of aluminium,[118] localised hardening occurs in these regions in the same way as in bulk specimens. However, metallographic evidence shows that the material in the crack tip may deform in ways not observed in normal bulk deformation. For example, thin foils containing the fatigue fracture surface of single and multi-phase materials showed sub-grains of about 0.1μmetres diameter. These are much smaller than ever observed under bulk deformation conditions. This suggests that the magnitude of strain in the crack tip is very high. Knowledge of the behaviour of materials under such high strain is scarce and hence prediction of material behaviour in the crack tip is difficult. However, the effects of such high strain on precipitate resolution and overageing have been studied in some alloys.[58,72] In an aluminium-zinc-magnesium

alloy,[72] re-solution of non-coherent precipitates was observed ahead of the growing crack. It was suggested that the re-solution was attributed to solute diffusion since at high crack growth rates and hence short diffusion times, the precipitates remained largely unaffected. In a commercial precipitation hardened aluminium-copper alloy, there was however no evidence of precipitate re-solution in the region of the crack tip but the reasons for this are not stated in the work.

The major features of fatigue fracture surfaces are the striations which lie approximately perpendicular to the local direction of crack growth. Since they were first reported[119] a lot of work has been done in the study of their features. For instance, it has been suggested that they form only under conditions of plane strain at the crack front.[3] Furthermore, the distance between each striation represents one cycle of stress although the reverse does not always apply; some stress cycles produce no striations since the strain concentration build up at the crack tip may be insufficient to increase the crack length. This association of stress cycles with striations has been examined in a number of programme loading tests.[120,121] These also showed that striation spacing increased as the stress increased.

Not all fatigue fracture surfaces show clearly defined striations. Their visibility is influenced by the testing method,[3] environmental conditions[122] and method of examination. Some may be visible under an optical microscope whereas others may require surface replication and electron microscope examination for resolution. Two types of striations have been

identified, namely a ductile or type A and a brittle or type B.[123] The ductile striations lie on curved plateaux which form a general fracture plane normal to the maximum tensile stress. The brittle striations lie on crystallographic facets which show considerable orientation differences to the general fracture plane. The two types may occasionally appear together under similar stress conditions but in general the brittle type is observed in corrosive environments[124] and cycling at low frequencies.[18]

Striations have been observed on the fatigue fracture surfaces of many metallic materials and polymeric materials,[125] covering a number of different crystal structures. In the metallic materials they have been observed irrespective of whether the crack path is transgranular or intergranular.[91] However, they are not the only features observed. Others include areas of micro-cleavage and void coalescence and of course these influence the rate of growth.[126] The types of features observed are dependent on the micro-structure and testing conditions. In work on pearlitic and spheroidised carbide structures in steel, fracture surfaces showed areas of cleavage where the structure was pearlitic in addition to striations. Cleavage was associated with crack growth through cementite plates. In the spheroidised carbide structure, the crack growth rate was lower and the fracture surface showed striations.

2.6.2. Mechanisms of Crack Growth in Fatigue

A number of mechanisms have been proposed for stage II crack growth and most of them are based on the explanation of

striation formation since this is the most common fracture surface feature. There are however other features, as mentioned earlier. Four mechanisms described are as follows:-

a) striation or ripple formation

b) micro-cleavage

c) void coalescence

d) intergranular separation

The most widely accepted mechanism for striation formation is the plastic blunting process proposed by Laird.[107] It is schematically shown in fig. 11. During tensile loading, plastic strain occurs at the crack tip and plastic deformation is concentrated in zones along planes of 45° to the crack growth direction. This results in crack blunting and an increased surface area. During the compression half of the cycle, the crack faces come together without complete reversal of the plastic deformation and the crack advances a certain distance. The crack is resharpened and ready to repeat the process on the next cycle. Each cycle produces a striation according to this model. Furthermore peaks on one side of the crack should correspond with peaks on the other and the same with valleys. This is observed in many cases but other types of striation profiles exist[3,127]. For example, peaks may correspond with troughs and undercutting of ridges does occur on some fracture surfaces. The profile is dependent on the symmetry and number of available slip systems [128] and in general, most F.C.C. materials show a uniform "saw-tooth" profile. This is not always the case in B.C.C. materials where high elastic anistropy may exist as for example in β-brass, $E\langle 111\rangle / E\langle 100\rangle = 8.94$. The different types of profile

indicate that there is no single mechanism which precisely satisfies all the observations. Nevertheless, the plastic blunting model is the most applicable.

Microcleavage may occur during crack propagation in materials containing brittle second phase particles. This has been observed in a coarse pearlite steel[129] and in high strength aluminium alloys.[130] This growth mechanism gives a higher propagation rate than a striation mechanism.[126] The increase in rate is dependent on the microstructure in pearlite steels.[131] For coarse pearlite structures, the growth rate and extent of micro-cleavage were greater than in a spheroidised structure.

Void or dimple formation during crack growth has been observed in several steels having fine microstructures.[3,132]

The mechanism proposed[133] is based on void formation ahead of the main crack and ultimate linking up of the two on subsequent cyclic loading.

Intergranular crack growth has been observed in several quenched and tempered high strength steels.[134] It was found to be associated with prior austenite grain boundaries particularly if the boundary strength was impaired by impurity elements.

2.6.3. Studies of Crack Growth Rates

The major aims of such studies have been not only measurement of crack growth rate but its dependence on material properties and testing conditions. A number of methods for crack growth measurement have been used. For example, the striations on fracture surfaces indicate localised growth and their spacings can be used to determine the localised growth rate. However, striations are not always present and they do not always

indicate the microscopic growth rate. The optical and electrical methods are widely used to measure crack growth. The optical method is suitable for surface crack studies but is time consuming and requires an observer. For thick specimens, the errors can be severe since a crack may branch off and tunnel to give, for example, the undercutting earlier mentioned in striation profiles. The electrical method overcomes these disadvantages. It measures the potential between the two faces produced by the growing crack and therefore gives a measure of the increase in fracture surface area. It is more practically convenient than the optical method but is standardised against the optical.

Fracture mechanics concepts have been widely used in the prediction of growth rates. The stress intensity range at the crack tip is the dominant parameter. A most widely accepted equation is that below,[136] which applies to the growth per cycle of a crack having length 2a;

$$\frac{da}{dN} = C\,(\Delta K)^m \qquad \text{——————} 8$$

where ΔK is the range of stress intensity

C is a constant which may be material dependent

m is the exponent in the power law relationship

This equation suffers from several limitations and unfortunately is often used for predictions in situations for which it is not valid. For example it should only be used where the plastic zone size at the crack tip is small compared to the crack length and specimen dimensions. Furthermore, it assumes that in

determining the plastic zone size for calculation of the stress intensity range ΔK, the yield stress remains constant throughout the test. As described in earlier sections, materials may show hardening or softening on cyclic testing. Finally, the equation takes no account of material properties. Nevertheless, there is much experimental data for several materials which satisfies the equation and justifies its use in certain circumstances.

Several other approaches to crack growth predictions have been made based on dislocation theories[137] and cyclic material behaviour.[138,139] From the metallurgical point of view, approaches based on the latter appear more attractive since the opportunity for material design is improved. In one approach,[138] the growth rate of several materials including multi-phase aluminium alloys and steels, was related to monotonic tensile properties and satisfied a universal relationship. The tensile properties involved were the yield stress and tensile strength, true strain at fracture and Youngs modulus.

A more realistic approach[139] is that based on cyclic properties which have been already defined in 2.2.1. The properties considered are the cyclic strength coefficient (K') and the cyclic strain hardening exponent (n'). In the derivation of this model, stage II crack growth was observed in a ductile metal and the pattern of crack tip deformation and crack growth deduced.[140] Intense plastic deformation occurred in localised bands at 45° to the tensile axis. The new crack surface formed by shear decohesion along these bands during the tensile loading. The model is described in the form of two equations, both given below (9 and 10). Each refer to the rate

of growth per cycle of a crack of length 2a. Equation 9 describes the model for low cycle fatigue conditions where the plastic strain predominates. Equation 10 refers to high cycle fatigue conditions where the elastic strain constitutes a predominant part of total strain.

$$\frac{da}{dN} = a\left[\frac{\pi}{32}\,\frac{\sigma_f^2}{\epsilon_f^{n'}(\sigma_y')^2}\right]\Delta\epsilon_p^{(2n'+1)} \qquad \text{——— 9}$$

$$\frac{da}{dN} = a\left[\frac{\pi}{32}\,\frac{\epsilon_f}{\sigma_f^{1/n'}(\sigma_y')^2}\right]\Delta\sigma^{(2n'+1/n')} \qquad \text{——— 10}$$

where n' = cyclic strain hardening exponent

σ_y' = cyclic yield stress

σ_f = true monotonic fracture stress

ϵ_f = true monotonic fracture strain

$\Delta\epsilon_p$ = plastic strain range

$\Delta\sigma$ = stress range

These equations show that for low cycle fatigue conditions, an increase of n' gives a decrease in crack growth rate. For a decrease in crack growth rate under high cycle fatigue conditions, a decrease of n' is required. These facts correlate with the statements made earlier and give simple indices of fatigue crack growth resistance.

2.7. Summary

The major objectives in this survey have been to review the work done on microscopic aspects and mechanisms of fatigue in that important group of materials, namely those based on multi-phase alloys. Such alloys constitute almost all those commercial

materials that are used for high duty applications. The survey has shown that almost all the earlier work on such aspects and mechanisms was concentrated on single phase materials. In more recent years this work has been extended to cover multi-phase materials.

A significant advance in fatigue knowledge that has been made in recent years is the identification of cyclic material parameters. These can be related to fatigue performance and enable the fatigue behaviour under specific conditions to be reliably predicted. This advance has been mainly attributed to the design and use of sophisticated testing machines. An underlying theme throughout much of the work covered in this survey has been the attempt to link such parameters with microstructural features. If this could be done then the design of microstructure for specific fatigue performance is then made possible.

The most significant cyclic parameter recognised to date is the cyclic strain hardening exponent (n'). Its value has been shown to influence fatigue behaviour in that it can be related to total life performance and crack growth resistance. The best correlation between this parameter and microstructure has been found with the mode of slip. High values are associated with structures which allow extensive dislocation and cross slip whilst low values are associated with restricted dislocation motion. However, the limiting range of values known for this exponent at the present time restricts the opportunity for extensive control of fatigue behaviour using this method. There is a need for further research into alloy design giving higher or lower values than the existing range for this exponent. Further research is

also required into the relationship between Stage I and II crack propagation on microstructure. Little work has been done to relate microstructure with stage I crack growth yet in high cycle fatigue conditions, this stage may occupy up to 90% of the life. In Stage II crack growth there has been more work done but the dependence on microstructure is still not clear. The fracture mechanics approach splits the basic crack-growth curve into three regions,[144] these being an initial threshold which is then followed by a region of uniform fatigue crack growth and finally catastrophic failure. The threshold region is reported as being strongly dependent on microstructure[144] and further work is required here.

3. EXPERIMENTAL PROCEDURE

3.1. CHOICE OF MATERIALS

The major objective of this work has been the study of crack initiation and propagation in a pearlite structure. The steel used, required a composition such that on suitable heat treatment, a fully pearlite structure could be achieved without the presence of pro-eutectoid ferrite or cementite. The most suitable steel available, at the time the work began, was a carbon spring steel, having the specification number En42CK (B.S.970). It had been made by the acid open hearth process and was supplied by, at that time the B.I.S.R.A. laboratories. Its composition is given in Table 1 and for this work is designated steel A. Metallographic examination of the steel showed only traces of a pro-eutectoid constituent but it did contain numerous non-metallic inclusions. Many were oriented in the rolling direction and the majority were identified as alumina and manganese sulphide. Because of their known influence on fatigue behaviour, it was considered that both crack initiation and propagation could be attributed to them as well as pearlite morphology. Arrangements were therefore made for a steel of similar composition to be made in a vacuum induction melting furnace. Two separate casts of steel were subsequently made using the melting facilities of the Sheffield Polytechnic. These are designated steels B and C and their composition is given in table 1. Both showed only traces of pro-eutectoid cementite and the inclusion content was extremely low. The orientation of inclusions with rolling direction was utilized in the subsequent examination of damage areas insofar that orientation of damage areas was easily identified with reference to rolled out inclusion direction.

3.2. PREPARATION OF MATERIAL

3.2.1. Specimen Design

The material was shaped into two forms, namely rolled strip 15mms. wide and about 5mms. thick and also rolled bar of 18mms. diameter. Each form was used for a supply of specimens for fatigue testing in an Avery reversed plane bending machine and a closed loop electrohydraulic servo-controlled machine. To avoid the presence of large residual stresses in the specimens prior to fatigue testing, samples were machined and roughly polished prior to heat treatment.

Flat specimens for reversed plane bending were machined to dimensions shown in fig. 12A such that all rolled edges and decarburised surfaces were removed. The round section specimens for push-pull fatigue were machined to dimensions shown in fig. 12B. The specimens were mechanically polished to a roughness of 15μm. For the round specimens, only the gauge length was polished and this was done using a Morrison machine.

In order to prevent decarburisation during the heat treatment, all specimens were encapsulated in a silica tube containing argon. Each specimen was first degreased and dried before inserting in the tube. One tube end was closed and the open end was fitted into a vacuum line. The system included a special valve which was fitted to an argon supply. The tube was evacuated and then filled with argon. This process of evacuation and argon filling was repeated several times. After final evacuation, argon was passed into the tube to a pressure of 180mms. of mercury. The tube containing the specimen was sealed off using an oxy-acetylene burner. It was calculated

that at about 1300°K which was the maximum temperature reached during heat treatment, the internal pressure in the tube would be about 1 atmosphere. This prevented tube explosion during heating.

3.2.2. Heat Treatment

Heat treatment cycles were designed to produce three different structures, these being a coarse pearlite, fine pearlite and a distribution of spheroidised carbides in ferrite. Most of the early work was done using a coarse pearlite and here the cycle was designed to give a structure that was readily resolvable using an optical microscope. For coarse pearlite production, the encapsulated specimens were austenitized at 1100°C for 4 hours to homogenize the austenite followed by transfer to and holding in a muffle furnace at 710°C for 20 hours and then cooling in air. For the three steels used in the work, this cycle produced a coarse lamellar pearlite having an average pearlite cell size of 30μm (range 20 - 50μmetres) as determined by lineal analysis. The mean interlamellar spacing was 3000 Angstrom units.

A fine pearlite was produced by a similar austenitization treatment to the above but followed by air cooling. This gave an average pearlite cell size of 12μm (range 1 - 28μmetres) and an interlamellar spacing of 700 Angstrom units. The spheroidised carbide structure was achieved by heating to and holding at 670°C for 36 hours and then cooling in air. It had a mean free ferrite path of about 5000 Angstrom units. The spheroidal carbide size was in the range of 1 - 4μmetres.

3.2.3. Surface Preparation

After heat treatment and prior to fatigue testing, the specimen surfaces were mechanically polished down to 6μm. Mechanical polishing was only minimal since surfaces had been polished down to 15μm before heat treatment. They were then electro-polished to provide a non-distorted surface layer. The electrolyte contained 25 grams of chromium trioxide, 133 mls of glacial acetic acid and 7 mls of distilled water. The apparatus used is shown in fig. 13. A cylindrical cathode of stainless steel allowed both surfaces of the flat specimens to be polished and a glass stirrer was immersed in the electrolyte. For cylindrical specimens, an additional item of equipment was used. Here the specimen was rotated by fixture in a chuck and driven by a motor.

The conditions for successful electropolishing varied slightly according to the type of structure. In general, with a fixed anode-cathode separation of 35mms, the required potential drop between anode and cathode for successful polishing was between 20 and 24 volts and the current density was approximately 0.15 amps/cm^2.

Electropolishing was often used for fatigue damaged specimens in order to examine the extent of damage within the specimen. Here it was necessary to remove known thicknesses from damaged surfaces. The conditions for satisfactory electropolishing were reproduced and the loss in weight during polishing a specific surface area was determined. Knowing the density of steel, the weight loss was converted into volume and subsequently into thickness of metal removed. Surface removal was controlled

by adjustment of polishing time. The conditions described above gave a removal rate of about 25μm/hour.

3.3. FATIGUE TESTING

Two types of fatigue tests were used in the work. Initially, the material available was tested in a reverse plane bending machine using the specimens machined from the strip (fig.12A). Later in the work, material was tested in uniaxial tension-compression using the equipment described below. The specimens for this work were produced from round bar (fig.12B).

3.3.1. Reverse Plane Bending Tests

Specimens were fatigue tested in an Avery reverse plane bending machine. Here the specimen was bolted at one end to a dynamometer and at the other end to a bending arm which is operated by a motor-driven eccentric through a connecting rod. The bending arm oscillates about an axis passing through the mid-point of the specimen. The throw of the eccentric was adjusted to give the required bending moment which is determined by the deflection of a measuring arm connected to the dynamometer. Knowing the bending moment and specimen dimensions, it was possible to determine the maximum theoretical bending stress at the specimen surface. It was however realised that the method of calculation is based on the assumption that the operative stresses are of an elastic nature whereas in fact some of the stresses will be plastic. The method has been used so that specimens of different thickness values can if necessary be tested at the same theoretical bending stress. To achieve this, the required bending moment was first determined using the formulae and the eccentric throw adjusted accordingly.

A series of tests was also performed to evaluate the magnitude of strain at a specimen surface corresponding to a range of values for eccentric throw settings. A strain gauge was fixed to the surface of several specimens in turn, each having different thicknesses. After calibration, the gauge readings were used to calculate the corresponding surface strain.

The number of specimens available was such that a full determination of the stress-life curves for each of the three structures was not possible. Nevertheless, an estimate of that portion of the curve between 10^3 and 10^6 cycles was aimed for from a few non-interrupted cyclic tests at various stress amplitudes. The majority of tests were conducted at surface stress amplitudes corresponding to failure at between 10^5 - 10^6 cycles and in these, specimens were periodically removed during the test for examination of damage. All tests were carried out at a frequency of 24 HZ.

3.3.2. Uniaxial Tension-Compression Tests

These tests were carried out using a closed-loop servo-hydraulic machine. Using this equipment either the load or deformation could be controlled. Load was measured by a load cell in series with the specimen and was applied by a hydraulic ram. This ram was energized by a hydraulic pump and controlled by an electro-hydraulic servo-valve. A clip-on extensometer was used to measure specimen deformation.

All the tests were carried out in strain control. With a pre-determined strain amplitude setting, the feedback signal from the extensometer was compared with this command by the servo-controller. The difference between the two

signals was used to drive the ram by means of a servo-valve. This machine was used to perform three different types of tests, these being:-

a) incremental step tests

b) constant amplitude strain-controlled tests

c) monotonic tension tests

Incremental step tests were used to establish the cyclic stress-strain curves for each structure. Such curves were earlier described in section 2.2.1. One specimen only was used to establish the curve for each structure. In the test, a specimen was subjected to a programme of continually increasing and then decreasing strain amplitudes. These ranged from a strain amplitude of approximately 0.0011 to 0.0168 in 15 equal steps. An X-Y plotter was used to monitor the load and strain measurements and the results from this plotter were used for measurement of these values. Continuous monitoring of strain and load was possible from a high speed strip chart recorder and an oscilloscope.

Each specimen was subjected to a total of about 45 blocks. The X-Y plotter was used to trace out load and strain values for a number of these blocks and in this way it was possible to record the changes in load required to maintain specific levels of strain amplitude. After only a few blocks, the cyclic behaviour as shown by load values began to stabilize. Once stability was achieved, the cyclic stress-strain curve was produced by joining up the tips of the loops on the trace from the X-Y plotter, which showed load values corresponding to levels of strain amplitude. The load values were of course converted

to stress. This curve was used to determine values for the cyclic strain hardening exponent n' and the cyclic strength coefficient K', both having been described earlier in 2.2.1. Equation 1 was used to determine the values, this being:

$$\sigma_a = K' \left[\frac{\Delta \epsilon_p}{2} \right]^{n'}$$

where σ_a is the stress amplitude corresponding to a plastic strain amplitude of $\frac{\Delta \epsilon_p}{2}$ in a cyclic stress-strain curve.

In the constant amplitude strain-controlled tests, specimens were tested at strain amplitudes giving failure in about 10^5 - 10^6 cycles or 2×10^5 - 2×10^6 reversals. Specimens were also tested under these conditions and removed for metallographic examination at the following stages of life: 25%, 50% and 75%. The frequency of cycling in all the tests was approximately 10 HZ. Prior to the commencement of this work, the relationship between strain amplitude and life to failure was predicted for each of the three structures using the methods described in 2.2.2. The information required for prediction was

a) the cyclic strain hardening exponent n'

b) the fatigue strength coefficient σ_f'

c) the fatigue ductility coefficient ϵ_f'

The appropriate value of the exponent n' was known from the incremental step test. Values of the coefficients σ_f' and ϵ_f' were not known but previous work[9,10,11] had shown them to be approximately equal to the monotonic true fracture strength and fracture ductility respectively. Monotonic tension tests were carried out under strain control in the hydraulic machine and the stress-strain curves were traced using the X-Y plotter for

each structure. From these the values for both the true fracture strength and fracture ductility were determined and hence completed the information required for prediction. The number of samples available was small and hence it was not possible to check the predicted curve over a wide range of strain amplitudes. The only checks made were at those amplitudes which had been predicted as corresponding to lives of about 10^5 - 10^6 cycles. In this way, any necessary corrections were possible before conducting the tests in which specimens were removed for metallographic examination.

In the cyclic tests to failure, readings of strain and load on the high speed recorder and traces on the oscilloscope could be used as indicators of the stage of cracking. For example, when a crack initiated, this manifested itself in a reduction of the tensile load required to maintain a given strain amplitude. However, the size of crack necessary to produce an effect that could be picked up by the equipment was such that, by the time the load reduction was observed, the crack would be well into the propagation stage.

3.4. METALLOGRAPHIC EXAMINATION

Pre-polished specimen surfaces were examined after cyclic and monotonic testing in order to determine the extent and form of damage. In the case of cyclic testing, specimens were also removed from the machine at specific stages of the life for metallographic examination and recycled. Further electro-polishing of a damaged surface and the removal of known amounts was also carried out in order to study the extent of damage below the surface. In almost all cases, an examination of an untested specimen was

conducted in parallel for comparison purposes. It also assisted in isolating those features that were not attributed to either cyclic or monotonic tests. Fracture surfaces of specimens cycled to failure were examined metallographically. In the reverse plane bend tests, a fracture surface was produced by stopping the test as near to final failure as possible and breaking the specimen in a vice. This minimised any destruction of surface features that was extensive if the specimen was allowed to proceed to complete cyclic failure.

A number of metallographic examination techniques were used in the work, all based on either optical or electron microscopy.

3.4.1. Optical Microscopy

Bright field and also dark field illumination were used in the normal optical microscope techniques for detecting early damage of surfaces of specimens having coarse pearlite and spheroidised carbide structures. For the fine pearlite, the resolving power of the microscope was insufficient.

In the examination of surface topography of damaged areas, specimens were first flash coated with copper and then nickel plated so as to preserve the surface features. Without the initial copper coating, the nickel deposit was not adherent. The copper plating solution was made up to contain the following materials:- 23 gms of copper cyanide, 35 gms of sodium cyanide and 15 gms of sodium carbonate, all in 1 litre of water. The solution was used at 50°C in a fume cupboard with all the necessary safety precautions. The anode-cathode potential was 2 volts and a copper anode was used. After washing, the copper plated specimens were immediately plated with nickel using a

solution containing 240 gms of nickel sulphate, 45 gms of nickel chloride and 30 gms of boric acid, all in 1 litre of water. A good adherent deposit was produced on plating at an anode cathode potential of 3 - 4 volts and an anode of annealed nickel. The solution temperature was 20°C. After about 2 hours plating the deposit thickness was sufficient to withstand the necessary sawing off of sections. These specimen sections were mounted at a taper angle of about $11\frac{1}{2}^{o}$ to give an apparent surface magnification of x 5.

3.4.2. Electron Microscopy

For high resolution microscopy, the transmission and scanning electron microscopes were used. Most of the work on the scanning electron microscope was carried out using the facilities of the British Rail Technical Centre at Derby. The majority of work was done using the transmission electron microscope and for this two separate preparation techniques were involved, these being:-

(a) the production of replicas

(b) the production of thin foils

Two methods were used for replica production. For surface damage examination where it was necessary to preserve the surface, a two-stage replica method was used. Cellulose acetate sheet of thickness 0.034 mms was first wetted with acetone and applied to the specimen surface. After drying, it was stripped off, shadowed with gold-palladium for improving contrast and then coated with carbon. Break-up of the replica during dissolution of the acetate film was minimised by first coating the carbon with a low melting point paraffin wax. This was done by cutting

the carbon coated film into suitable sized pieces required for the microscope. Each piece was then placed carbon face down into the molten wax and the wax allowed to solidify. The acetate film was dissolved in acetone and the wax subsequently dissolved in petroleum ether so as to leave the carbon replica.

Interpretation of some fields obtained in the replicas was at first difficult since it was not known whether certain features were true ones attributed to fatigue damage or whether they were artefacts of replication. Since a scanning electron microscope was not readily available, it was decided early on in the work to develop techniques whereby such features could be positively identified. Comparison with unfatigued specimens was used but not considered to be completely satisfactory. It was however thought that if a feature was seen repeatedly on several replicas of the same area, it was unlikely to be a replication artefact.

A method was therefore developed for obtaining a replica from the same area. This consisted of replicating in acetate sheet as before but then carefully mounting the dried plastic replica on a glass slide for examination in an optical microscope. It was possible to identify areas corresponding to particular features of interest during optical microscope examination. The area of interest was then marked for subsequent reference and the process repeated with a second plastic replica and the same area identified. After shadowing with gold-palladium and carbon, the areas of interest were cut out and processed as above for examination in the electron microscope. With care, it was possible to examine several replicas from about the same

area using this two-stage method. If a feature was attributable to fatigue damage it would show itself in each replica from the area containing that feature.

Single stage replicas were produced of fracture surfaces and those damaged surfaces where preservation was not necessary. Here carbon was evaporated onto the surface and stripped off by etching. This method was mainly used on the cylindrical specimens which had been cycled in uniaxial tension-compression tests.

Thin foils were prepared of the cylindrical specimens by cutting discs perpendicular to the cyclic stress axis. These were mechanically polished in a holder down to a thickness of about 150μmetres. They were electrolytically polished at 10^{o}C using a solution of 25% perchloric acid in methanol. Final dishing and perforation was carried out using the electro-jet technique in a solution of 10% perchloric acid in methanol at -10^{o}C and a potential of 14-16 volts depending on the structure. Two electron microscopes were used for examination of the foils. These were:-

(a) an A.E.I. 1000 KV microscope

(b) a JEM 100B microscope

4. RESULTS

All the results presented are from tests on the three steels A, B and C whose composition is shown in table 1. As mentioned previously, three separate structures were produced by heat treatment of each of these steels and the structural characteristics are as follows:-

a) coarse pearlite having an average pearlite cell size of 30μm (range 20 - 50 μmetres) and a mean interlamellar spacing of 3000 Angstrom units (Fig.14a)

b) fine pearlite with an average pearlite cell size of 12μm (range 1 - 28 μmetres) and a mean interlamellar spacing of 700 Angstrom units (Fig.14b)

c) spheroidised carbides in ferrite having a carbide size range of 1 - 4 μmetres and a mean free ferrite path of 5000 Angstrom units (Fig.14c)

4.1. CYCLIC AND MONOTONIC PROPERTIES

These properties were assessed mainly from tests on steel C. The monotonic tension stress-strain curves are shown in Fig.15 and values for some of the important properties given in table 2. Values of the monotonic true fracture stress and strain have also been determined because each is utilised in deriving the total strain-life plots as discussed in 2.2.2. The fine pearlite shows higher values than the other structures for those parameters which define monotonic strength. The spheroidised carbide has a much higher fracture ductility than the other structures.

The results of incremental step tests are shown in two forms. Firstly the cyclic properties are listed in table 3. Secondly, the cyclic stress-strain curves are produced for comparison with

the monotonic stress-strain curves in figures 16 - 18. The values in table 3 indicate that both the cyclic yield stress and strength coefficient are highest for the fine pearlite structure. Its cyclic strain hardening exponent is lower than that for the other structures. All three values lie in the narrow range 0.228 - 0.248. Typical values of this exponent for a large number of different materials have been shown to lie in the range 0.10 - 0.25.[12] High values are associated with those structures which allow extensive cross slip and dislocation motion.[11] All three structures show high values for the cyclic strain hardening exponent and these are attributed to the presence of ferrite as the dominant phase. Calculations based on the iron-cementite equilibrium diagram give a volume proportion of 85% for ferrite in pearlite. It is well known that the stacking fault energy for this phase is high and cross-slip is hence easy.

The second phase is shown to influence the exponent value since that for the fine pearlite is lower than the coarse pearlite and spheroidised carbide structures, the values of the latter two being very similar. From the above observations,[11] this would suggest that cross slip and dislocation motion are less extensive in the fine pearlite than the other two structures. It will be shown later in the metallographic results that fine pearlite shows the least concentrated slip damage of the three structures.

A comparison of the monotonic and cyclic stress-strain curves (figs. 16 - 18) shows that the fine pearlite behaves in a different manner to that of the coarse pearlite and spheroidised carbide. The monotonic is above the cyclic stress-strain curve for fine pearlite over the range of strain values used in the tests. This

indicates cyclic softening. Such behaviour has been observed in many steels.[7,68] In both the coarse pearlite and spheroidised carbide structures, cyclic softening is observed for the lower values of strain but a cross-over occurs where the cyclic curve is above the monotonic curve. This indicates cyclic hardening. This transition from softening to hardening occurs at a strain value of 0.003 for the coarse pearlite and 0.004 for the spheroidised carbide structure. It means that on cyclic testing at a strain amplitude below the cross-over value for the respective structure, the stress required to maintain the amplitude will initially decrease. At amplitudes above the value, the stress required will initially increase. This behaviour is observed in several steels. For example, the steel represented by Fig.3 shows similar characteristics. The reasons for this cross-over are discussed later.

The predicted strain-life curves for the three structures are shown in Figs. 19 - 21. As mentioned earlier, these have been produced from results of the monotonic and incremental step tests using the methods described in 2.2.2. The major reason for their production was to predict the strain amplitude corresponding to failure at between 10^5 and 10^6 reversals. The majority of tests for subsequent metallographic examination have been conducted at such strain amplitudes. The number of specimens available was limited and checking of the predicted curves was not possible over the range of strain values. Checks were restricted to that portion of the curve for each structure corresponding to failure at around 10^6 reversals. Such checks showed very good agrement with values on the prediction curve.

In the high cycle region of the prediction curve corresponding to failure at around 10^5 - 10^6 reversals, the fine pearlite has a greater fatigue resistance than the other two structures. This is shown by the fact that for a given life of say 3×10^5 reversals, a strain amplitude of 0.0026 can be tolerated by the fine pearlite whereas both the coarse pearlite and spheroidised carbide structures can tolerate an amplitude of 0.0024. At a strain amplitude of 0.0024, the life for the fine pearlite is approximately double that for each of the other structures.

In the low cycle region of the prediction curves corresponding to strain amplitudes of above 0.01, the spheroidised carbide structure possesses the greatest fatigue resistance. At a strain amplitude of 0.1, the curves show that the life for this structure is up to ten times that of either the coarse or fine pearlite. In this region, the fine pearlite has the lowest fatigue resistance. In the high cycle region, the position is exactly reversed and the reasonsfor this predicted behaviour are discussed later.

In order to produce fatigued specimens of steels B and C for metallographic examination, a series of tests were performed using the closed loop servo-hydraulic testing system. Specimens were removed for examination at various stages of the life. In the main, the strain amplitudes selected were those which gave failure between 10^5 - 10^6 reversals. For steel C, the values used are shown in Figs. 19 - 21. For steel B a range of strain amplitudes were used to cover the low cycle and high cycle regions. During these tests, strain and load were continuously recorded.

In such tests on steel C, softening initially occurs as

predicted from the comparison of monotonic and cyclic stress strain curves. Softening is completed within the first 100 reversals and the load required to maintain the preset amplitude stabilizes. This stability corresponds to the saturation region shown in Fig.8. In tests on steel B, a similar softening effect is observed on initial testing at either high or low strain amplitudes.

In the few tests conducted on steel B, a behaviour pattern was observed that involved a change in load required to maintain a pre-set strain amplitude. In some of the tests on this steel, samples were removed from the machine for observation at say 10, 20 or 30% of the life and then replaced for subsequent testing at the same amplitudes. The delay between removal and replacement for testing ranged from 30 minutes to 24 hours. It was found that whilst softening occurred on testing of virgin specimens as previously mentioned, a further softening effect followed by stability was observed each time the specimens were recycled. Further investigation of this behaviour pattern is necessary.

In the continuous measurement of load and strain it was possible to examine the effects of crack growth, in the final stages of tests to failure, on the load required to maintain a given strain amplitude. Since the cycling frequency was constant in all tests, an increase in the rate at which the load amplitude decreased for a given strain amplitude indicated an acceleration of crack growth rate. These observations predicted that in the spheroidised carbide structure, the crack growth period extended over a large number of stress reversals than both the coarse and fine pearlite.

4.2. METALLOGRAPHY

A large proportion of the metallographic work involved the observation of surface damage throughout the complete test to failure. These tests were conducted using either a reverse plane bending machine or the closed-loop servo-hydraulic machine. The tests included not only the period leading up to crack initiation but also that involving crack propagation. The results of this work are presented in three sections covering initiation sites, crack growth and general surface damage observations. A fourth section covers results of the transmission electron microscopy where the associated dislocation structures were examined. Unless otherwise stated, all the results refer to fatigue tests conducted under conditions giving failure at around 10^5 - 10^6 reversals of stress.

4.2.1. Observation of surface damage

a. Form of damage

A comparison of damage in the three structures at 25 and 75% of their life is shown in the electron micrographs of Figs. 22 - 27. In all structures, damage appears as wavy slip bands and continued cycling increases the number of slipped areas and intensifies some of the existing slipped areas. This is shown clearly in the optical micrographs Figs. 28 - 30 which relate to a coarse pearlite and show build-up of damage in one area at 2% and 5% of the life. In both coarse pearlite and spheroidised carbide structures surface damage can be observed at 1% of the life. All the early damage observed appears in the ferrite matrix and further examples are shown in Figs. 31 and 32. The damage

as viewed in optical micrographs is similar in appearance to that found in previous work[75,141] on fatigued specimens of ferrite-pearlite structures. In this previous work however, the damage appeared in the free ferrite grains and rarely in the ferrite within pearlite.

In the lamellar structures, slip damage appears at pearlite cell boundaries (Fig.23a) and within the pearlite (Figs. 22a and b). The orientation of the slip bands nearly always follows that of the cementite lamellae (Figs. 22-25,33) but there are exceptions to this as shown in Figs. 31 and 32. Many of the slip bands show ripples along their length as indicated by the arrows in Figs. 23 and 24. Similar effects have been observed by other workers and interpreted as slip band extrusions.[142] Whilst some areas may show heavy damage (Figs. 22a and b) other areas immediately adjacent show no apparent damage and this can exist right up to the final stages of failure. This concentration of damage is found in the coarse pearlite whereas in the fine pearlite, damage is less severe at an equivalent stage of the life and is more widely dispersed throughout the structure. A comparison of the two structures is obtained from Figs. 23b and 25a which represent typical areas after cycling to 75% of the fatigue life.

In the spheroidised carbide structure, slip band damage appears in the ferrite grains and at their boundaries. Fig. 27 shows a concentration of damage within the grains of ferrite which appears isolated from the boundaries. After cycling to 75% of the fatigue life, surface damage is more

uniformly distributed around grain boundaries and within the grains (Figs. 26a and b).

In both pearlite structures, slip band damage appears first in those pearlite cells where the cementite lamellae are oriented between 30 and 90° to the principal stress axis. This is shown in Figs. 28 - 30 and 33. Here the inclusions are elongated in the specimen length direction and hence define the principal stress axis. Cells having lamellae of orientation outside the above stated range show little surface damage throughout the whole life. The effect of orientation on sites of damage has been demonstrated in several experiments and Figs. 34 and 35 show the results of one conducted on a coarse pearlite. Here the surface damage after fatiguing to 5% of the life is shown in Fig.34. After electropolishing to remove 2μmetres, the surface was cleared of visible damage (Fig.35a) and again fatigued for the same number of cycles as before. Fig. 35b shows similar damage sites and this is attributed to the influence of cementite lamellae orientation on location of damage. Since the pearlite cell size in this structure lies in the range 20 - 50μmetres, the removal of 2μmetres has little effect on the existing pearlite cells prior to polishing. The cementite lamellae orientation at a particular site will not therefore be greatly altered. On removal of about 25μmetres by polishing, a large proportion of the existing cells are removed and the new surface shows many new cells. At a given site, the lamellae orientation may not be the same as that which existed before. After such removal and sub-

sequent fatiguing for the same number of cycles as before, there is a change in the sites of slip damage.

b. Influence of non-metallic inclusions on damage

The areas of damage shown in Figs. 28 - 30 and 33 show an extensive number of inclusions. These refer to the first steel used in the work (steel A). Subsequent steels B and C were processed so as to be low in inclusions. In spite of its high inclusion content, steel A has been used for much of the earlier work. The inclusions are mainly alumina and manganese sulphide. Previous work[143] has shown that alumina inclusions are detrimental to the fatigue characteristics of high strength steel. In this investigation the inclusions have little detrimental effect on the fatigue behaviour. Slip damage appears within the ferrite and there are only a few areas where damage concentrates around inclusions. In the stages of crack growth, inclusions appear to have no major influence.

c. Taper Sections

A comparison of specimens in the fatigued and unfatigued condition using taper sections shows surface disturbance after cycling and this can be detected early in the fatigue life. Typical sections are shown for the three structures in Figs. 36 - 39. In general, the surface damage is associated with a very shallow notch peak topography. Where features are observed they exist mainly as extrusions, and crevices. The maximum height of extrusions observed is approximately 0.5μ metres.

The fine pearlite shows the least surface disturbance

of the three structures. At magnifications of 1000 there is no apparent disturbance from the unfatigued condition. The coarse pearlite and spheroidised carbide structures show changes and examples of features in the coarse pearlite are shown in Figs. 36 and 37. Two features of interest are the extrusions and crevices. Extrusions appear in favourably oriented pearlite cells (Fig. 36a and 37a) and emerge from the ferrite. The root of the notches formed between extrusions coincides with the emergence of cementite lamellae at the surface. The average height of extrusions measured over a number of sections is 0.2μmetres. Crevices appear in the structures shown in Figs. 36 and 37. In Fig. 37b one crevice is associated with an inclusion stringer and its depth is approximately 2μmetres. There is some slip damage around its root. Adjacent to this are other smaller crevices but not associated with inclusions. These two show damage at their roots. Examples of other crevices are shown in Fig. 36.

The spheroidised carbide shows disturbance over the whole surface in the section. The form of disturbance differs from that in the coarse pearlite in two ways. Firstly the extrusions are broad and rounded (Fig. 38b) as opposed to the sharp peaks in the coarse pearlite. Secondly they are distributed over the surface whereas those in the coarse pearlite appear only from favourably oriented cells.

The effect of high strain amplitude testing on surface disturbance in a coarse pearlite is shown in Fig.39. There are more severe extrusions produced than in the lower strain

amplitude tests. Further more cracks appear at the pearlite cell boundaries. These latter results are not unexpected since crack initiation at grain boundaries has been observed in many metallic materials under conditions of high cyclic strain.[6]

4.2.2. Dislocation Structures in Fatigued Specimens

Transmission electron microscopy has been used for examination of interior structures of specimens at various stages throughout the fatigue life in order to support the observations of surface damage. The work has been confined to specimens of steel C which were fatigued in the closed-loop servo-hydraulic testing system using uniaxial cycling. For comparison purposes, the examination was extended to include structures in the as-received condition and after tensile fracture. Typical structures are shown in Figs. 40 - 46.

The structure corresponding to tensile fracture shows considerable differences from that for cyclic testing. Fig. 40 shows a coarse pearlite after tensile fracture. There are numerous sites of shear fracture in the cementite lamellae and these closely correspond with cracks in the ferrite. The areas of high dislocation density which are apparent after cyclic testing are either difficult to resolve or not apparent.

The features observed in foils of specimen's after cyclic testing have been closely examined to distinguish those that are attributed to true structural effects and those which are not (e.g. bend contours). All structures show a build-up of dislocations in the ferrite. After

25% of the life, samples show several areas of high dislocation density in the ferrite and after testing to 75% of the life, such areas appear more intense and extend over larger areas. The ferrite-cementite interface is an important source of dislocations which move into the ferrite. Figs. 41 and 42 show this effect clearly by comparison of typical areas in the unfatigued and fatigued condition for a coarse pearlite. A fine pearlite shows a similar effect.

In the spheroidal structure, dislocation build-up in ferrite appears to emanate from almost all carbide spheroids. This differs from the lamellar pearlite where dislocation activity appears to concentrate in small areas on the lamellae interface. Trails of dislocations are readily apparent in the ferrite (Fig. 46a) and a dislocation cell structure forms (Fig. 46b).

Figs. 41a and 44a show features that exist throughout whole cells of pearlite and continue through cementite lamellae without any apparent effect. Such features move across the image when the foil is tilted and are attributed to bends in the foil. However, similar features are observed in Figs. 43a, 44b and 45a. These do not move on tilting the foil and are true structural features associated with areas of high dislocation density.

Figs. 42a and 43b show dark features emanating from cementite lamellae into ferrite. At first sight they appear crack like but there are no indications of perforation

in these areas at very high magnification. Instead they are dislocation concentration areas. Fig. 45b shows features resembling arrow shaped markings across cementite lamellae. There is no displacement of the lamellae and further investigation is required to explain these features.

4.2.3. Studies of Crack Initiation Sites

The objectives of this aspect of the work have been to detect how soon cracks initiate at the surface during fatigue and locate the sites of such cracks. The work has involved the use of the optical and electron microscopy techniques described earlier in the experimental procedure. The detection of crack sites by optical microscopy is limited by the low resolution. This has been overcome by electron microscopy techniques using selected area replication methods so as to isolate artefacts of replication. The scanning electron microscope has been used to confirm some of the evidence obtained.

In both the coarse pearlite and spheroidised carbide structures cracks are observed in specimens fatigued to about 25% of the life. These can be clearly distinguished by optical and electron microscope examination technique. Their presence is confirmed by limited use of the scanning electron microscope. Examples for both lamellar and spheroidal structures are shown in Figs. 26, 27, 31, 32, 47, 48 and 49. Figs. 31 and 32 are electron micrographs of surface replicas from coarse pearlite. Careful examination shows cracks within the ferrite (A) and also at

ferrite-cementite interfaces (B). The shadowing effect produced during replica preparation enables such cracks to be distinguished. The shadow direction is shown by the cementite lamellae which protrude above the ferrite. Similar features are shown in a scanning electron micrograph (Fig.47). Here several cracks are shown all of which may have initiated either in a slip band or at the ferrite-cementite interface. In general, the coarse pearlite shows crack initiation at three sites under the stress conditions used in this work. These sites are slip bands, pearlite cell boundaries and the ferrite-cementite interface. Sites near the cell boundaries appear to be deeper in the early stages of the life. This fact is shown up in Figs. 48 and 49. These show coarse pearlite fatigued to 25% of its life and then electropolished to remove 2μmetres. The heavily slipped regions seen before polishing cannot be detected but micro-cracks exist, some of which are up to 20μmetres long. These cracks occupy pearlite cell boundaries and continue within the cells where their exact location is difficult to determine.

In the spheroidised carbide, Figs. 26 and 27 show damage concentration at ferrite cell boundaries and within the grains. Cracks are detected both at slip gands and at the cell boundaries. The shadowing effect is very severe at the cell boundaries and this indicates some considerable disturbance in these zones as a result of cycling. The effect becomes more accentuated in samples fatigued to 75% of the life.

In the fine pearlite, cracks cannot be detected in specimens fatigued to 25% of the life. It has already been reported earlier here that surface damage was minimal after such testing.

Cracks can be detected at 75% of the life and appear at cell boundaries and within slip bands (Fig.50). Because of the fineness of the pearlite, it has been difficult to identify whether cracks initiate at ferrite-cementite interfaces. Nevertheless, the overall results show quite conclusively that the propensity for crack initiation is far less than in either the coarse pearlite or spheroidal structure.

4.2.4. Studies of Crack Growth

Crack propogation has been studied using metallographic examination of the initial surface cracking and the final fracture surface. In the case of fracture surface examination, the cyclic test was stopped in most cases just prior to failure, so as to minimise the structural disturbance by rubbing of the two surfaces. The sample was removed and broken open to reveal the fracture surfaces.

Surface cracking studies have been conducted for the coarse pearlite and spheroidised carbide structures. Both show crack propagation which is mainly transgranular. In a coarse pearlite a specimen surface may show several cracks some of which can extend over several pearlite cells. Typical areas are shown in Figs. 51 - 53. Some cracks may grow through areas which are comparatively free of slip damage whilst neighbouring pearlite cells which are heavily damaged form no part of the fracture path. This is shown in Fig. 52a which represents a sample fatigued for 50% of its life.

Cracks may grow along ferrite-cementite interfaces, across cementite lamellae and ferrite and sometimes cell boundaries in the coarse pearlite. Typical areas from fracture surface

examination show examples of these crack routes (Figs. 54 - 56). Analysis of the surface crack path shows that the route followed at the surface is dependent on orientation of the cementite lamellae to the principal stress direction. Where the lamellae orientation is between 0 - 45° to the principal stress axis, the crack path is mainly through the lamellae. Figs. 54 and 55 show scanning electron micrographs of this path.

Crack growth along the ferrite-cementite interface in coarse pearlite is an important route and this again is influenced by orientation of lamellae to the principal stress axis. Where the orientation range is between 45 and 90°, the surface crack path is favoured along this interface. Fig. 55 shows an example of cracking along this interface. The almost featureless appearance on the interfacial areas indicates a cleavage mechanism. However, there are interruptions to crack growth along the interface since in some areas it passes through cementite lamellae. Cleavage may not necessarily be the only crack propagation mechanism in this structure. Closer examination of the interface in Figs. 55 and 56 shows markings which resemble striations. Surface replication of the fracture area of coarse pearlite fails to show the typical striation markings however which have been observed in many fatigue fractures by other workers.

The two routes mentioned about account for nearly 95% of the total fatigue crack path in the coarse pearlite. Where cell boundaries are followed there is no obvious reason for this route. In this structure, the overall fracture surface shows the largest area corresponding to catastrophic failure in the three structures. This indicates that the critical crack area

for catastrophic failure is smaller in the coarse pearlite than in the other two structures.

In the spheroidised carbide structure, the surface crack path is sensitive to structure in as much that it deviates its route in order to avoid a carbide spheroid. This may sometimes involve an abrupt change of direction. Fig. 57 shows examples of this change. In only one instance has a crack been observed to pass through a carbide particle and on this occasion, it was attributed to the particle being of exceptionally large size (slightly more than 4μ metres). The crack path is almost always in the ferrite and along the ferrite-carbide interface. Fig.58 shows a scanning electron micrograph of a fracture surface in this structure. It shows no fatigue striations. A surface replica of the fracture area is shown in Fig. 59 and this does show markings which are similar to the striations reported. These markings all lie in the same general direction but do not exist over the whole area of the fracture. This may be attributed to either a second propagation mechanism being operative or that the replication method failed to reproduce the markings existing elsewhere. In those markings observed, there are slight disturbances along their length which are probably a result of structural effects.

The spheroidised carbide structure shows the smallest area corresponding to catastrophic failure of the three structures. This shows that the critical crack area for catastrophic failure is greatest in this structure. This corresponds with the observations of surface crack growth where several cracks grew to considerable length across the specimen width before final fracture.

Crack propagation studies in the fine pearlite have been based only on fracture surface examination. As mentioned earlier, surface crack observation was difficult since catastrophic failure occurred almost immediately a surface crack was visible. This structure has therefore received a more concentrated examination of its fracture surface than either the coarse pearlite or spheroidised carbide in order to compensate for the lack of surface crack observation. Fracture surfaces of specimens fatigued between 10^5 and 10^7 cycles show a single initiation site (Figs. 60 and 61). The site is distinguished by its apparent lack of surface features compared with its surroundings. This featureless appearance is attributed to the inclination angle of the site with respect to the overall fracture. By tilting the stage containing the specimen in the chamber of the scanning electron microscope, the site can be shown to contain some features which tend to be striation like markings. In specimens fatigued to failure in under 10^4 cycles the fracture surface shows several crack initiation sites.

Cracks radiate from the initiation site and in general they propagate in a transgranular manner. The crack path is across the cementite lamellae and also along the ferrite-cementite interface. There are also areas of inter-granular cracking (Figs. 62 and 63) which are much more extensive than observed in the coarse pearlite. The areas along the ferrite-cementite interface are not as clear as seen in the coarse pearlite (Fig.55) but then this is due to the smaller grain size of the fine pearlite. Where a crack follows this interface it meets a grain boundary quickly and on crossing it, the

crack path is likely to alter. Transgranular cracking is extensive and crack growth across cementite lamellae is commonly observed (Fig.65). A striation mechanism of crack growth is detected from single stage replicas of the fracture surface (Fig.66). These markings on the replica are extensive and occupy large areas of replicas produced from several fatigue fractures.

This structure shows a relatively large proportion of the total fracture area corresponding to catastrophic failure. Its proportion is not as high as that for the coarse pearlite. Fig. 64 shows a region of transition from fatigue fracture to catastrophic failure. The critical crack length for catastrophic failure in this structure falls between that for the two other structures. This fact together with the speed at which failure occurred so soon after a crack was visible indicates that the crack growth rate in the fine pearlite must be very rapid.

5. DISCUSSION

5.1. THE DEPENDENCE OF CYCLIC PROPERTIES ON STRUCTURE

Two aspects of cyclic behaviour are considered in this discussion, namely, the predicted strain-life behaviour and the cyclic strain hardening exponent, n'.

The predicted strain-life behaviour shows differences in fatigue performance between the three structures under similar cyclic conditions. For example, under high cycle conditions as defined earlier in 2.3, the fine pearlite has the highest fatigue resistance. This prediction has been confirmed from the results of fatigue tests. Further confirmation is given in table 3 which shows that the cyclic yield stress is highest in the fine pearlite. Other investigators[145] have shown that the value of the cyclic yield stress is almost identical with the fatigue limit and hence is an indication of the stress below which fatigue will not occur.

Under low cycle conditions, the spheroidised carbide shows the highest fatigue resistance and the fine pearlite has the lowest resistance. This change of behaviour can be explained in the following way and part of the explanation is based on metallographic observations from the present investigation.

As previously mentioned in the literature review, the fatigue failure process is divided into three stages, these being:-

a) the initiation of a crack

b) the propagation of the crack into the material and

c) the attainment of a critical crack size at which the material then completely fractures in a rapid manner.

The proportion of fatigue life spent in either the initiation or propagation stage is dependent on cycling conditions and whether the specimen is plain or notched. With plain specimens, the

initiation stage predominates at strain amplitudes giving failure at around 10^5 cycles and above. Under low cycle fatigue conditions, the propagation stage is dominant. Several examples exist where the predominance of each stage has been studied in materials under various conditions[20,70,79,84,146]. In various F.C.C. metals, the proportion of life spent in stage II decreased from 70% at 100 cycles to less than 10% at 10^5 cycles to failure.[70] A similar trend has been observed in austenitic steel.[146]

Metallographic observations in the present investigation have shown that the fine pearlite has the greatest resistance to crack initiation of the three structures when tested under high cycle fatigue conditions. Observations of crack propagation do not give the same pattern. Both coarse and fine pearlite structures give fracture surfaces showing very small areas corresponding to fatigue crack growth. That in the spheroidised carbide structure is much larger. Such observations indicate smaller values for the critical crack size corresponding to rapid fracture in both lamellar structures compared with the spheroidal carbide structure. Results show that the coarse pearlite has the smallest value for the critical crack size.

Surface crack observations in the fine pearlite show that conditions for rapid failure are reached after only a small number of cycles once a crack is visible. As mentioned earlier, this has made surface crack examination difficult. In the coarse pearlite, however, once a surface crack is visible and grows during cycling, its path can be readily traced by interrupting the test. The fracture surface observations show a smaller area corresponding to fatigue crack growth in the coarse pearlite than

in the fine pearlite. The extent of fatigue crack growth is therefore greater in the fine than in the coarse pearlite. Since the conditions for rapid failure are reached in a small number of cycles for the fine pearlite, the above observations indicate that the fatigue crack growth must be higher in the fine than in the coarse pearlite. This is an important fact in the explanation of differences of fatigue resistance between the three structures.

A number of investigations[126,129] into crack growth measurement have been conducted which are relevant to this work. In one study,[126] a comparison was made of crack growth rates in a 1% carbon steel having either a spheroidised or lamellar pearlite structure. The growth rate was lower in the spheroidised than in the pearlite structure. The magnitude of the difference was dependent on the stress conditions during testing. The results of this work[126] have been used to consolidate and supplement the findings of the present investigation. The spheroidised carbide structure used in the work showed the most extensive area corresponding to fatigue crack growth of the three structures used. If one then assumes that the crack growth rate in this structure is the lowest of the three, based on the work of other investigators,[126,129] the following explanation can be offered to account for difference of superiority of structures.

In low cycle fatigue conditions giving failure in say 10^3 cycles, the plastic strain component predominates and the propagation stage occupies most of the life. The crack propagation resistance and the extent of fatigue crack growth before rapid failure therefore predominate the factors influencing fatigue

resistance. Both factors are most superior in the spheroidised carbide and hence account for this structure having the best fatigue resistance in low cycle fatigue.

In high cycle fatigue, the crack initiation resistance is the predominant factor influencing total fatigue resistance. The fine pearlite shows the greatest resistance to fatigue crack initiation of the three structures. In spite of its high crack growth rate and limited extent of fatigue crack growth, it is this high crack initiation resistance which accounts for its superior fatigue resistance in high cycle fatigue conditions.

In practice, fatigue cracks normally start at the surface. Two treatments which may be used to improve fatigue resistance of certain steels are carburising and nitriding. Both produce a hard surface skin and in the case of carburising, this is attributed to the formation of a tempered martensite structure. The hard skin possesses a high crack initiation resistance. In a similar way, the results of the investigation suggest that a skin of fine pearlite produced by suitable heat treatment will give high crack initiation resistance which is required for high cycle fatigue conditions. If this can be coupled with a core of spheroidised carbide then a structure having a combination of high crack initiation resistance and propagation resistance is achieved. The optimum combination for high cycle fatigue resistance is that where the case depth of fine pearlite is controlled to a level such that crack propagation begins in the structure of spheroidised carbide. Such a structure combination could be produced in a eutectoid carbon steel by first subjecting the material to a spheroidising anneal and then induction heating

to give the fine pearlite case.

The cyclic strain hardening exponent, (n'), has been identified as probably the most important parameter influencing the fatigue behaviour. Its relationship with microstructure has been studied[11] and high values are associated with those structures which allow extensive cross-slip and dislocation motion. Low values are associated with structures which restrict dislocation motion and have a limited number of slip systems. The difference between high and low values for a number of materials examined by other workers is not great. Typical values have been shown to be within a narrow range, 0.10 to 0.25.[12]

The values obtained for the three structures used in this investigation lie in the range 0.228 to 0.248 and hence are described as high values. These suggest structures having extensive cross slip and dislocation motion. All three structures consist of the cementite phase distributed within the more ductile ferrite matrix. Ferrite is the dominant phase in all three. Calculations based on data from the iron-cementite thermal equilibrium diagram show that all three structures contain 87% by volume of ferrite and 13% of cementite. It is only the size, shape and distribution of cementite which differentiates the three structures. Ferrite has a very high stacking fault energy and hence dislocations can readily cross slip. Furthermore, it contains a large number of available slip systems at room temperature. The high values obtained for the cyclic strain hardening exponent in the three structures are attributed to the dominance of ferrite and its associated characteristics as defined above.

Although all three values for the cyclic strain hardening

exponent fall in a very narrow range, the difference in value between that for the fine pearlite, which is the lowest, and the other two structures, which have similar values, is sufficient to warrant some explanation. On the basis of what has been stated earlier, the lower value for fine pearlite indicates that cross slip and dislocation motion are less extensive than in the other two structures. Results in table 3 show the fine pearlite to have the highest cyclic yield stress. Since this property is a measure of the stress required to move dislocations through the structure, it means that there are more effective barriers to dislocation motion in this fine pearlite than in the other two structures. Slip occurs in the ferrite and the volume of this phase is the same in all the structures. The greater restriction on dislocation movement in the fine pearlite is attributed to the cementite lamellae. These are effective barriers to dislocation movement although as shown in Figs. 41 and 42, their interface with ferrite is a principal source of mobile dislocations. If the cementite phase is the principal barrier, then the smaller the distance between barriers, the more effective is their restriction on dislocation motion into ferrite. The barrier spacing in both lamellar pearlite structures is measured by the mean interlamellar spacing; in the spheroidal carbide structure, by the mean free ferrite path. On this basis alone, the barrier spacing is smallest in the fine pearlite.

Two additional barriers are grain boundaries and cell walls. The latter are known to form in several materials on plastic deformation.[147] Observations in pearlite[147,148] have shown that a cellular dislocation sub-structure develops during plastic

deformation. The cell walls act as dislocation barriers and the cell size influences the extent of barriers. In the case of pearlite[147] the initial cell size is determined by the interlamellar spacing. The smaller the spacing, the smaller is the cell size and hence the greater the barrier effect. In the electron microscope work, there is evidence of a dislocation cell structure formation in the spheroidised carbide (Fig.46b) and within some areas in the lamellar structures. Further examination is necessary to pursue this sub-structure phenomenon.

Confirmation of the effect of cementite morphology on dislocation motion is seen in some of the micrographs which show surface slip damage (Figs. 22 - 27). Both the coarse pearlite and spheroidised carbide structures show concentrated damage in some areas. This indicates extensive dislocation movement in some isolated zones. At equivalent stages of the fatigue life, the fine pearlite shows much less severe damage; instead it is more widely dispersed throughout the structure. This means that the movement and accumulation of dislocations from a given source is restricted. Instead, plastic strain occurs by the movement of dislocations from new sources in other areas and the process is repeated. As will be discussed later, this has an important effect on crack initiation characteristics.

5.2. CYCLIC HARDENING AND SOFTENING PHENOMENA

The three structures show differences of behaviour in their response to cyclic hardening or softening. The fine pearlite shows softening over a wide range of strain. The coarse pearlite and spheroidised carbide structures show softening at small values of strain but a changeover to cyclic hardening occurs above a

strain value which is similar for both structures. Results of tests on several materials performed by other investigators[7,68] show a range of behaviour patterns. For example, the steel shown in Fig.3 cyclically softens at small strains but hardens at high strain levels in a similar manner to the coarse pearlite and spheroidised carbide. On the other hand, softening is found over a range of strain levels in a hardened and tempered 0.4% carbon steel (SAE 4340)[7]. In another carbon steel (SAE 4142), a hardened and tempered structure shows softening or hardening according to the hardness after heat treatment and prior to cyclic testing.[68] A high hardness value in the range of 500 - 670 Brinell leads to cyclic hardening whilst a value below 500 leads to cyclic softening.

According to the literature,[12] materials which show cyclic hardening are desirable for good fatigue performance. Whether or not this performance is under high or low cycle conditions is not stated. In the case of the three structures used in this work, fine pearlite shows the best performance under high cycle conditions yet shows softening. Cyclic softening indicates a decrease in the structural resistance to dislocation motion. Plastic deformation is therefore possible at lowered values of stress and the accumulation of fatigue damage accentuated. If crack initiation is then accentuated as a result of damage accumulation one expects softening to be an undesirable contributory factor to good fatigue performance. However, if damage accumulation can be readily dispersed throughout a structure then the deleterious effects of softening are overcome. The micrographs in this work (Figs. 23b and 25a) show the damage in fine pearlite

to be very uniformly distributed in the structure. Damage build-up to levels sufficient for crack initiation under conditions of high cycle fatigue therefore requires a much larger number of cycles than in other structures. Assuming then that softening is an undesirable factor, the ability for slip damage dispersal in the fine pearlite outweighs the disadvantage of softening. The next step in the argument is how can one develop the structure to maintain this ability for damage dispersal yet replace the softening by a hardening response? This will improve further the high cycle fatigue performance. This is an important area for further research although much work has already been done into the mechanisms of softening in several structures.[65] Some of the reasons proposed for the softening effect in the fine pearlite are proposed later in this section.

A prediction of cyclic hardening or softening is possible from a knowledge of the monotonic strain hardening exponent. A high value of above 0.1 for this exponent indicates a material that will probably cyclically harden whilst if below 0.1, cyclic softening is likely. A similar basis for prediction is that of the ratio given by $\frac{\text{tensile strength}}{\text{yield strength}}$. Where this ratio is above 1.4 materials are expected to harden.[8] If below 1.2, cyclic softening is predicted. In the case of steel SAE 4142 mentioned earlier, the influence of hardness on the cyclic hardening/softening response is attributed to changes in the above ratio, produced by the effects of different tempering treatments used in the work.[68] Calculation of the ratio from tests on the fine, coarse pearlite and spheroidised carbide gives values of just under 1.4, over 2.1 and 1.9 respectively. From these values, the observed behaviour

does not completely correspond with the predicted behaviour, based on the above ratio. For instance, the values for coarse pearlite and spheroidised carbide predict hardening whereas some softening is observed at low strains. In the case of fine pearlite, cyclic softening is observed but not predicted from the value. It is clear that the above methods of predicting hardening or softening responses are not valid for the three structures used in this investigation.

A number of mechanisms have been proposed in previous work to account for cyclic hardening and softening behaviour.[48,68,149] In the investigations where hardening and softening were observed in heat treated steels,[7,68] no mechanisms were proposed. It is however well established that cyclic hardening indicates an increase of resistance to the to-and-fro motion of dislocations in the structure and this resistance arises for a number of reasons. In single phase materials, the principal reason is the accumulation of dislocations and their interaction with each other and point defects. In multi-phase alloys an additional source of resistance is from precipitate particles that obstruct dislocation motion. Cyclic softening indicates a decrease of resistance to dislocation motion. This decrease arises from the release of dislocations from networks and dislocation annihilation. In multi-phase alloys a further cause is structure degradation where strengthening precipitates can be sheared by dislocations and reach sizes where they re-dissolve in the matrix.[50] A further source of softening is the relaxation of residual stresses set up during heat treatment or cold work.[150]

Softening in the three structures used in this investigation is not attributed to the relief of micro-residual stresses that

are formed during heat treatment. All samples were given a low temperature heat treatment after metallographic preparation that would have been sufficient to relieve any internal stresses produced by the austenite to pearlite transformation. Reversion of cementite is not thought likely in the early stages of the cyclic test. Electron transmission microscopy was used for the examination of non-fatigued specimens and those fatigued for 25 up to 75% of the life. If reversion had occurred early in the life to account for the softening phenomenon, it would have been more accentuated in samples fatigued for as little as 25% of the life. This would have shown up as areas containing surface slip bands and denuded of cementite. Comparison of structures in the fatigued and non-fatigued condition did not show such features that could be clearly attributed to a reversion effect. Some caution is required relating to statements on reversion in the investigation. Of the metallographic techniques used in this work those based on electron transmission microscopy are the only ones that can reveal any reversion effect if it does exist. Such techniques have not been extensively used and this is an area where further work is necessary. Low carbon steels, for example, have been shown to exhibit this reversion effect on cyclic testing.[46]

From the evidence of this investigation, the major cause of cyclic softening is the release of mobile dislocations from the interface between ferrite and cementite. Figs. 41 and 42 show this interface to be a principal source of dislocations. These are unpinned and move into the ferrite when the shear stress at the interface reaches a sufficiently high level. The orientation of the interface to the principal stress direction determines the

magnitude of the acting shear stress. The importance of orientation is discussed later. Once unpinned, these dislocations can readily move within the ferrite and hence the stress required to maintain their motion is decreased giving softening. The saturation period that quickly follows the softening, indicates that the stress required to maintain the dislocation motion remains constant. It signifies a balance between the continued unpinning of dislocations from the interface and the build up of dislocations in the ferrite that oppose the motion of newly released dislocations. Alternatively, it may be the result of the release of dislocations from interfaces having orientations such that the required level of shear stress for unpinning of dislocations requires an increase of the applied principal stress.

Whereas the fine pearlite shows cyclic softening over a range of strain amplitudes, both the coarse pearlite and spheroidised carbide show a change-over to cyclic hardening when tested at strain amplitudes above a certain level. This behaviour difference is explained in terms of the availability of dislocations. Since the contributions to strain are the number of dislocations moving under stress and their slip distance, then if either the number available or distance moved is increased the overall effect is an increase of strain. If the principal source of dislocations is the ferrite-cementite interface, then the number of available dislocations is proportional to this interface area. Calculations based on the metallographic data and using the method shown in Appendix 1 give the following ratios for area in the three structures:

coarse pearlite	- 1.0
fine pearlite	- 4.5
spheroidised carbide	- 0.2

The fine pearlite shows a much greater interface area than the other two structures. There is therefore a much greater source of available dislocations in this than the other structures. This means that at those amplitudes where cyclic hardening occurs in coarse pearlite and spheroidised carbide whilst softening remains in fine pearlite, the strain can be accommodated in the fine pearlite by the release of further dislocations into the ferrite. In both coarse pearlite and spheroidised carbide, the lower number of available dislocations have to move over greater distances into the ferrite and here they must overcome the obstacles such as dislocation pile ups and point defects. An increase in the applied stress is therefore required to maintain their movement; hence the cyclic hardening effect.

Since cyclic hardening is a desirable feature for improved fatigue performance as previously suggested[12] the ideal situation is that of the fine pearlite structure showing hardening and yet maintaining its characteristics that give a uniform dispersal of slip. On the basis of this mechanism, such hardening could be achieved by ensuring a sufficiently effective obstruction to dislocation motion in the ferrite once the dislocations are unpinned. This implies an adjustment to ferrite composition such that its friction stress is increased without detrimental effects on the cementite lamellae morphology. This is an area for further investigation. In the wire drawing industry for example, small quantities of molybdenum (up to 0.2%) in eutectoid carbon steel have enabled very fine pearlites[151] to be produced by patenting treatments and these have been subsequently cold drawn to give very high strength wire. Here the molybdenum has not only

altered the transformation characteristics of austenite during heat treatment but also is an effective ferrite strengthener. This is cited as an example of the sort of investigation that could be carried out.

It has been reported earlier that in the case of steel B, samples of fine pearlite that were cycled for up to 10, 20 or 30% of the life, showed further softening and then stability on re-testing after delay times of up to 24 hours. This behaviour requires further study but suggests an ageing-type phenomenon similar to that of the yield point re-appearance. Alternatively, the softening may result from the relief of micro-residual stresses that arise during cycling.

5.3. THE INFLUENCE OF ORIENTATION ON SURFACE DAMAGE

In both lamellar pearlites, surface damage is more readily apparent in those cells containing cementite lamellae that are oriented between 30 and 90° to the principal stress direction. It is however realised that in those cells where the lamellae orientation lies outside this favourable range, slip may occur but not manifest itself as slip bands at the surface. This could happen if the Burgers vector for atom displacement has a direction parallel to the surface of examination. In the spheroidised carbide there is no clear relationship between the location of damage and orientation of spheroids based on results of low resolution microscopy. The dependence of surface damage on lamellae orientation (shown in Figs. 34 and 35) is attributed to the stresses acting on the ferrite-cementite interface. Since the shear stress is at a maximum in a direction of 45° to the principal stress axis, then such interfaces will be subject to

this maximum shear stress where the cementite lamellae are oriented at 45°. Such interfaces are regions where the atom arrangement changes from B.C.C. in the ferrite to orthorhombic in the cementite. To accommodate this atomic pattern change, the transition zone contains a high density of atomic imperfections such as vacancies and dislocations. On cycling, dislocations are unpinned where the operative shear stress is sufficiently high. Movement of dislocations into the cementite is difficult because of its restricted plasticity. Movement into ferrite is much easier since it has a large number of available slip planes at room temperature along which the dislocations can move. Slipping therefore occurs in the ferrite along those planes where the resolved shear stress reaches a critical value. The movement of many dislocations along atomic planes manifests itself as slip bands at the ferrite surface.

In the spheroidal carbide structure, the extent of the interface area between ferrite and cementite is considerably less than that in the other structures. Consequently the number of available dislocations from this interface is small. To account for the plastic strain such dislocations would have to move over large distances into the ferrite. As shown in the micrographs, figs. 26 and 27, slip bands appear in the ferrite and some are closely associated with ferrite grain boundaries. From the low resolution microscopy, there appears to be no correlation of damage with orientation of these boundaries or the interfaces. Evidence from high resolution microscopy as shown in Fig. 46 indicates that there may be some dependence of the damage areas on orientation. Dislocations are seen to emanate more from some

areas of the interface than others and areas of common orientation appear relatively free of dislocations. In this latter work, specimens are in the form of thin foils produced from discs taken across the specimen diameter. The principal stress direction is therefore coincident with a normal to the photograph surface. Further work is necessary to establish whether any orientation dependence of damage areas exists.

5.4. STAGE I CRACK GROWTH

As defined earlier in section 2.5, this stage includes the period of crack initiation and also that where the crack grows along a plane of high shear stress.

5.4.1. Effect of Cyclic Stress on Surface Topography

In general, a fatigue crack initiates at a free surface and in regions of plastic strain concentration. For most of the materials examined, the most common site is a slip band and the formation of slip bands is associated with the development of a surface topography containing grooves and ridges. These are more often called intrusions and extrusions respectively.[32,36,37] Their formation is detrimental to fatigue performance since they create areas of stress concentration and cracks readily develop within them. Clearly this effect of surface topography on overall performance is most marked under high cycle conditions. Here the stage I crack growth, as defined in 2.5 occupies such a large part of the total fatigue life.[3]

In spite of the surface slip bands observed, taper sections show no pronounced notch-peak topography in any of the three structures after testing under high cycle fatigue conditions. There is surface disturbance shown from comparison of fatigued

and non-fatigued specimens but it is slight and more apparent in the coarse pearlite than in the other two structures. In the coarse pearlite the maximum height of extrusions is 0.5μmetres (μm) and some crevices exist of up to 2μm is depth. This disturbance is nowhere near as severe as that which has been observed in other materials. For example, extrusions of up to 10μm in length have been reported for some aluminium alloys.[18] In low cycle fatigue, there is a greater amount of surface disturbance. Rumpling is observed and extrusions of up to 5μm in length are measured in the three structures. Location of extrusions and intrusions with respect to microstructural features has been easier in the spheroidised carbide structure where the rounded form of shallow extrusions has been within the ferrite. Surface displacement between the ferrite and carbide spheroids has not been observed. In the coarse pearlite, extrusions appear in the ferrite but usually close to its interface with the cementite. Intrusions are invariably associated with the region where cementite lamellae meet the interface and this is significant with regard to crack initiation sites and is discussed later.

Cementite morphology clearly influences the surface topography produced on cycling. The superiority of the fine pearlite structure with respect to high cycle fatigue performance is attributed in part to the minimum amount of surface disturbance which impedes the formation of sites of high stress concentration. A more uniform dispersal of slip damage in the structure is the major cause for this minimum disturbance. Most of the mechanisms proposed for extrusion/intrusion phenomena are based on

studies of single phase materials.[3,4,5,6,152] The ease of cross slip of dislocations has been identified as an important factor yet in some materials where cross slip is easy, extrusions are not formed. In a recent study[109] on multi-phase specimens containing both soft and hard phases, a model for extrusion/intrusion formation has been proposed. It states that extrusions and intrusions are associated with thin soft phases that are surrounded by harder phases. The soft phases show preferential deformation and for extrusions and intrusions to form, a sub-grain structure must develop. Such a structure is favoured by easy cross slip. The three structures used in this investigation are based on the soft phase ferrite, which predominates, and the hard cementite. Ferrite has a high stacking fault energy and cross-slip is easy. Hence cycling must promote sub-grain formation.

Assuming that the sub-grain structure formation is the significant factor influencing surface topography after cycling, the following is offered as an explanation for the differences of topography between the three structures. Studies of pearlite[147,148] have shown that a sub-grain structure exists in the ferrite and its size, in terms of cell dimensions, is influenced by interlamellar spacing. The larger the spacing the greater the cell size. In the spheroidised carbide the dependence of cell size is less clear. In both lamellar structures therefore, the starting cell size in ferrite is not the same in the coarse and fine pearlite. It is smaller in the fine pearlite and hence the yield stress of ferrite here is greater, according to prediction based on the traditional Hall-Petch

relationship. Since plastic strain is more uniformly distributed in the fine than coarse pearlite, the overall effect on the sub-grain structure should be different. What this difference means is not yet clear; it is assumed that the cell size in the structure will show considerable differences between coarse and fine pearlite. In the present work using transmission electron microscopy, a cell structure was observed in the spheroidised carbide (Fig.46) and within some areas in the lamellar structures. This is a field for further study using high resolution metallographic techniques.

5.4.2. Crack Initiation Sites

It is difficult to establish the exact location of an initiating crack. In this investigation, initiating cracks have been identified early in the life for coarse pearlite and spheroidised carbide structures; the structural features that dominate the crack length have been examined. Clearly the crack size should be kept small and its transition to shear mode growth obstructed in order to achieve improved fatigue performance. Some cracks initiate very early in the life but show negligible growth on subsequent cycling and appear to have little role in the fatigue failure process. It is important that the causes for such cracks to become dormant are known. A knowledge of those structural features within which the initiating crack grows is an important step towards identifying these causes.

In Fig. 31, two examples of initiation sites are shown. In that indicated at B, a crack has initiated at a ferrite-cementite interface. At A, the site is more difficult

to define. Much of the surface crack length is within the ferrite and associated with areas showing heavy slip damage. It is therefore more likely that the crack has initiated within a slip band. Slip bands and the ferrite-cementite interface are the two principal sites for crack initiation in the coarse pearlite. Additional sites are pearlite cell boundaries and, as shown in Fig. 37b, a surface protruding inclusion, although these are rare. Initiation at pearlite cell boundaries is thought to be attributed to boundary embrittlement by impurity elements such as copper. The steel contained trace levels of copper and this element is known to migrate to austenite grain boundaries during prolonged heat treatment. In the fine pearlite, the principal cracking site is within slip bands whilst in spheroidised carbide, cracks initiate mainly at slip bands and ferrite cell boundaries.

Crack initiation at the ferrite-cementite interface is observed only in the coarse pearlite. Here initiation is attributed to:-

a) debonding at the interface during cyclic stress

b) formation of surface notches coincident with lamellae emerging at the surface (Figs. 37a and b)

Debonding occurs as a result of the build-up of vacancies to a sufficiently high level at the interface. These vacancies form and accumulate in the interfaces where dislocations are released for movement into ferrite by the acting shear stresses during cyclic testing. The accumulation of vacancies is most severe at those interfaces where the shear stresses are high enough to release large numbers of dislocations. Coherency

between ferrite and cementite is destroyed with consequent weakening of the interface. Its ability to support stress is thus impaired and where the operative stress is sufficiently high, a crack may be formed at the interface. Such a level of stress is most likely to be reached in the roots of surface notches formed. Where such notches coincide with the interface, as shown in Figs. 37a and b, the possibility of crack initiation is very high. Observations of cracks show that such sites exist at interfaces oriented at around 45° to the principal stress axis (Fig.31).

Other studies of two phase alloys [78,107] have shown a similar type of interface crack initiation to that above. In a titanium alloy,[78] crack initiated at the interface between α and β grains during high cycle fatigue. Because slip band damage was not detected, the cracking was attributed to interfacial debonding. In a zirconium alloy,[107] the interface between zirconium hydride and the matrix grains was susceptible to cyclic damage because of its low coherency. Void initiation was prevalent at the interface and this would account for its tendency for crack initiation. Surface crack initiation within slip bands is common to all three structures. Slip bands are regions of dislocation build up and previous studies [153] have shown that cracks initiate in regions of high strain concentration. In both the coarse pearlite and spheroidised carbide structures, a shallow surface notch peak effect leads to distribution of stress which produces areas of stress concentration. These accentuate the crack initiation. In the fine pearlite the notch peak effect is so shallow as to be

undetectable by the metallographic techniques used here.

The highest resistance to crack initiation under high cycle fatigue conditions is found in the fine pearlite. This is attributed to a capacity for more homogeneous distribution of plastic strain in this structure than the others. The build-up of plastic strain to levels sufficient for crack initiation therefore requires a larger number of strain cycles than in the other structures. The more homogeneous distribution of strain arises from the extensive interface area between ferrite and cementite. It is from this interface, as previously mentioned, that dislocations move into ferrite so as to accommodate the plastic strain. The fine pearlite has the smallest value for mean free ferrite path in the three structures and at first, it was thought that this might have had a detrimental effect on strain build up due to its limiting the distance for movement of dislocations into ferrite. This does not appear to have been the case.

In the sub-surface zones, foils have shown that dislocations emanate from the ferrite-cementite interface and build up in the ferrite. A cellular arrangement of dislocations appears in both lamellar and spheroidal structures as shown in Figs. 42b and 46b. Cracks have not been detected in any of the foils produced. However crack-like features are seen in Figs. 43b, 44b and 45b and these are closely associated with the ferrite-cementite interface. These features have been closely examined and are attributed to areas of high dislocation density. They are not, for example, bend or thickness contours.

Transmission electron microscopy was used only in the final stages of the work and it is clear from the results obtained so far that a more thorough use of this technique in fatigue studies is necessary.

5.4.3. Shear Mode Growth

Evidence of shear mode growth following crack initiation has been difficult to produce because of the limited amount of fractographic examination in this work. Nevertheless, both lamellar structures show areas characteristic of this type of growth. No such areas have been observed in the spheroidised carbide structure. Fig. 60 shows an example in the fine pearlite. The area corresponding to shear mode growth is small and extends from the specimen surface. Fracture examination using the scanning electron microscope reveals few features of significance in the area. Under high cycle fatigue conditions both structures show only one such area whereas in low cycle fatigue there are several, all of which extend from the surface. Their orientation is estimated to be around 45^{o} to the principal stress axis. Although further examination is necessary, using say single stage replication and electron microscopy, the evidence for shear mode crack growth following initiation is conclusive for both lamellar structures.

As mentioned earlier, three crack initiation sites are identified in the lamellar structures. The relatively flat surface of the shear mode crack area is likened to that appearance characterizing cleavage at the interface between ferrite and cementite. An example of such an appearance is shown in the stage II fracture in Fig. 55. These features would indicate

that of the three initiation sites, shear mode crack growth begins from a ferrite-cementite interface and continues along this interface. Transition to stage II crack growth occurs after only a small crack depth is reached. Subsequent growth is then along planes normal to the principal stress and catastrophic failure occurs.

5.5. STAGE II CRACK GROWTH

Structural differences between the three materials studied influence the stage II crack growth under high cycle fatigue conditions. The effects of structure are shown up as differences in characteristics based on:-

1. the crack propagation rate
2. the route followed by a propagating fatigue crack
3. the extent of fatigue crack growth before catastrophic failure

5.5.1. Propagation Rate

Relative crack propagation rates at the surface have been estimated in the work and based on metallographic observation at various stages of the life. They show a similar trend to results of other workers[126,129] using more sophisticated measuring techniques. For example, the fatigue crack propagation rate for spheroidised carbide is lower than for coarse pearlite. There is however no agreement in results showing pearlite structure effects on propogation rates. An increase of pearlite lamellar spacing was shown in previous work[126,129] to increase propagation rates whereas in the present investigation, a more rapid rate is found in the fine pearlite. A principal cause of this disagreement is likely to be difference of chemical composition of the steels used. The carbon content of the steel

used in previous work[126,129] was 1% and the other alloying elements indicated that it was likely to give pro-eutectoid cementite on transformation from the austenitic condition. This would be accentuated during slow cooling to produce coarse pearlite. In the present investigation, the steel used contained around 0.75% of carbon and metallographic examination showed only traces of cementite. The presence of this brittle cementite at pearlite grain boundaries would be detrimental to crack propogation in that the propagation rate would no doubt be increased and intergranular propogation would be evident. In the results of this work[126,129] no mention is made of intergranular appearance on the fracture surface. Nevertheless, the highest propagation rate for coarse pearlite in the work[126,129] is attributed mainly to the larger amount of pro-eutectoid cementite in this structure than in fine pearlite. The disagreement in results for pearlite structure effects is therefore attributed to the significant reduction in amount to trace levels of pro-eutectoid cementite found in steels used in the present investigation.

Differences in fatigue crack propagation rates between the three structures are attributed to a number of reasons, namely:-

a) behaviour of material in the crack tip
b) effects of cyclic properties, e.g. cyclic strain hardening exponent
c) route followed by the propagating crack

As mentioned earlier in 2.6, a small plastically deformed zone is created at the tip of a growing crack. Its size is dependent on the stress intensity factor[114] and material properties[115] at the crack tip. It has a significant influence

on fatigue propagation rate. Plastic strain is concentrated within this zone and its level increases throughout the test even though the overall strain amplitude may be kept constant as was the case in most cyclic tests performed in this investigation. Although the levels of plastic strain concentration reached are not known, the cyclic stress-strain curves of Figs. 16 - 18 do show a transition from cyclic softening to hardening as the strain level increases for both coarse pearlite and spheroidised carbide structures. Softening is observed in fine pearlite over a range of strain levels. Hence, if strain levels in the plastic zone are sufficiently high, localised cyclic hardening occurs in both coarse pearlite and spheroidised carbide. The effect of this is to promote the re-distribution of plastic strain in regions where it can be more readily accommodated. This could account in part for observed crack growth along certain routes and then obstruction: further growth continuing along other routes from the main crack. Branch cracking is a manifestation of such characteristics. Clearly this is a field for further study but a significant point is that branch cracks were apparent in coarse pearlite and spheroidised carbide but not fine pearlite structures. In the latter structure, cyclic softening occurs at all strain levels shown in the cyclic stress-strain curve and hence localised softening occurs in the plastic zone. Its effect is to concentrate plastic strain at the tip of the growing crack and hence intensify dislocation motion therein. Deviation from the main crack is not apparent from metallographic observation and its high rate of propagation has been mentioned earlier. Both observations correlate well

with expected behaviour arising from this localised softening.

In the work of Tomkins,[139,140] an approach has been made towards prediction of crack growth rate that is based on cyclic material behaviour. The model is described in the form of two equations, both of which are given (9 and 10) in section 2.6.3. That equation referring to high cycle fatigue conditions is reproduced below:-

$$\frac{da}{dN} = a \left[\frac{\pi}{32} \frac{\epsilon_f}{\sigma_f^{1/n'} (\sigma_y')^2} \right] \Delta\sigma^{(2n'+1/n')} \quad \text{---10}$$

This indicates that a decrease in the crack growth rate, da/dN is achieved by a lowering of the cyclic strain hardening exponent, n', all other terms being equal. The results in table 3 show fine pearlite to have the smallest value for this exponent, n' : it does however have the highest growth rate. The results from this investigation do not therefore correspond with the predicted behaviour from equation 10 and the disagreement may be attributed to the following reasons:-

1. the validity of crack growth measurement in this investigation. It was difficult to resolve detail in the fine pearlite structure and crack growth could have remained undetected for a long time. The rapid crack growth observed at the surface may therefore have represented the final stages only of the crack growth period.
2. the validity of equation 10 for the structures used in the work. As mentioned earlier, the model[139,140] was derived from observations of cracking in a ductile metal. Cementite is recognised as a brittle constituent and hence those stages of crack growth throughout cementite may not comply with conditions under which the model applies.

5.5.2. Microstructural Features of Propagating Crack Paths

Two of the major characteristics of stage II cracking have been known for a long time to be transgranular propagation and striation formation on the fatigue fracture surface. Since striations were first reported,[119] much work has been done in the study of their features. They have been observed in many metallic and non-metallic materials.

In the three structures used in this investigation, fatigue cracks propagate almost always in a transgranular manner. Where intergranular cracking has been observed, it is associated with both lamellar structures but never occupies significant portions of the fatigue fracture area. In both the coarse and fine pearlites, crack growth is along ferrite-cementite interfaces and across cementite lamellae whilst maintaining a path that is approximately normal to the principal stress axis. Cementite fracture is preferred where the lamellae are orientated nearly normal to the crack path. If lying at angles greater than about 45° to the crack path, the resolved stresses at the crack tip may be insufficient to crack the lamellae but sufficient to propagate the crack along the ferrite-cementite interface where voids may already exist and provide an easy potential route.

Cracking of cementite lamellae may be explained in terms of a fibre loading mechanism.[154] Such a mechanism is justified since pearlite simulates many fibre reinforced materials in so far as it contains hard particles within a ductile matrix. It predicts that the highest stress is developed at the centre of lamellae and fracture occurs here. Furthermore, the tendency

for cementite lamellae to crack depends on thickness, thin lamellae being easier to crack than thick ones. Results obtained show that fracture of lamellae does not always occur along their mid-length. However, the results for fine pearlite show extensive crack propagation across cementite lamellae and this could be attributed to the lamellae being easier to crack. Other results that can be readily explained in terms of the mechanism are found for the spheroidised carbide structure. Here the crack path is rarely through the spheroids and this is most likely attributed to spherical particles not being subject to significant fibre loading. When fracture does occur there is less energy available to propagate the crack into the ferrite matrix than that released from a fractured lamella. The concept of energy release from lamellae fracture can be applied to explain the rapid crack growth across lamellae in fine pearlite. With a small interlamellar spacing of 700 Angstrom units, the energy released from fracture of one lamella may be sufficient to propagate the crack through the ferrite and on to the next lamellae where the process is then repeated. The effect is shown most clearly in Fig.44b where several individual cracks are shown to propagate across cementite lamellae and continue their growth in ferrite. There are however other cracks which on meeting a lamella grow some distance along the interface before cutting across the lamella. This behaviour could be attributed to the presence of growth faults in the cementite lamellae.[155] It is clear from the limited amount of crack propagation studies in this investigation that no single mechanism can explain all the observations so far.

Crack growth along the ferrite-cementite interface is most apparent in the coarse pearlite as shown in Fig.55. At first sight, growth along this interface appears to be of a cleavage type. Striation formation is not apparent on the fracture surfaces of coarse pearlite but is present on both fine pearlite and spheroidised carbide structures. This difference in appearance is difficult to reconcile. On the basis of microstructure it is difficult to explain the higher propagation rate found in fine pearlite. The only feature is the greater proportion of intergranular fracture in this structure but even so this represents a very small proportion of the fatigue area. In general, the overall picture emerging from results of crack propagation studies in this investigation is not clear. This is attributed to only a small amount of the total time being spent on crack propagation studies. The small amount of time has been justified since the overall investigation was concerned with high cycle fatigue behaviour and un-notched specimens. As mentioned earlier, the crack propagation stage represents only a small amount of the total life under such conditions.

5.5.3. Conditions for Catastrophic Failure

A fatigue crack grows within a specimen until the crack length and stress intensity at the crack tip reach levels at which catastrophic failure occurs. This transition to rapid fracture falls within the field of fracture mechanics and fracture toughness concepts and has not received much attention in this investigation. Nevertheless, the concept of fatigue fracture toughness has been proposed[156] and shown to be related to the cyclic strain hardening exponent. A decrease in value

for this exponent is claimed[156] to increase the fatigue fracture toughness in that the area of the fatigue fracture zone is increased. Results from this investigation contradict this claim; the lowest value for the exponent is found in the fine pearlite which is shown to have the lowest fatigue fracture toughness.

6. CONCLUSIONS

1. Fatigue damage appears early in the life in both lamellar and spheroidal carbide structures. Surface damage exists as slip bands in the ferrite. In both the coarse and fine lamellar structures, surface damage is more intensive in those regions having cementite lamellae oriented at between 30 and 90° to the principal stress axis. At a given stage of the fatigue life, the damage in these preferred regions is more localised in the coarse than in the fine pearlite.
2. Surface damage in all three structures, tested to failure under high cycle fatigue conditions, is associated with a very shallow surface topography. The maximum height of extrusions is about 0.5μmetres in the coarse pearlite and spheroidised carbide structures. There is almost no notch peak effect distinguishable by optical metallography in the fine pearlite.
3. Cyclic stressing leads to a dislocation build-up in the ferrite. The principal source of dislocations is the ferrite-cementite interface.
4. Cracks appear at slip bands and interfaces between ferrite and cementite in all the three structures. Cracks also appear at pearlite cell boundaries in lamellar structures and at ferrite cell boundaries in spheroidal structures. Microscopic cracks can be detected at up to 25% of the life in coarse pearlite and spheroidised carbide structures whereas in fine pearlite they are detected at between 50 and 75% of the life.
5. The mechanisms of crack propagation in the three structures are not the same. There are large areas of micro-cleavage at ferrite-cementite interfaces and crack cutting across cementite

lamellae in the coarse pearlite. Fine pearlite shows extensive cutting across lamellae by a growing crack and some intergranular cracking. A striation mechanism is detected. Crack growth is concentrated within ferrite or along the ferrite-cementite interface in the spheroidised carbide structure.

6. In all three structures, fatigue crack propagation follows a stage I - II sequence and terminates when the conditions for catastrophic failure are attained. Results suggest greater surface crack propagation rates in lamellar than spheroidal structures. Furthermore, the proportion of the full fracture zone occupied by the fatigue crack area is greatest in the spheroidal structure and least in the coarse pearlite.

7. The predicted strain life curves show that the highest fatigue resistance in the low cycle region is found in the spheroidised carbide structure. For the high cycle region beyond 10^5 cycles, the fine pearlite structure has the highest fatigue resistance. These predictions are confirmed from the strain-life tests.

8. The three structures differ in their change of deformation resistance over a range of strain of up to 0.015. The fine pearlite cyclically softens over the whole range. The coarse pearlite and spheroidised carbide structures cyclically soften at strains of up to about 0,004. On cycling at strains above this level, both structures harden and then reach a saturation level.

7. RECOMMENDATIONS FOR FURTHER WORK

Throughout the discussion section of this thesis, several areas have been identified where further investigation is recommended. In general, all the areas are associated with an identification of the important microstructural features that influence the fatigue performance of pearlite structures. It is recommended that the transmission electron microscope be more extensively used in several of these areas. The specific areas for investigation are as follows:-

a) to identify the microstructural features that influence the mechanism of cyclic softening and hardening,

b) to examine the effects of cyclic testing on the reversion of cementite in ferrite,

c) to examine the ageing-type phenomenon observed in the work and identify those factors which influence it,

d) to evaluate the fatigue performance of structures having a spheroidised carbide core and a case of fine pearlite,

e) to examine the mechanisms of fatigue crack propagation.

REFERENCES

1. H.J. Gough and D. Hansen. Proceedings Royal Society (London) Series A. 1923, 104, 538.
2. J.A. Ewing and J.W.C. Humfrey. Phil. Trans. Royal Society (London) Series A. 1903, 200, 241.
3. W.J. Plumbridge and D.A. Ryder. Met. Rev. 1969, 14, 119.
4. N. Thompson and N.J. Wadsworth. Advances in Physics 1959, 7, 72.
5. J.C. Grosskreutz. Phys. Stat. Sol. (b) 1971, 47, 11.
6. J.C. Grosskreutz. Phys. Stat. Sol. (b) 1971, 47, 359.
7. R.W. Landgraf, JoDean Morrow and T. Endo. J. Materials. 1969, 4(1), 176.
8. R.W. Smith, M.H. Hirschberg and S.S. Manson. The Fatigue Behaviour of Materials under Strain Cycling in Low and Intermediate Life Range. NASA Report. TN-D1574. April 1963,
9. R.W. Landgraf. ASTM. STP.467, 1970, 3 .
10. JoDean Morrow. ASTM. STP.378, 1965, 45.
11. C.E. Feltner and C. Laird. Acta Met. 1967, 15, 1621.
12. J.C. Grosskreutz. Met. Trans. May 1972, 3, 1255.
13. C.E. Feltner and P. Beardmore. ASTM. STP.467, 1970, 77.
14. O.H. Basquin. Proc. ASTM. 1910, 10, 625.
15. S.S. Manson. NACA Tech. Notes. 1954, 2933.
16. L.F. Coffin. Trans. ASME. 1954, 76, 931.
17. S.S. Manson and M.H. Hirschberg. Fatigue - An Interdisciplinary Approach. Syracuse University Press. New York. 1964,133.
18. P.J.E. Forsyth. A Two-Stage Process of Fatigue Crack Growth. Proceedings of the Crack Propogation Symposium. Cranfield, 1961.
19. L.F. Coffin. Fatigue at High Temperature - Prediction and Interpretation. Inst. of Mech. Engineers. 1974, 188. September.
20. P. Watson. Ph.D. Thesis. Dept. of Civil Engineering. Univ. of Waterloo, Canada. January 1971.
21. W.P. Mason. ASTM. STP.237, 1958, 36.
22. P.J.E. Forsyth. J.I.M. 1951-2, 80, 181.
23. P.G. Partridge. Phil. Mag. 1965, 12, 1043.
24. C.J. Beevers and M.D. Halliday. Met. Sci. J. 1969, 3, 74.
25. D.I. Golland and P.L. James. Met. Sci. J. 1970, 4, 183.
26. G.F. Modlen and G.C. Smith. J.I.S.I. 1960, 194, 459.
27. A.J. McEvily and T.L. Johnston. Proc. 1st Int. Conf. Fracture, Sendai, Japan, 1965.
28. F.G. Ostermann. Met. Trans. 1971, 2, 2897.
29. F.G. Ostermann and W.H. Reimann. ASTM. STP.467, 1970, 169.
30. P.R. Swann. Ph.D. Thesis. Univ. of Cambridge, 1960.
31. H.J. Gough. Proc. ASTM. 1933, 33, 3.
32. P.J.E. Forsyth. Nature. 1953, 171, 172.
33. N. Thompson, N.J. Wadsworth and N. Louat. Phil. Mag. 1956, 1, 113.
34. W.A. Wood. Phil. Mag. 1958, 3, 692.
35. R.C. Boettner and A.J. McEvily. Acta Met. 1965, 13, 937.
36. P.J.E. Forsyth. Proc. Royal Society. 1957, A242, 198.
37. A.H. Cottrell and D. Hull. Proc. Royal Society 1957, A242, 211.
38. S.J. Basinski, Z.S. Basinski and A. Howie. Phil. Mag. 1969, 19, 899.
39. E.E. Laufer and W.N. Roberts. Phil. Mag. 1966, 14, 65.
40. P. Lukas, M. Klesnil and J. Krejci. Phys. Stat. Sol. 1968, 27, 545.

41. D.F. Watt and R.K. Ham. Nature. 1966, 211, 734.
42. C.E. Feltner. Phil. Mag. 1965, 12, 1229.
43. C.H. Wells. Acta. Met. 1969, 17, 443.
44. N.M. Grinberg. Fiziko-Khim. Mekhan. Mat. 1972, 8(3), 18.
45. D. Munz, V. Bachmann and H. Rachmantio. Mat.Sci.Eng. 1971, 8(4), 244.
46. J.T. McGrath and W.J. Bratina. Acta. Met. 1967, 15, 329.
47. C.H. Wells and C.P. Sullivan. Trans. ASM Quarterly. 1964, 57, 841.
48. C. Calabrese and C. Laird. Mat.Sci.Eng. 1974, 13(2), 141.
49. G.R. Leverant. Trans. AIME. 1967, 239, 1992.
50. A.J. McEvily, J.B. Clark, E.C. Utley and W.H. Herrnstein III. Trans. AIME. 1963, 227, 1093.
51. J.E. Pratt. Acta. Met. 1967, 15, 319.
52. M. Klesnil and P. Lukas. J.I.S.I. 1965, 203, 1043.
53. Y. Bergström, O. Vingsbo and G. Lagenberg. Mat.Sci.Eng. 1969/70, 5, 153.
54. J. Krejci and P. Lukas. Phys. Stat. Sol. (a) 1971, 5, 315.
55. R.P. Wei and A.J. Baker. Phil. Mag. 1965, 12, 1005.
56. J.T. McGrath and W.J. Bratina. Phil. Mag. 1965, 12, 1293.
57. M. Klesnil and P. Lukas. Fracture 1969. Proceedings of Brighton Conference 1969. Ed. P.L. Pratt. Pub. Chapman and Hall. London. 1969, 725.
58. J.C. Grosskreutz and G.G. Shaw. Acta. Met. 1972, 20, 523.
59. A.H. Purcell and J. Weertman. Met. Trans. 1973, 4, 349.
60. K. Hatanaka and H. Kawabe. J.Soc.Mat.Sci. Japan. Dec.1971, 20, 219, 1278.
61. J.F. Tavernelli and L.F. Coffin. Trans. ASM. 1959, 51, 438.
62. D.H. Avery and W.A. Backofen. Acta.Met 1963, 11, 653.
63. M. Klesnil and P. Lukas. J.I.S.I. 1967, 205, 746.
64. J.T. McGrath and W.J. Bratina. Phil. Mag. 1970, 21, 1087.
65. A. Abel and R.K. Ham. Acta. Met. 1966, 14, 1495.
66. M. Klesnil, M. Holzmann, P. Lukas and P. Rys. J.I.S.I. 1965, 203, 47.
67. J. Polak, M. Klesnil and P. Lukas. Mat.Sci.Eng. 1974, 15(2,3), 231.
68. R.W. Landgraf. Dept. of Theoretical and Applied Mechanics, Univ. of Illinois. Rep. No.320, Nov. 1968.
69. D.S. Kemsley. J.I.M. 1956-57, 85, 420.
70. C. Laird and G.C. Smith. Phil. Mag. 1963, 8, 1945.
71. M.J. May and R.W. K. Honeycombe. J.I.M. 1963-64, 92, 41.
72. S. Lynch and D.A. Ryder. Scripta Met. 1972, 6(2), 181.
73. D. Munz. Eng. Frac. Mech. 1973, 5(2), 353.
74. G. Lutjering, H. Doker and D. Munz. Proc. Conference on Microstructure and Design of Alloys. Cambridge, August 1973, 87, 421.
75. M. Hempel. Fracture. 1958. Proceedings of Swampscott Conference. Pub. Wiley. 1959, 376.
76. T. Yokobori, M. Nanbu and N. Takeuchi. Rep. Res. Inst. Strength Fracture Material. Tohoku Univ. Nov. 1969, 5, 1, 1.
77. C.M. Gilmore and W.A. Wood. Proc. Conf. on Microstructure and Design of Alloys. Cambridge. August 1973, 92, 451.
78. D.K. Benson, J.C. Grosskreutz and G.G. Shaw. Met. Tran. 1972, 3(5), 1239.
79. C. Laird and C.E. Feltner. Trans. Met. Soc. AIME. 1967, 239, 1074.
80. N.F. Mott. Acta. Met. 1958, 6, 195.
81. A.N. May. Nature. 1960, 185, 303.

82. A.J. Kennedy. Phil. Mag. 1961. 6, 49.
83. J. Porter and J.C. Levy. J.I.M. 1960-61, 89, 86.
84. R.C. Boettner, C. Laird and A.J. McEvily. Trans. Met. Soc. AIME. 1965, 233, 379.
85. C. Laird and A.R. Krause. Int. J. Fract. Mech. 1968, 4, 219.
86. K.U. Snowden. Phil. Mag. 1966, 14, 1019.
87. H.E. Tipler and P.G. Forrest. Inst. Mech. Eng. Conf. on Fatigue. London. 1956.
88. D.I. Golland and P.L. James. Met.Sci.J. 1970, 4, 113.
89. H.D. Williams and G.C. Smith. Phil. Mag. 1966, 13, 835.
90. H.M. Clark. Nature. 1966, 209, 193.
91. P. Beardmore and P.H. Thornton. Acta. Met. 1970, 18, 109.
92. G.C. Smith. Proc. Royal Society. 1957, A242, 189.
93. D.W. Hoeppner and F.M. Vitovec. Trans. Met. Soc. AIME. 1964, 230, 1378.
94. J.C. Swearengen and R. Taggart. Acta. Met. 1971, 19, 543.
95. J.P. Owens, P. Watson and A. Plumtree. Proc. of 1971 International Conference on Mechanical Behaviour of Materials. Japan, Vol.II pp. 131-142.
96. R.C. Boettner, A.J. McEvily and Y.C. Liu. Phil. Mag. 1964, 10, 95.
97. C.H. Wells and C.P. Sullivan. Trans. ASM. 1967, 60, 217.
98. W.E. Duckworth. Metallurgia. 1964, 69, 53.
99. J.C. Grosskreutz and G.G. Shaw Fracture 1969. Proceedings of Brighton Conference 1969. Ed. P.L. Pratt. Pub. Chapman and Hall. 620.
100. J. Lankford and F.N. Kusenberger. Met. Trans. 1973, 4, 553.
101. R.J. Wanhill, D. Ryder and T. Davies. J.Nucl. Mat. 1972 May, 43, 75.
102. A.J. McEvily, R. Ebara and K.M. Prewo. Proc. Conf. on Microstructure and Design of Alloys. Cambridge. 1973, 52, 256.
103. J.B. Clark and A.J. McEvily. Acta. Met. 1964, 12, 1359.
104. C.A. Stubbington. ibid 931.
105. H.I. Kaplan and C. Laird. Trans. Met. Soc. AIME. 1967 239, 1017.
106. C.E. Feltner. Acta. Met. 1963, 11, 817.
107. C. Laird. ASTM. STP.415, 1967, 131.
108. D.J. Duquette and M. Gell. Met. Trans. 1971, 2, 1325.
109. S.P. Lynch. Metal Sci. 1975, 9, 401.
110. R.K. Ham and M.L. Wayman. Trans. Met. Soc. AIME. 1967, 239, 721.
111. C.A. Stubbington and P.J.E. Forsyth. Metallurgia. 1966, 74, 15.
112. A.W. Thompson and W.A. Backofen. Acta. Met. 1971, 19, 597.
113. P.G. Forrest and A.E.L. Tate. J.I.M. 1964-65, 93, 438.
114. T. Yokobori, K. Sato and Y. Yamaguchi. Rep. Res. Inst. Strength Fracture Mat. Tohoku Univ. 1970, 6, 49.
115. G.R. Chanani, S.D. Antolovich and W.W. Gerberich. Met. Trans. 1972, 3, 2661.
116. P. Lukas, M. Klesnil and R. Fiedler. Phil, Mag. 1969, 20, 799.
117. M.A. Wilkins and G.C. Smith. Acta. Met. 1970, 18, 1035.
118. J.C. Grosskreutz and G.G. Shaw. ASTM. STP.415, 1967, 226.
119. C.A. Zappfe and C.D. Worden. Trans. ASM. 1949, 41, 396.
120. P.J.E. Forsyth and D.A. Ryder. Aircraft Engineering. 1960, 32, 96.
121. J.C. McMillan and R.M. Pelloux. ASTM. STP.415, 1967, 505.
122. D.A. Meyn. Trans. ASM. 1968, 61, 42.
123. P.J.E. Forsyth, C.A. Stubbington and D. Clark. J.I.M. 1961-62, 90, 238.
124. P.J.E. Forsyth. J.I.M. 1965, 93, 456.
125. R.W. Hertzberg, H. Nordberg and J.A. Manson. J.Mat.Sci. 1970, 5, 521.
126. C.E. Richards and T.C. Lindley. Eng.Fract.Mech. 1972, 4, 951.

127. E. Smith and J.T. Barnby. Met. Sci. J. 1967, 1, 1.
128. C.E. Richards. Acta. Met. 1971, 19, 583.
129. T.C. Lindley and C.E. Richards. Conf. on Effect of Second Phase Particles on Mech. Props. of Steel. Scarborough 1971. I.S.I. Publ. 1971, 119.
130. D. Broek. Fracture 1969. Proc. of Brighton Conference 1969. Ed. P.L. Pratt. Pub. Chapman and Hall. 754.
131. P.T. Heald, T. C. Lindley and C.E. Richards. Mat.Sci.Eng.1972, 10, 235.
132. R.W. Hertzberg. ASTM. STP.415, 1967, 305.
133. P.J.E. Forsyth and D.A. Ryder. Metallurgia. 1961, 63, 117.
134. W.A. Spitzig and R.P. Wei. Trans. ASM. 1967, 60, 279.
135. D.M. Gilby and S. Pearson. RAE Tech. Rep. 66402, 1966.
136. P.C. Paris and F. Erdogan. J. Basic Eng. 1963, 85, 528.
137. J. Weertman. Int.J. Fract.Mech. 1969, 5, 13.
138. A.J. McEvily and T.L. Johnston. Int.J.Fract.Mech. 1967, 3, 45.
139. B. Tomkins. Phil. Mag. 1968, 18, 1041.
140. B. Tomkins, G. Sumner and J. Wareing. Fracture 1969. Proc. of Brighton Conference 1969. Ed. P.L. Pratt. Pub. Chapman and Hall. 712.
141. P. Fox. M. Phil. Thesis. Sheffield Polytechnic, 1969.
142. R.C. Boettner. Trans. Met.Soc. AIME. 1967, 239, 1030.
143. R. Kieesling. Non-Metallic Inclusions in Steel. I.S.I. Publication 115, Part III, 1968.
144. J.F. Knott. Metals and Materials. May 1975, 45.
145. C.E. Feltner and J. Morrow. J.Basic.Eng., Trans. of ASME. 1961, 83, 15.
146. A.T. Price and W.J. Elder. J.I.S.I. 1966, 204, 594.
147. J.D. Embury and R.M. Fisher. Acta.Met. 1966, 14, 147.
148. J.D. Embury, A.S. Keh, R.M. Fisher. Trans. Met. Soc. AIME. 1966, 236, 1252.
149. C. Laird and G. Thomas. Int.J.Fract.Mech. 1967, 3, 81.
150. C.T. MacKenzie and P.P. Benham. The Engineer. 1962, 214, 1104.
151. Private Communication
152. P.J.E. Forsyth. Physical Basis of Metal Fatigue. 1969. Blackie & Son Ltd. (London).
153. W.A. Wood. ASTM. STP.237. 1958, 110.
154. T.C. Lindley, G. Oates and C.E. Richards. Acta. Met. 1970, 18, 1127.
155. K.E. Puttick. J.I.S.I. 1956, 185, 167.
156. T. Yokobori and T. Aizawa. Rep.Res. Inst. Strength and Fracture of Materials. Tohoku Univ. 1969, 6, pp.19.

STATEMENT OF POST GRADUATE STUDY

During the period in which the research work was carried out, a number of courses, seminars and conferences were attended. These included the following:-

a) the production and presentation of a paper entitled "Initial Fatigue Damage in Pearlite" at the Institute of Metals Conference, "Modern Metallography in Metallurgy". This was held at Liverpool University in September, 1971,

b) the presentation of a paper at a research colloquium at Sheffield Polytechnic and attendance at several of these colloquia,

c) attendance at several colloquia arranged by the Fatigue Research Group at the British Rail Technical Centre,

d) a series of lectures based on Advanced Dislocation Theory in Fracture at Sheffield Polytechnic,

e) a series of lectures based on Quantitative Metallography at Sheffield Polytechnic.

A paper has been submitted and accepted for presentation at the forthcoming International Conference on Fracture to be held at Waterloo, Canada, in June 1977. The paper is entitled "Metallographic Aspects of Fatigue in Pearlite Structures".

ACKNOWLEDGEMENTS

This thesis is based on work carried out at the Sheffield City Polytechnic whilst the author was a part-time research student in the Department of Metallurgy from October 1969 to September 1975.

My ideas owe much to the help and advice given to me by Peter Warin, my college supervisor, and Peter Watson of the British Rail Technical Centre, Derby. I wish to thank the many colleagues at the Technical Centre who provided valuable experimental assistance and stimulating discussion. I am indebted to the technical staff at the Polytechnic, particularly Russell Day for workshop facilities and Ray Codd for assistance in preparation of some of the foils.

I would also like to thank the British Steel Corporation for use of their microscope facilities at Swinden Laboratories and their information service at the Hoyle Street laboratories. My thanks go to Patricia Cooper who typed the thesis and also to the Principal at Rotherham College of Technology who supported my initial move into part-time research.

Finally, I wish to thank my family, Janet, Sarah, and Rachel for their moral support and co-operation throughout the whole period of this work.

APPENDIX 1

METHOD OF CALCULATION USED FOR THE DETERMINATION OF RELATIVE AREAS OF FERRITE-CEMENTITE INTERFACE IN STRUCTURES

Consider the interface area within a cube of the material, whose dimensions are 1 x 1 x 1 mm.

In both lamellar pearlites, the total area is given by:

number of lamellae in cube x interface area x 2

In both cases, the interface area is assumed to be 1 square millimetre.

Coarse pearlite

No. of lamellae = $\frac{1 \text{ mm.}}{\text{thickness of lamellae + mean free ferrite path}}$

Lamellae thickness = 0.043 μ metres

Mean F.F. path = 0.300 μ metres

No. of lamellae = $\frac{1 \text{ mm.}}{0.343 \mu \text{ metres}}$ = 2900

A. Total interface area = 2 x 1 x 2900 = 5800 mms^2

Fine Pearlite

Lamellae thickness = 0.008 μ metres

Lamellae spacing = 0.07 μ metres

B. Total interface area = 12900 x 2 x 1 = 25800 mms^2

Spheroidised Carbide

Consider the average number of spheroids within the cube having the dimensions stated earlier.

Total interface area is then given by:-

Number of spheroids x surface area of spheroids

To find average number of spheroids

Av. diameter of spheroid = 2μ metres

Mean free ferrite path = 0.5μ metres

No. along 1 mm. $= \frac{1 \text{ mm}}{2.5\mu \text{ metres}} = 400$

No. in cube = $400 \times 400 \times 400$

To find surface area of spheroid

Area of sphere = $4\pi r^2$

r = average radius of spheroid

$\therefore r = 1\mu$ metre

Total surface area = $400 \times 400 \times 400 \times 4 \times \pi \times 1 \times 1$

$C = 800 \text{ mms.}^2$

Summarising, the total interface area within the cube for each structure is given by:-

A - coarse pearlite	=	5800 mms^2
B - fine pearlite	=	25800 mms^2
C - spheroidised carbide	=	800 mms^2

TABLE 1

CHEMICAL COMPOSITION OF STEELS USED IN THE INVESTIGATION

Weight %

	STEEL A	STEEL B	STEEL C
Carbon	0.78	0.78	0.74
Silicon	0.20	0.20	0.21
Manganese	0.70	0.68	0.66
Sulphur	0.039	0.025	0.020
Phosphorus	0.020	0.010	0.010
Nickel	0.40	0.42	0.37
Chromium	0.24	0.28	0.22
Copper	0.12	Not Analysed	
Aluminium	0.015	Not Analysed	
Lead	0.05	Not Analysed	

TABLE 2

MONOTONIC PROPERTIES OF STEEL C

AS MEASURED IN A TENSILE TEST

STRUCTURE	0.2% Proof Stress N/mm^2	Tensile Strength N/mm^2	True Fracture Stress N/mm^2	True Fracture Strain
Coarse Pearlite	375	776	945	0.28
Fine Pearlite	780	1145	1285	0.16
Spheroidised Carbide	392	724	1080	0.71

TABLE 3

CYCLIC PROPERTIES OF STEEL C AS

DETERMINED FROM A CYCLIC STRESS-STRAIN CURVE

STRUCTURE	Cyclic Yield Stress N/mm^2	Cyclic Strength Coefficient N/mm^2	Cyclic Strain Hardening Exponent n'
Coarse Pearlite	220	1750	0.245
Fine Pearlite	275	2620	0.228
Spheroidised Carbide	210	1670	0.248

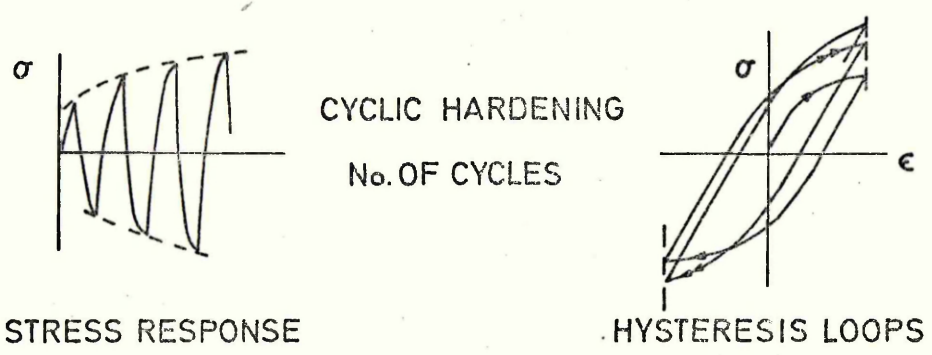

FIG. 1 SCHEMATIC REPRESENTATION OF THE RESPONSE OF METALLIC MATERIALS TO CYCLIC STRAIN.[9]

Fig. 2 Monotonic and Cyclic Stress-Strain Curves for Steel SAE 4340 (Annealed) After Landraf[7]

COMPARISON OF THE MONOTONIC AND CYCLIC STRESS STRAIN CURVES FOR STEEL SAE 4340 (ANNEALED).

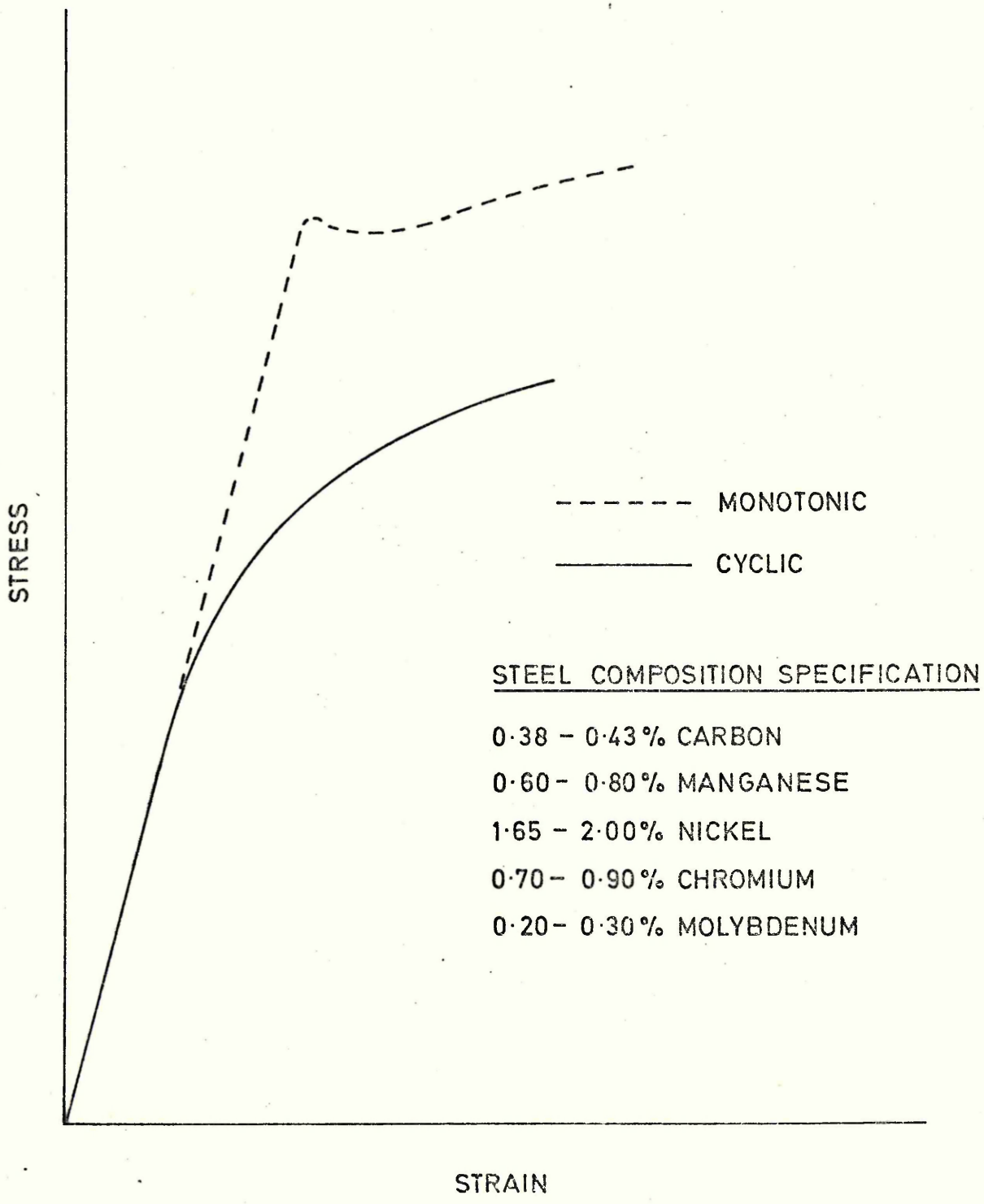

FIG. 2

Fig. 3 Monotonic and Cyclic Stress Strain Curves for Man-ten Steel and Waspaloy.
After Landgraf.[7]

STRAIN CURVES

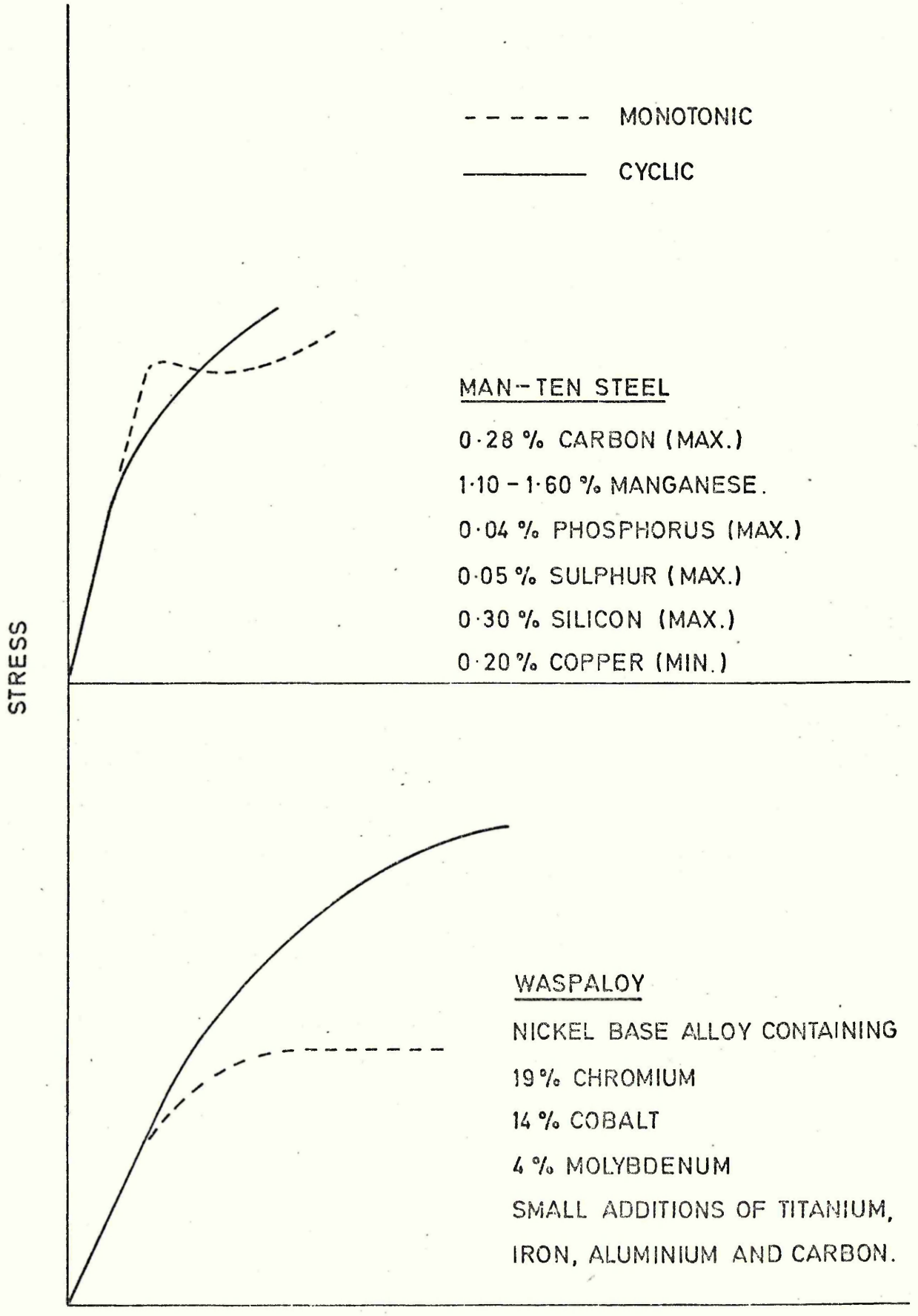

FIG. 3

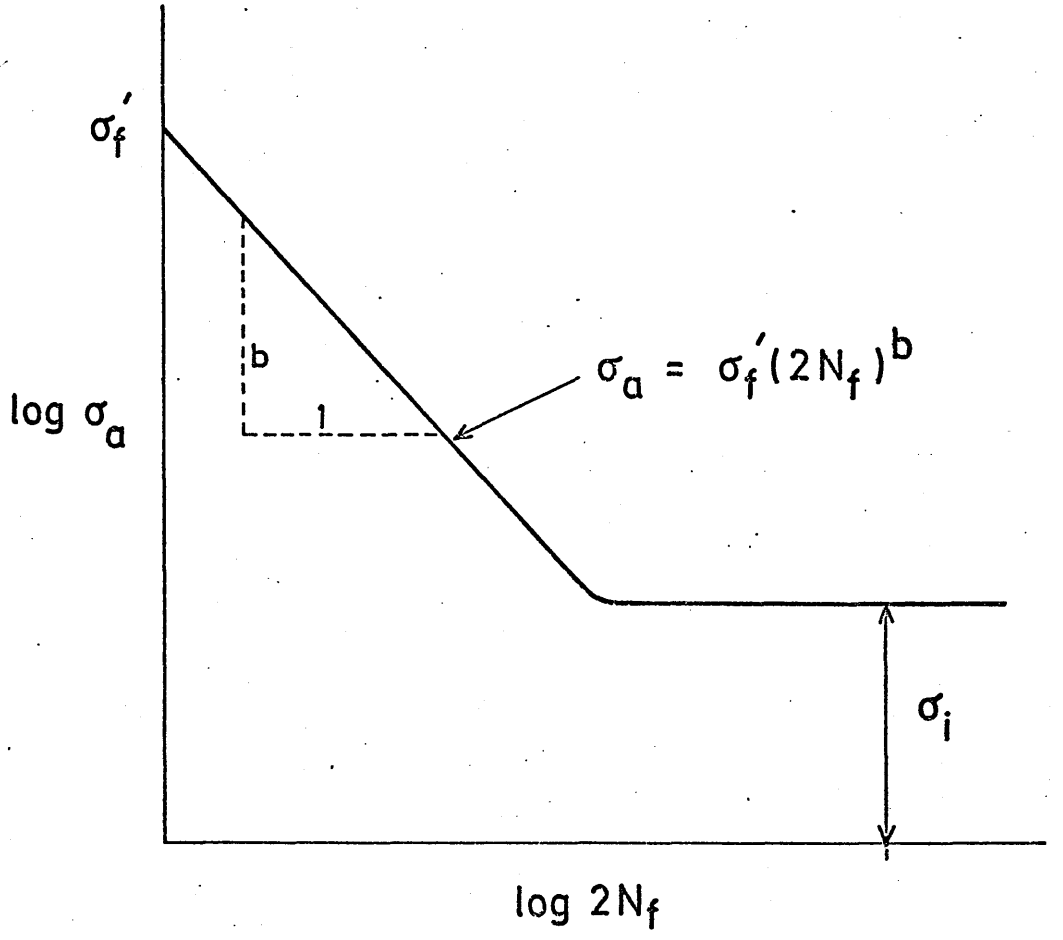

FIG. 4

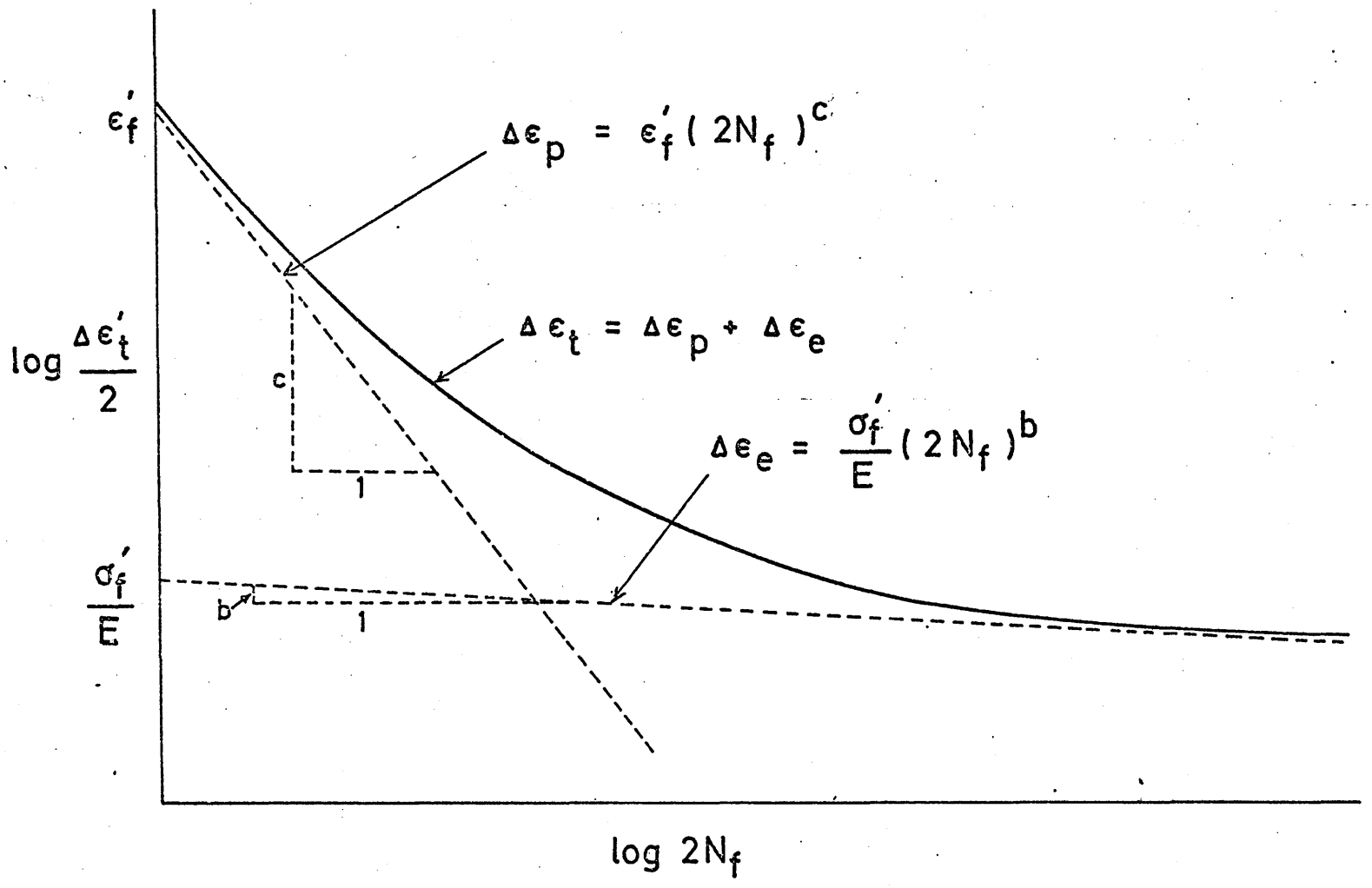
ϵ_f'
$\Delta\epsilon_p = \epsilon_f'(2N_f)^c$
$\log \frac{\Delta\epsilon_t'}{2}$
$\Delta\epsilon_t = \Delta\epsilon_p + \Delta\epsilon_e$
c
1
$\Delta\epsilon_e = \frac{\sigma_f'}{E}(2N_f)^b$
$\frac{\sigma_f'}{E}$
b
1
$\log 2N_f$

FIG. 5

Fig. 6 Schematic variation of the fatigue strength and ductility exponents, (b and c) and the true fracture strength and strain (σ_f and ϵ_f) with the cyclic strain hardening exponent, n'.

Fig. 7 Schematic diagram of stage I and stage II crack propagation in a polycrystal. After Laird.[107]

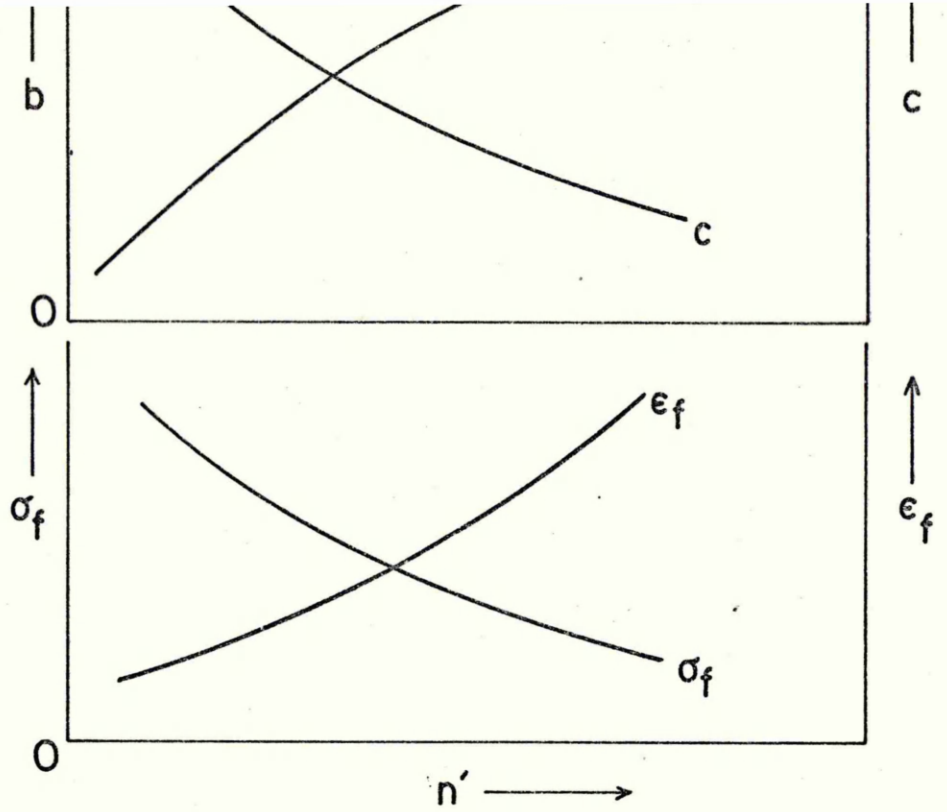
b
c
O
c
ϵ_f
σ_f
ϵ_f
σ_f
O
n′

FIG. 6

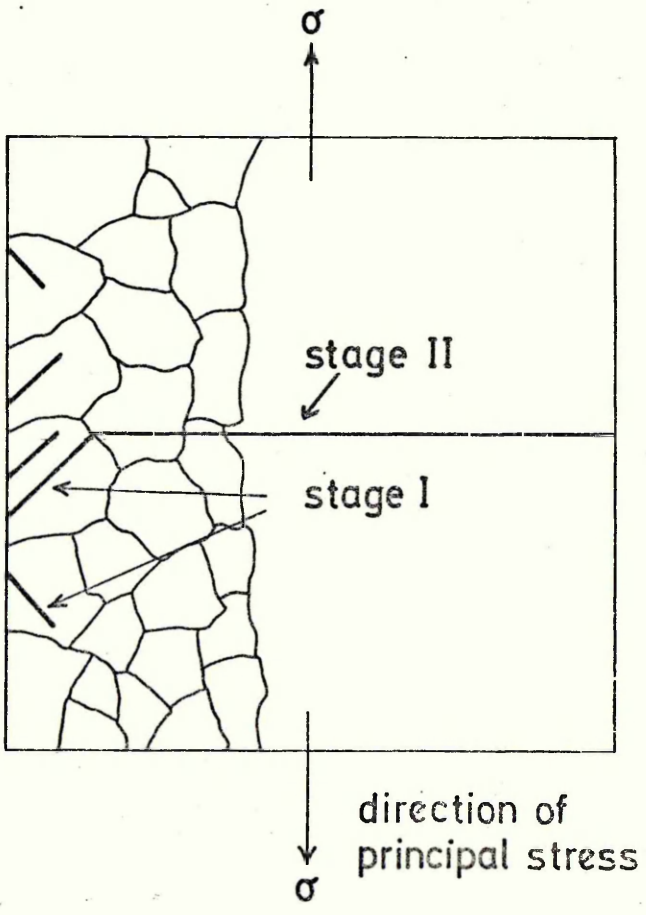
σ
stage II
stage I
direction of
principal stress
σ

FIG. 7

Fig. 8 Schematic representation of a fatigue hardening curve.

Fig. 9 Schematic representation of dislocation structures produced in single phase materials by cyclic stressing.

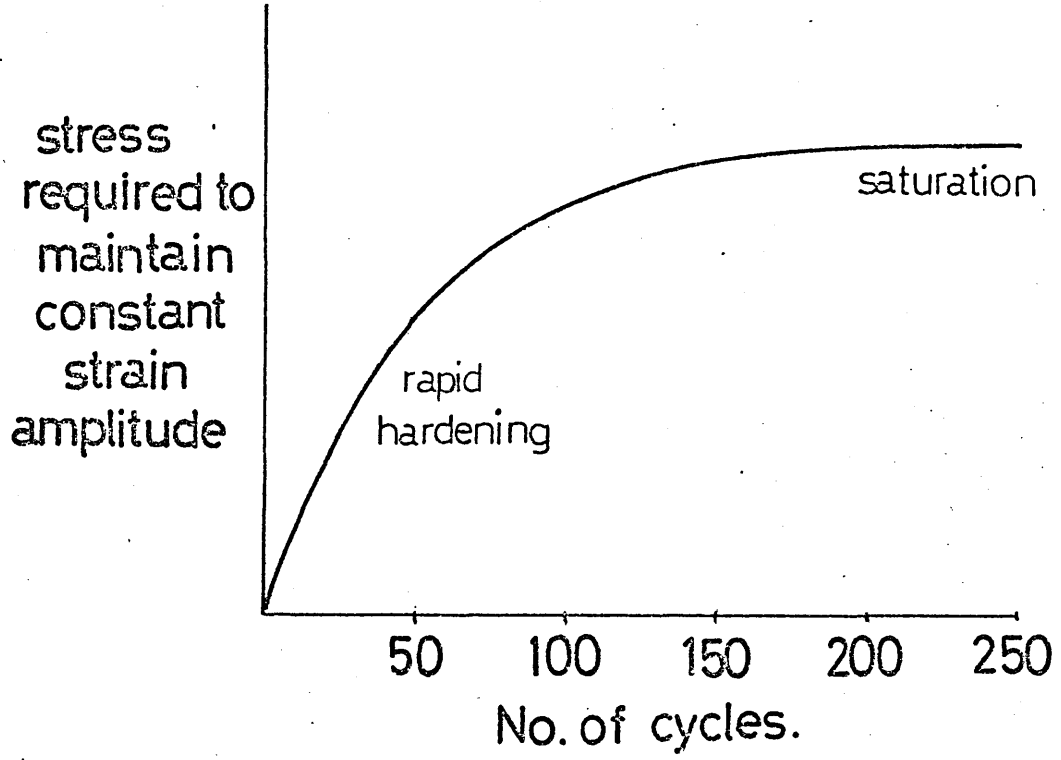

FIG. 8

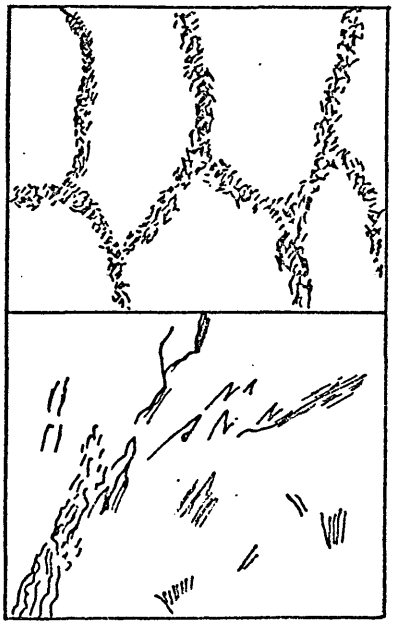

A. CELLULAR NETWORK

B. BUNDLES.

MAG. X 15,000

FIG. 9

Fig. 10 An illustration of two mechanisms for shear mode crack growth. Type A is associated with materials of wavy slip character where screw dislocations can readily cross slip. Type B is associated with materials of planar slip character.
After Kaplan and Laird.[105]

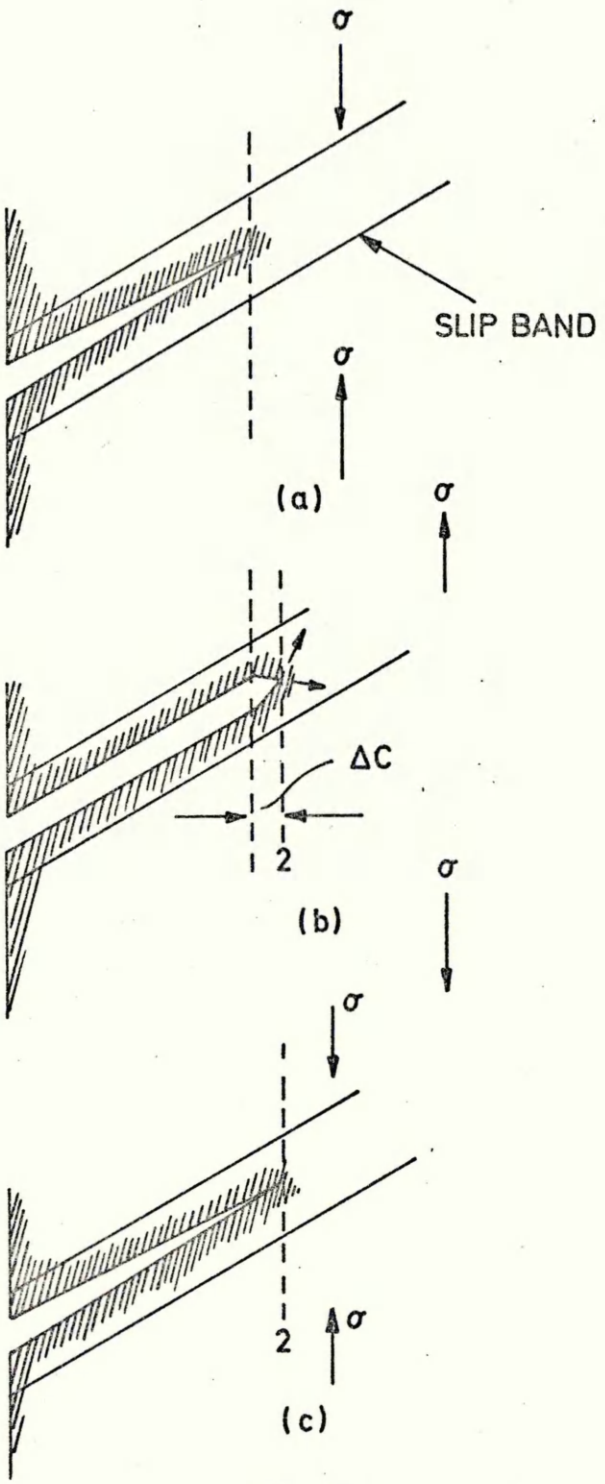

FIG. 10 A

Stage I crack growth by the plastic blunting process: (a) compression (b) tension (c) compression.

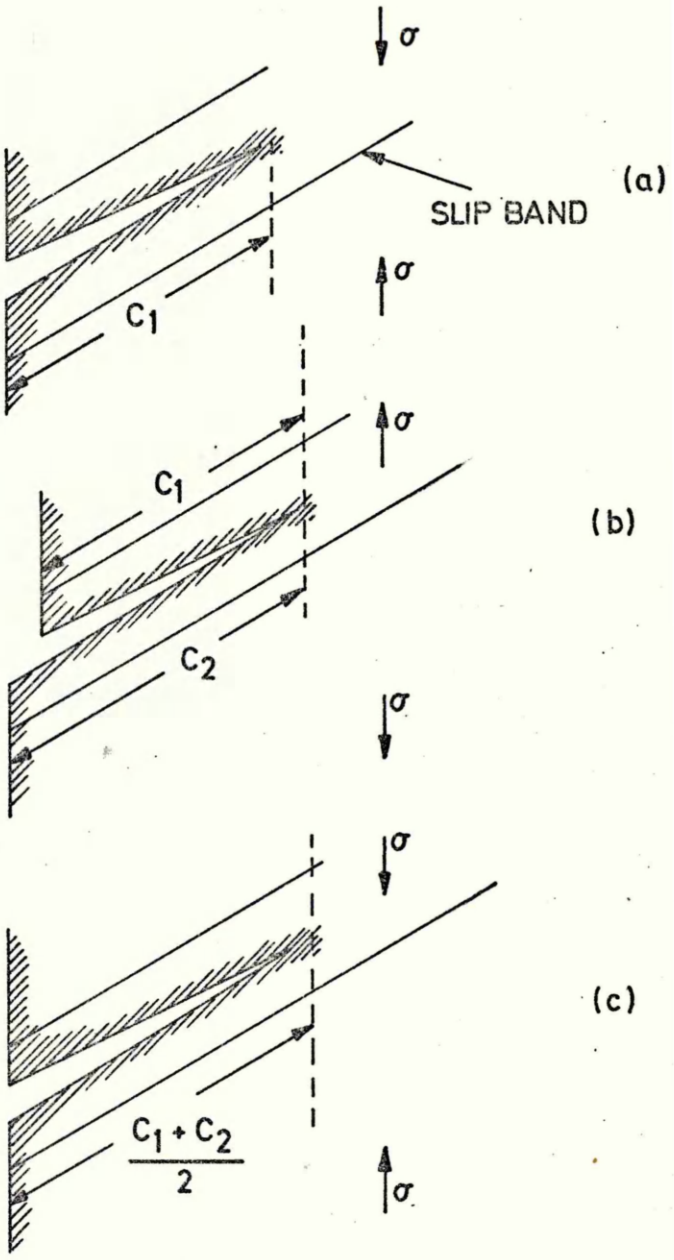

FIG. 10 B

Stage I crack growth by the unslipping analog of the plastic blunting process: (a) compression (b) tension (c) compression.

Fig. 11 The plastic blunting process.
Drawings at left indicate points on the cyclic hysteresis loop to which the crack-tip geometry applies. The plastic zone size is measured along planes of maximum shear.
After Laird.[107]

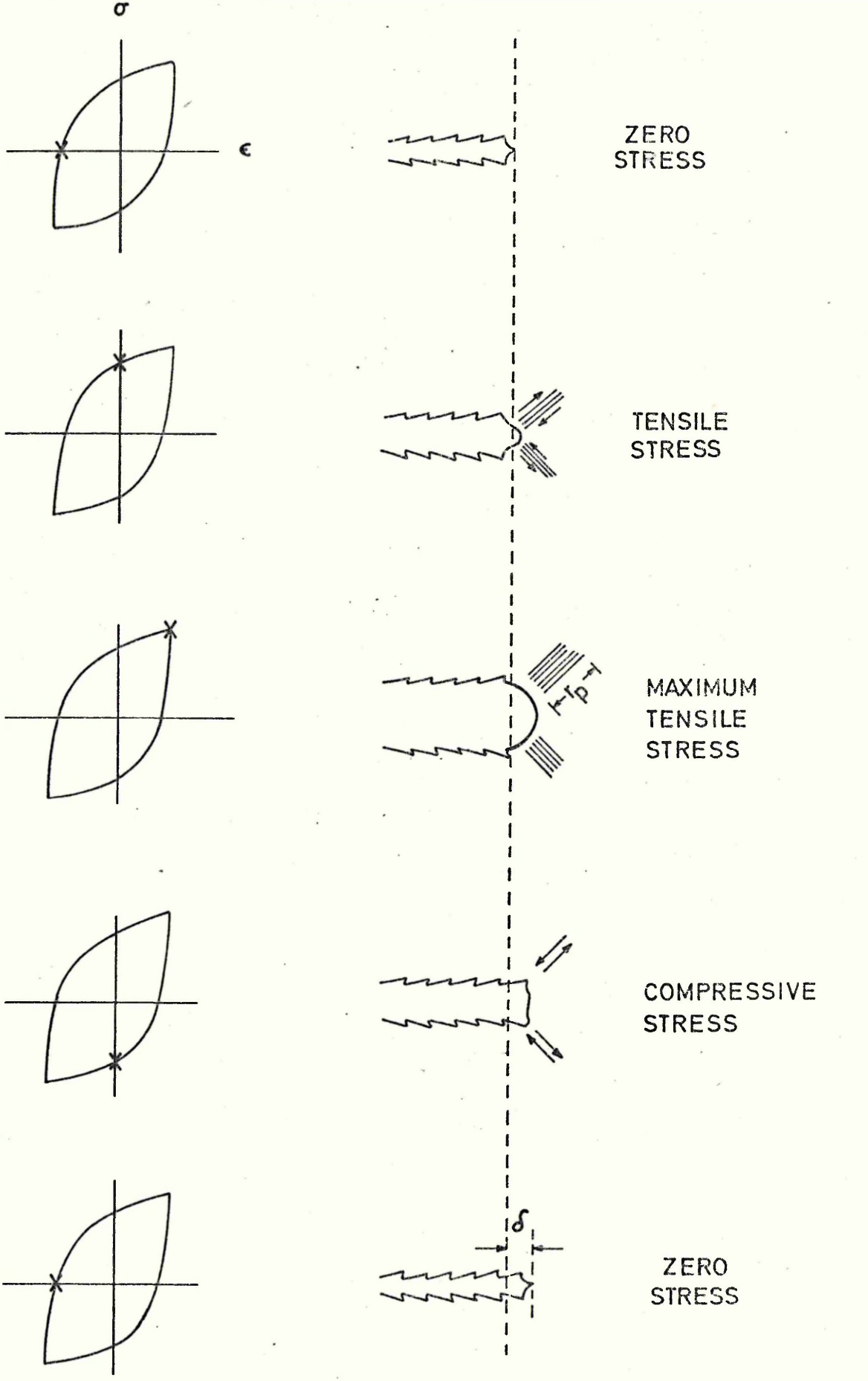
σ
ε
ZERO STRESS
TENSILE STRESS
MAXIMUM TENSILE STRESS
COMPRESSIVE STRESS
ZERO STRESS
δ
HYSTERESIS LOOPS
r_p = plastic zone size
δ = crack advance distance

FIG. 11

Fig. 12 Specimen design.

Upper diagram shows dimensions of flat specimens used for reverse plane bending.

Lower diagram shows round section specimen dimensions.

Fig. 13 Apparatus used for electropolishing specimens.

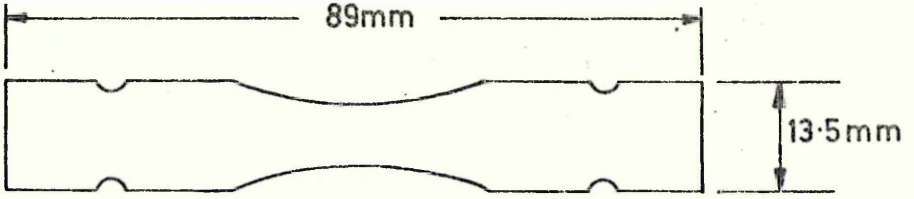
89mm
13·5mm

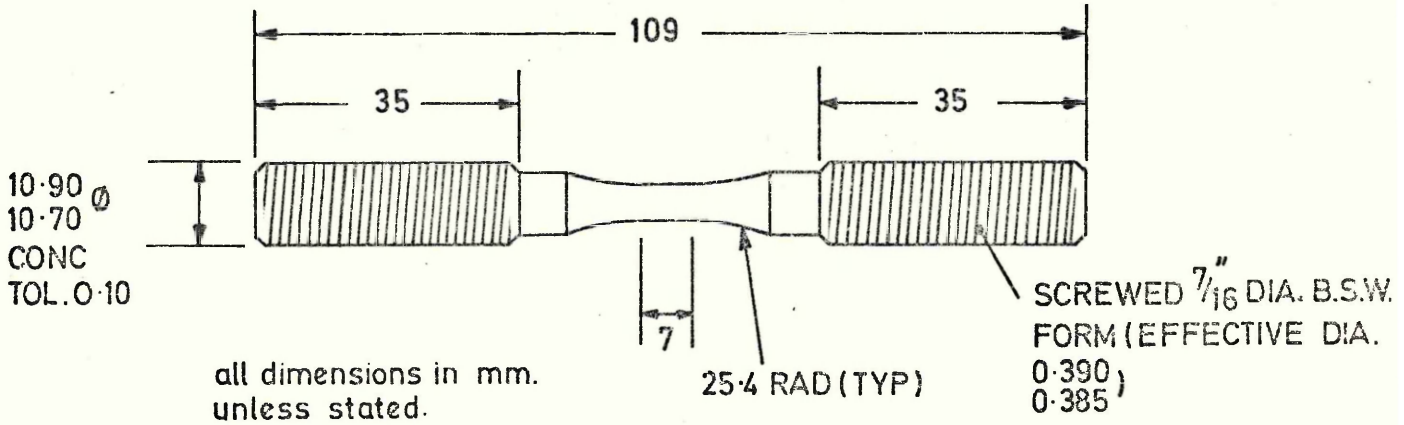
109
35
35
10·90 Ø
10·70
CONC
TOL. 0·10
7
all dimensions in mm.
unless stated.
25·4 RAD (TYP)
SCREWED 7/16 DIA. B.S.W.
FORM (EFFECTIVE DIA.
0·390
0·385)

FIG. 12

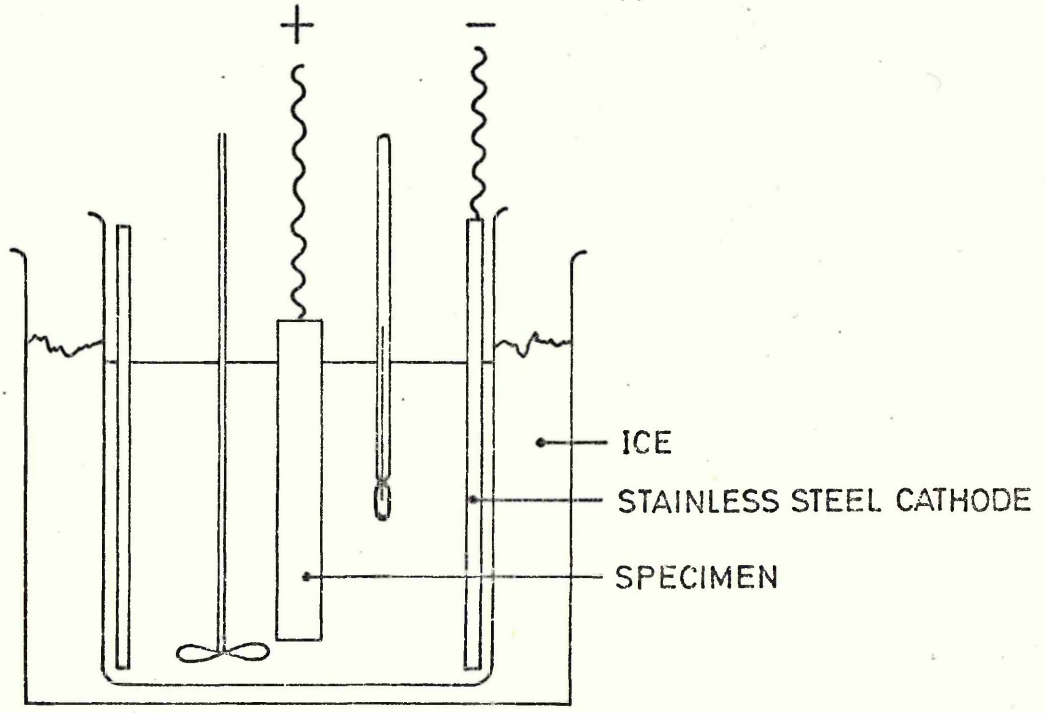
+
−
ICE
STAINLESS STEEL CATHODE
SPECIMEN

FIG. 13

Fig. 14 Typical areas of the three structures used in the investigation (in the heat treated condition).

a. Coarse pearlite Mag. x 500

b. Fine pearlite Mag. x 700

c. Spheroidised carbide Mag. x 15000

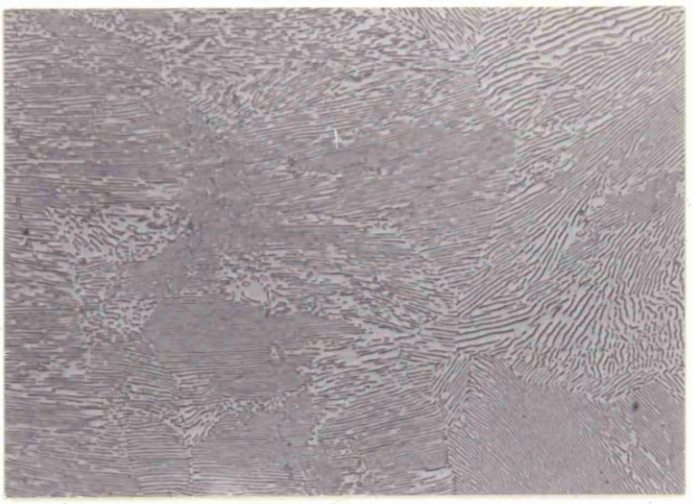

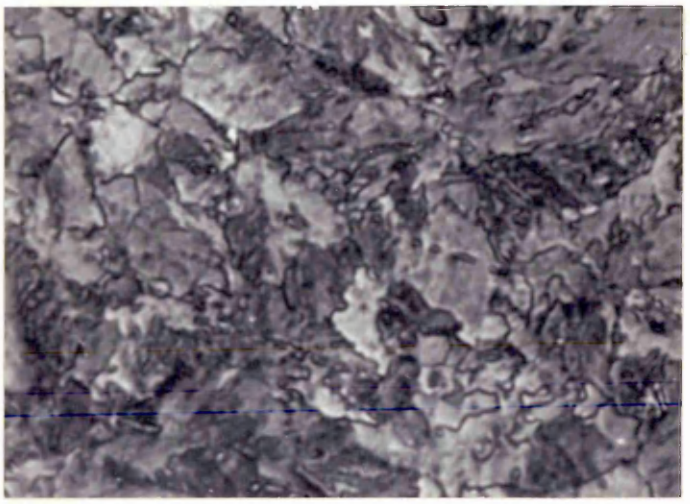

FIG. 15 THE INFLUENCE OF MICROSTRUCTURE ON THE MONOTONIC TENSION STRESS - STRAIN CURVE (STEEL C)

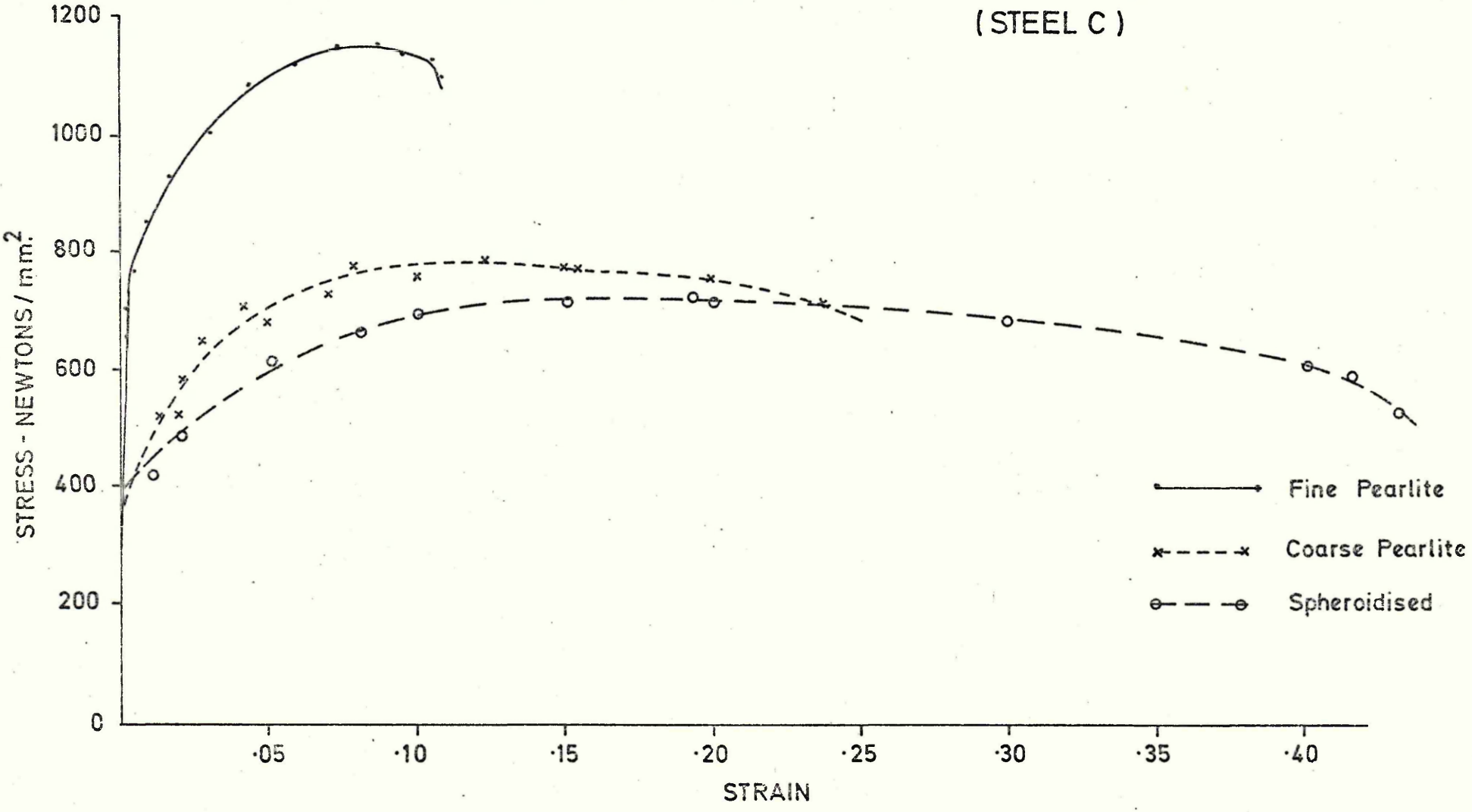

CYCLIC TENSION STRESS - STRAIN CURVES
(STEEL C)

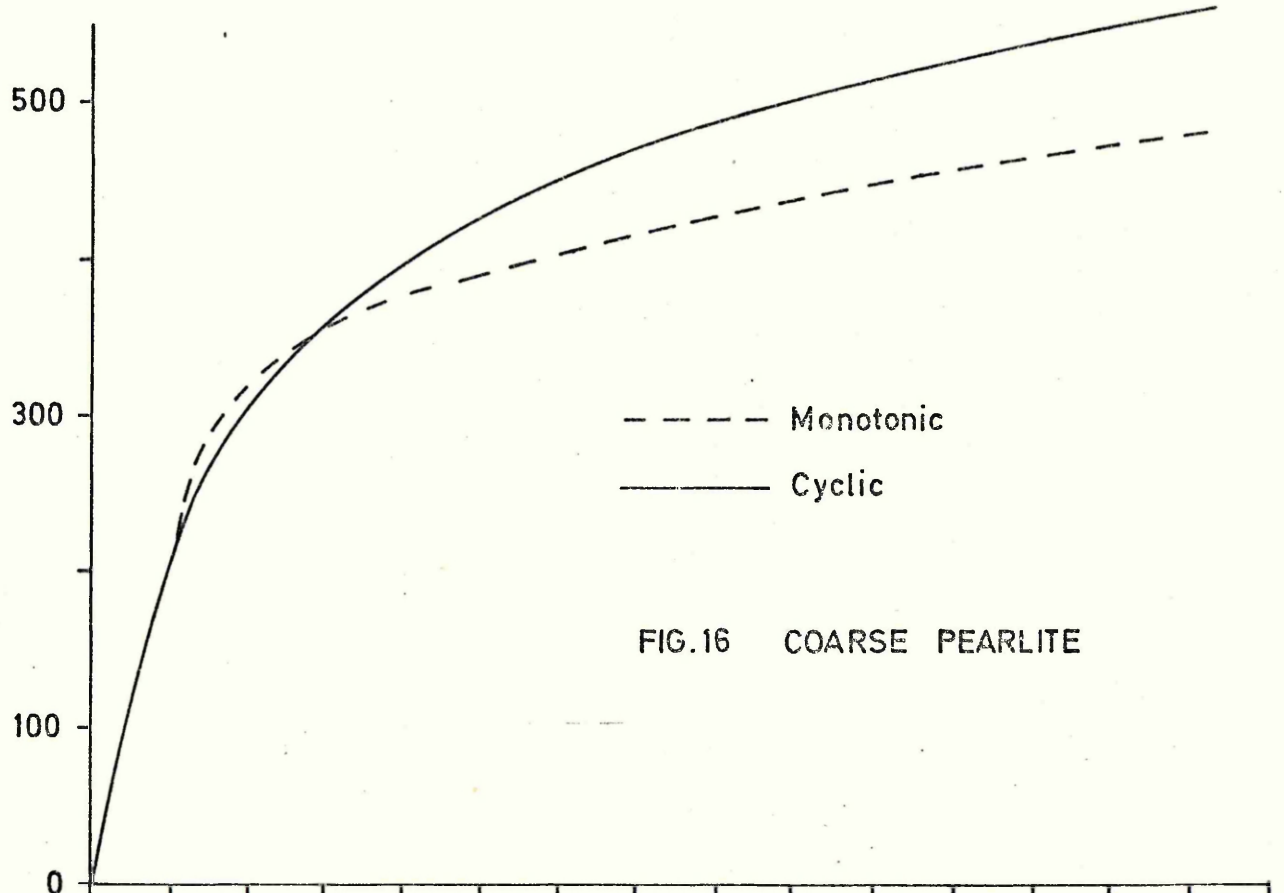

FIG. 16 COARSE PEARLITE

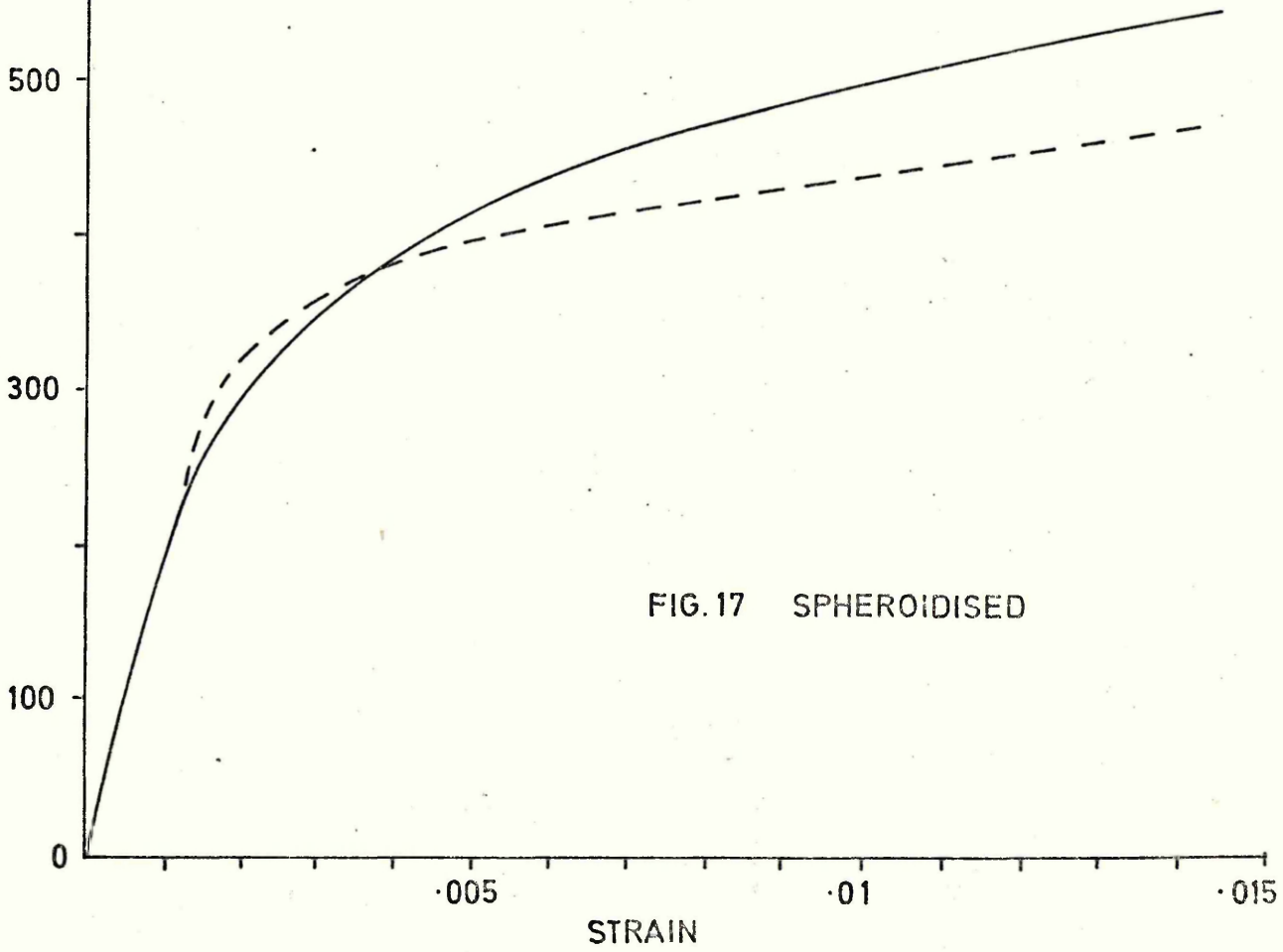

FIG. 17 SPHEROIDISED

CYCLIC TENSION STRESS-STRAIN CURVE
(STEEL C)

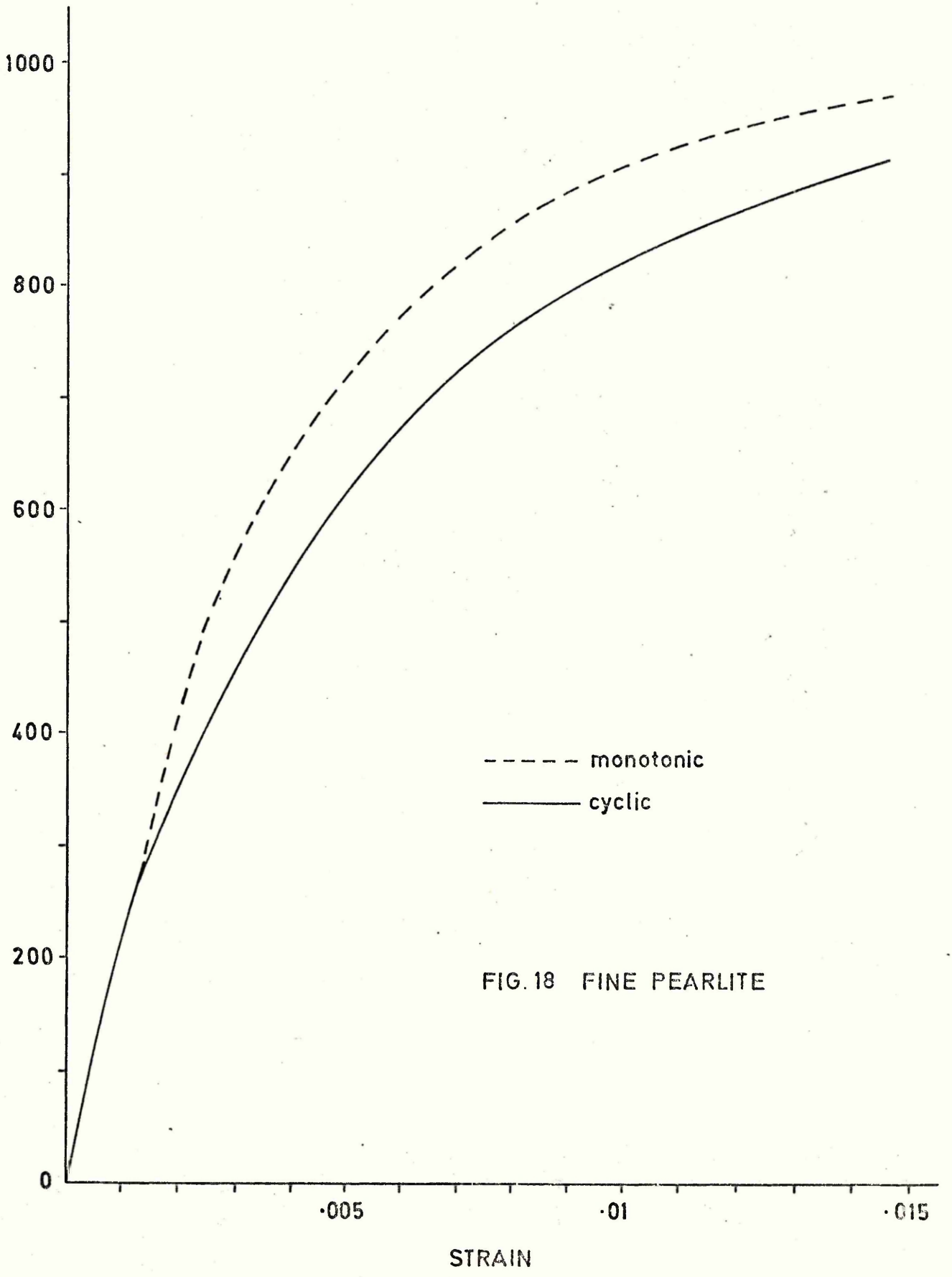

FIG. 18 FINE PEARLITE

FIG. 19 PREDICTED STRAIN-LIFE CURVE
(COARSE PEARLITE)

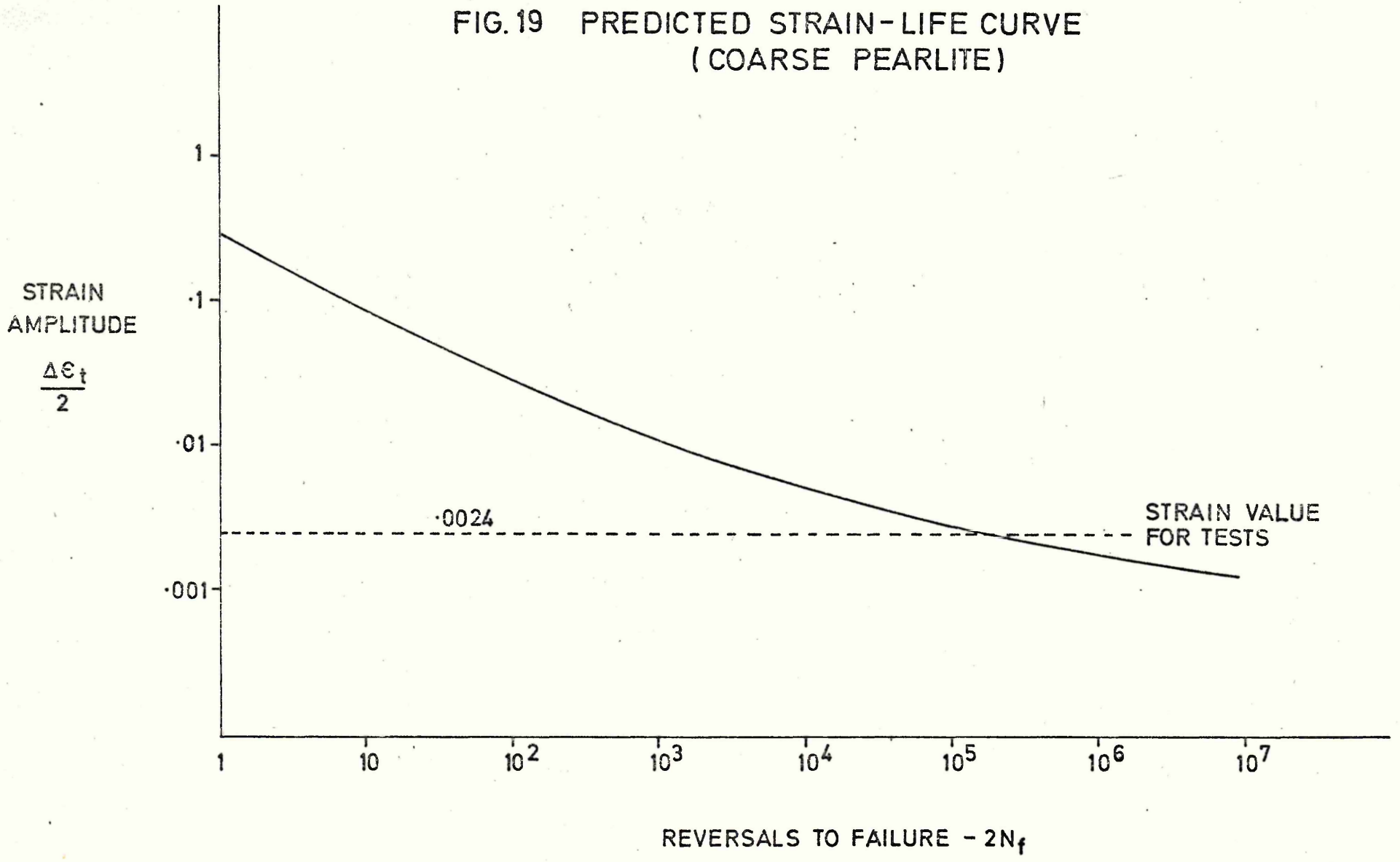

FIG. 20 PREDICTED STRAIN-LIFE CURVE
(FINE PEARLITE)

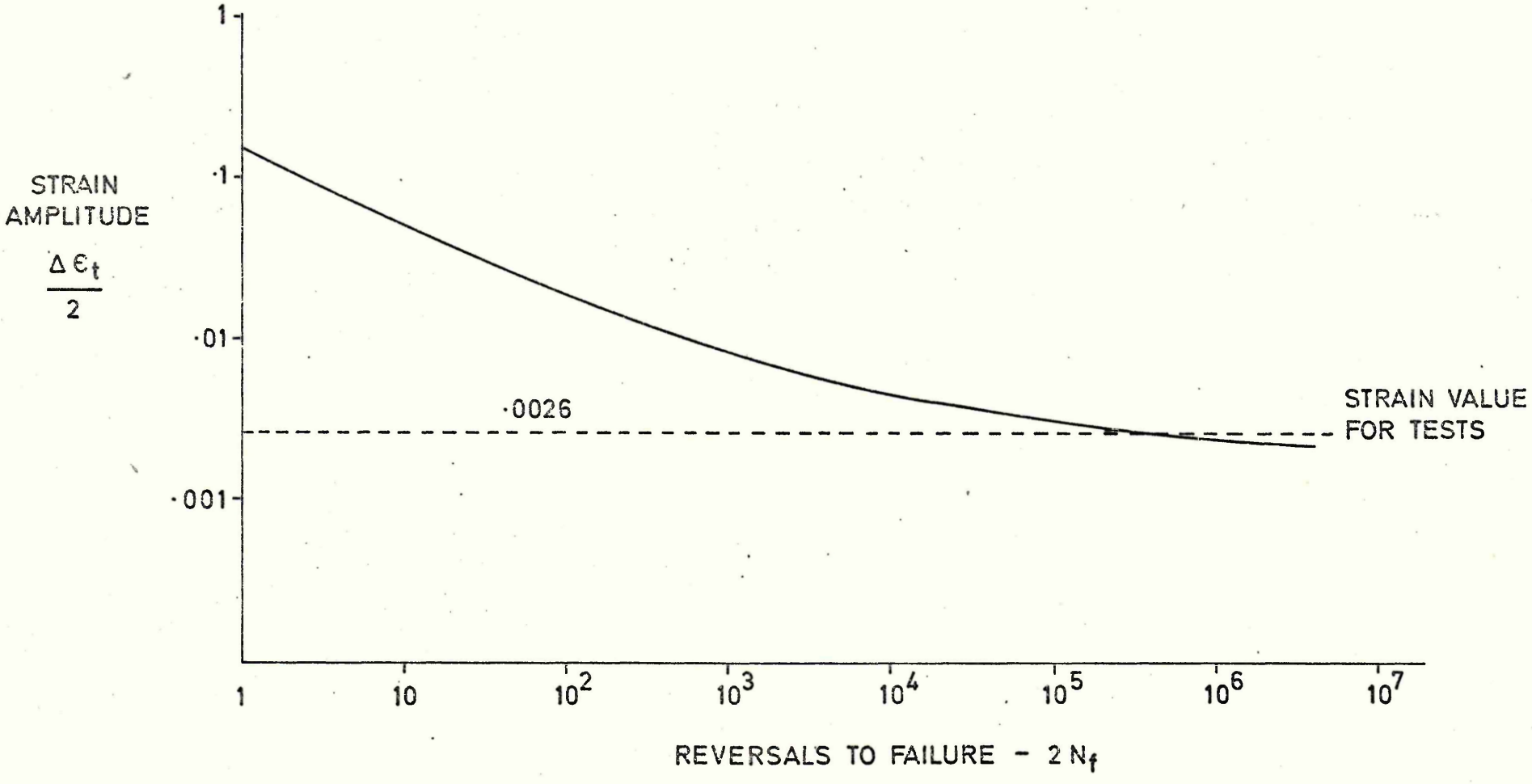

FIG. 21 PREDICTED STRAIN-LIFE CURVE
(SPHEROIDISED CARBIDE)

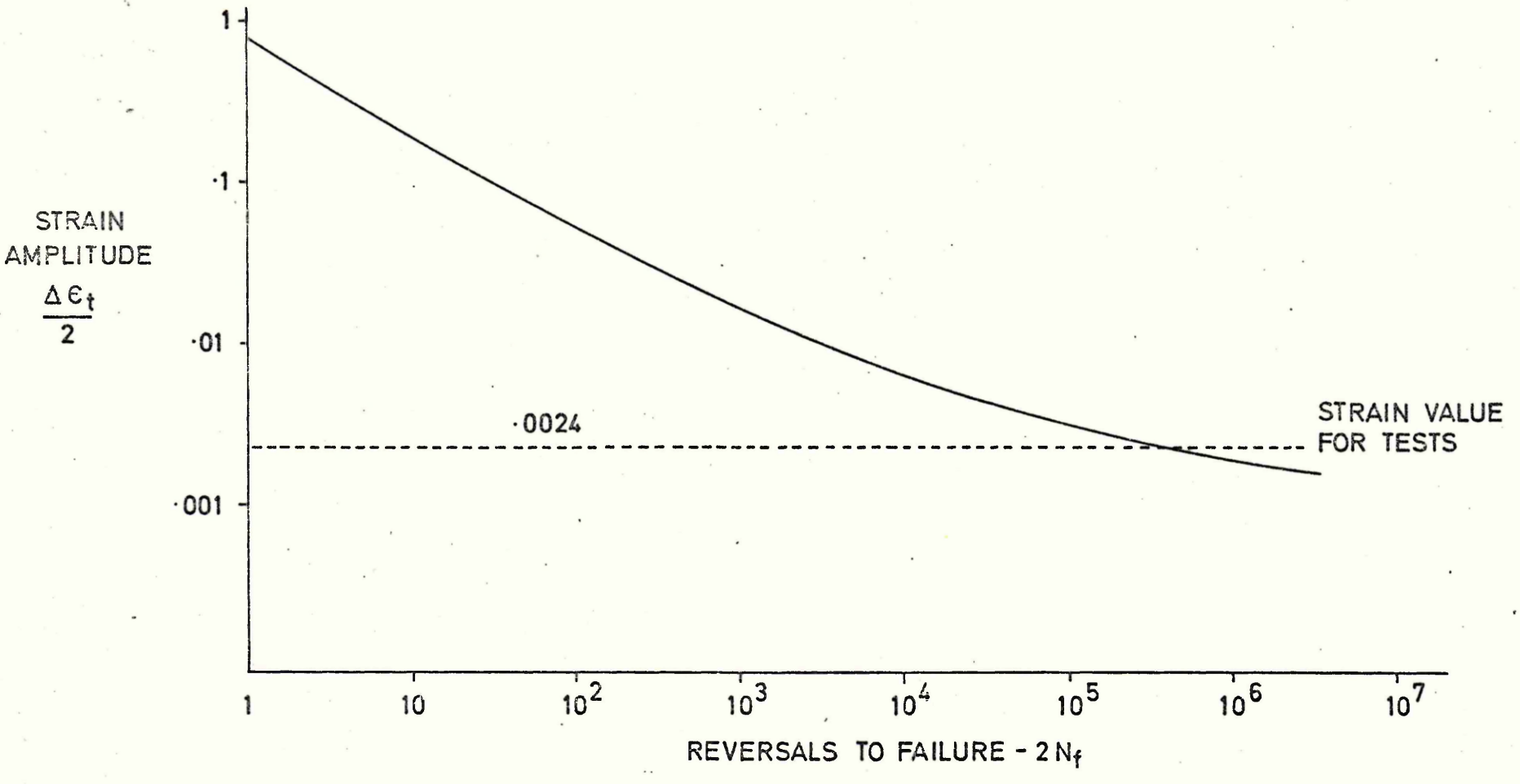

SURFACE FATIGUE DAMAGE IN COARSE PEARLITE

Fig. 22 Cycled for 25% of life
Mag. x 2000

a. Note the area free of damage

b.

Fig. 23 Cycled for 75% of life

a. Mag. x 8000
Note damage at pearlite cell boundaries

b. Mag. x 5000
Note the ripples indicated by arrows

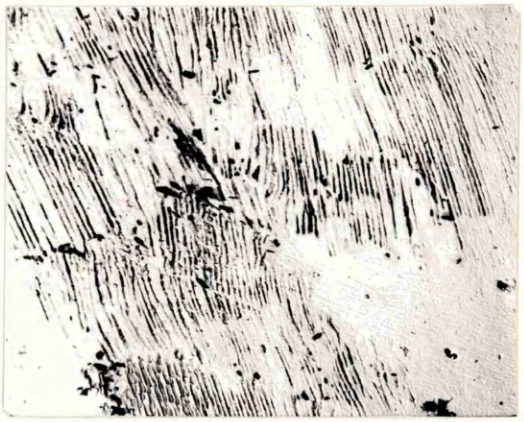

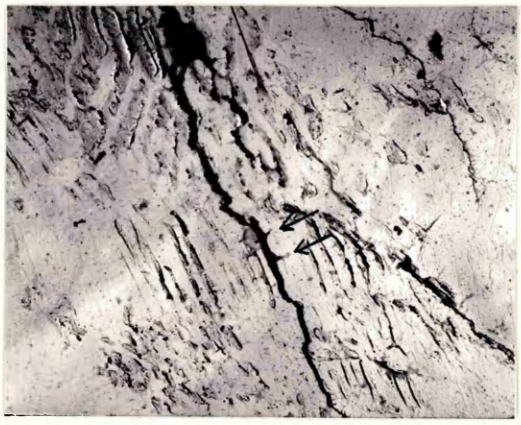

Surface Fatigue Damage in Fine Pearlite

Fig. 24 Cycled for 25% of life.

a. Mag. x 8000

b. Mag. x 15,000

Fig. 25 Cycled for 75% of life

Mag. x 15,000

Surface Fatigue Damage in Spheroidised Carbide.

Fig. 26 Cycled for 25% of life.
Mag. x 8000

a.

b.

Fig. 27 Cycled for 75% of life
Mag. x 10,000

a.

b.

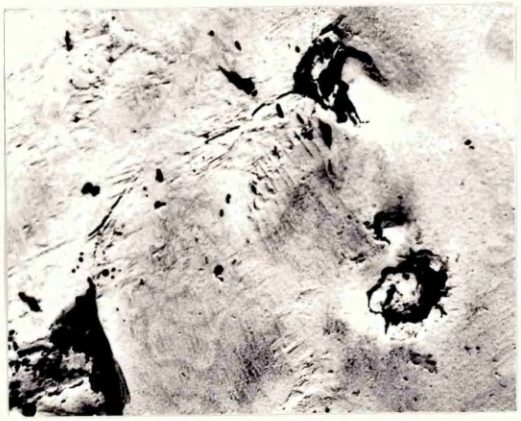

The Development of Surface Fatigue Damage in the same area of Coarse Pearlite.
Mag. x 500

Fig. 28 2% of life

Fig. 29 5% of life

Fig. 30 Final failure

Principal Stress Direction

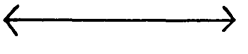

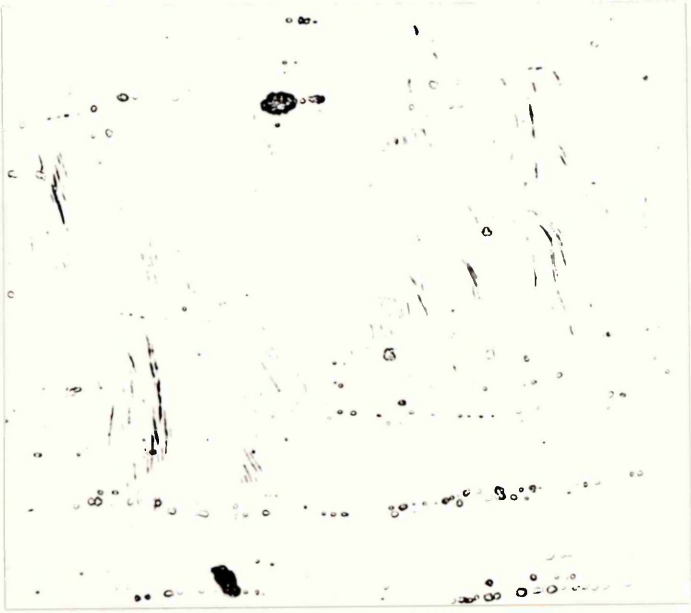

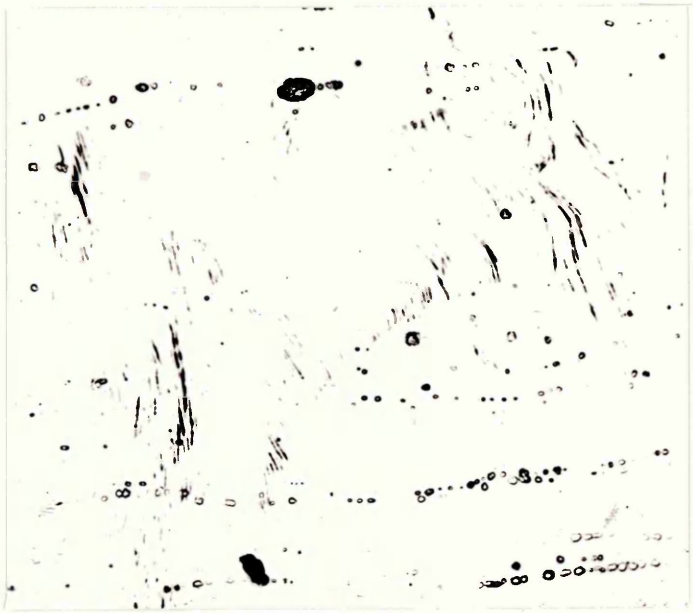

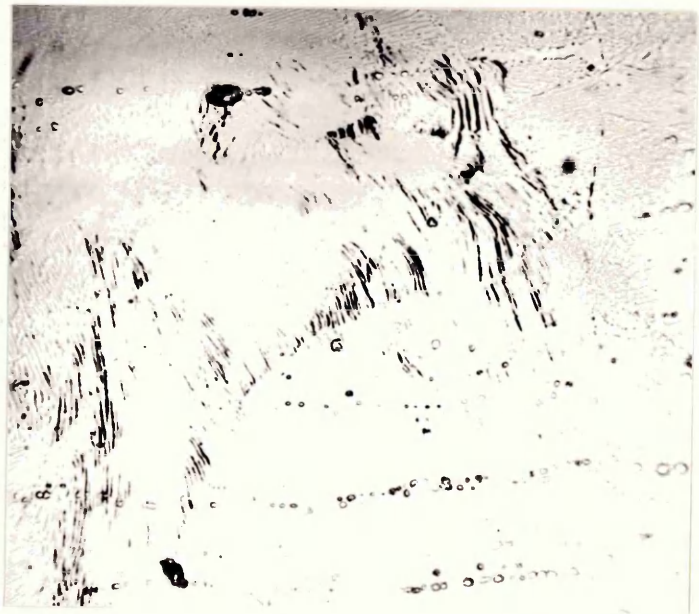

An Electron Microscope Study of Replicas from Fatigue Damaged Surfaces in Coarse Pearlite.

Cycled to 25% of life.

Fig. 31 Mag. x 10,000
The arrows indicate cracks within ferrite (A) and also at ferrite-cementite interfaces (B)

Fig. 32 Mag. x 8000
Note the appearance of slip bands within ferrite and the absence of slip in some areas of ferrite.

Principal stress direction

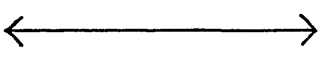

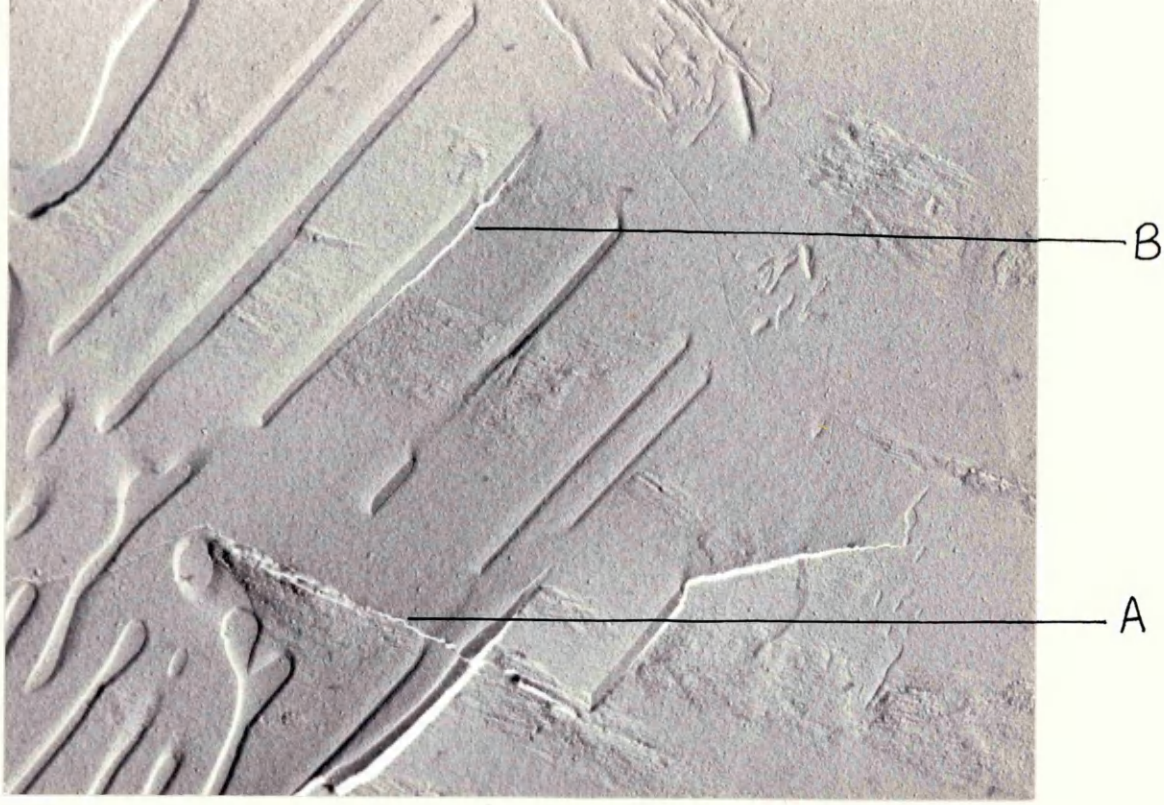
B
A


A
B

Fig. 33 Surface fatigue damage in Coarse Pearlite.

Fatigued to 10% of life.

Mag. x 1500

Principal Stress Direction

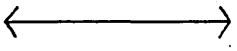

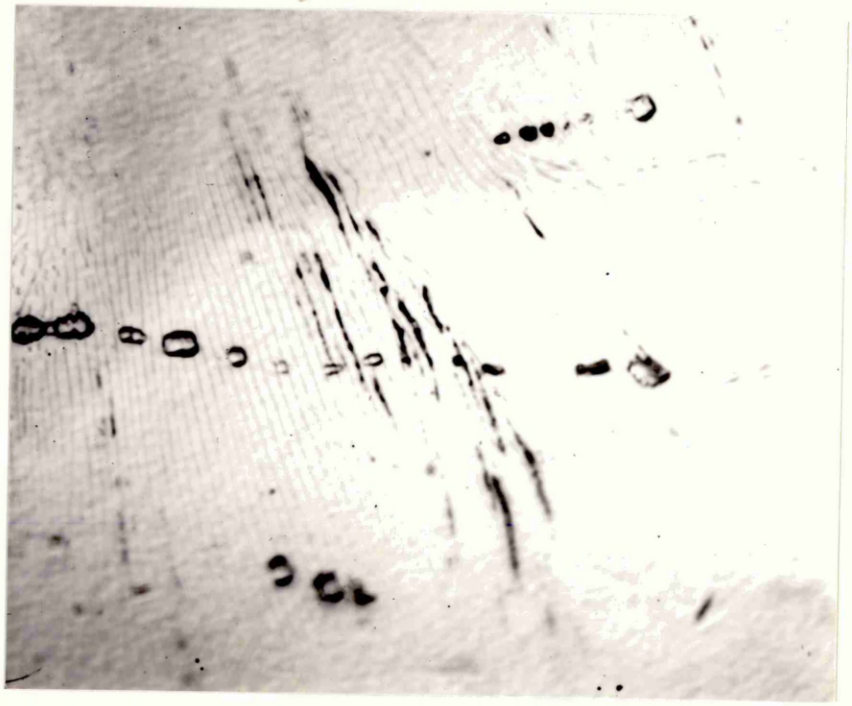

The Effect of Cementite Lamellae Orientation on location of surface damage in coarse pearlite. Mag. x 200

Fig. 34 Area of damage - fatigued to 5% of life (i.e. 28 x 10^3 cycles)

Fig. 35a Same area after electropolishing damaged surface to remove 2μ metres.

Fig. 35b Same area after fatigue testing for a further 28 x 10^3 cycles.

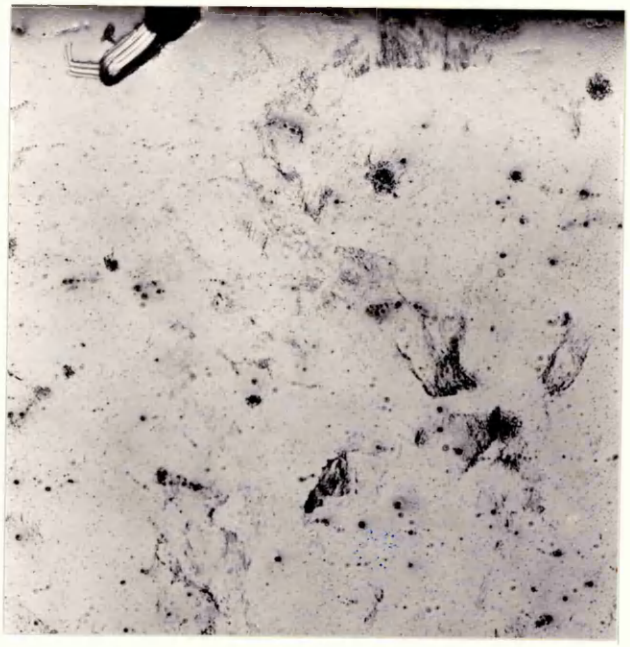

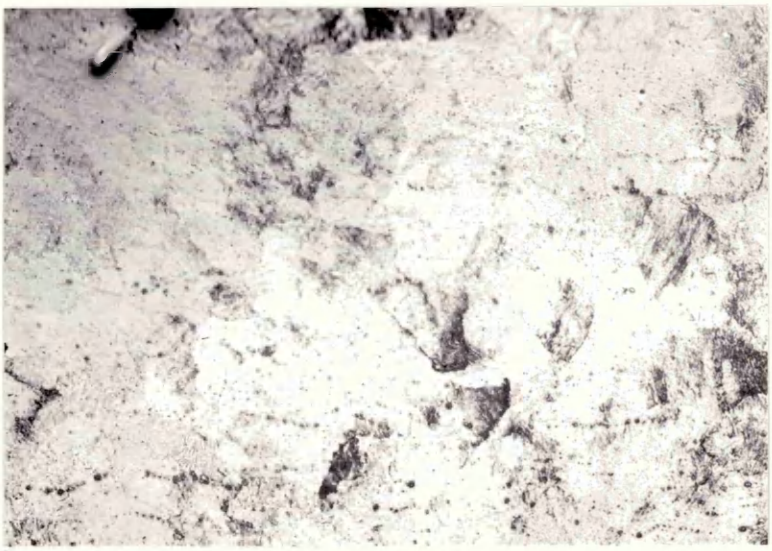

Taper Sections of Specimens showing Fatigue Damage.
Taper magnification x 5

Fig. 36 Coarse pearlite fatigued to 10% of life.

a. Mag.x1000

b. Mag. x 500

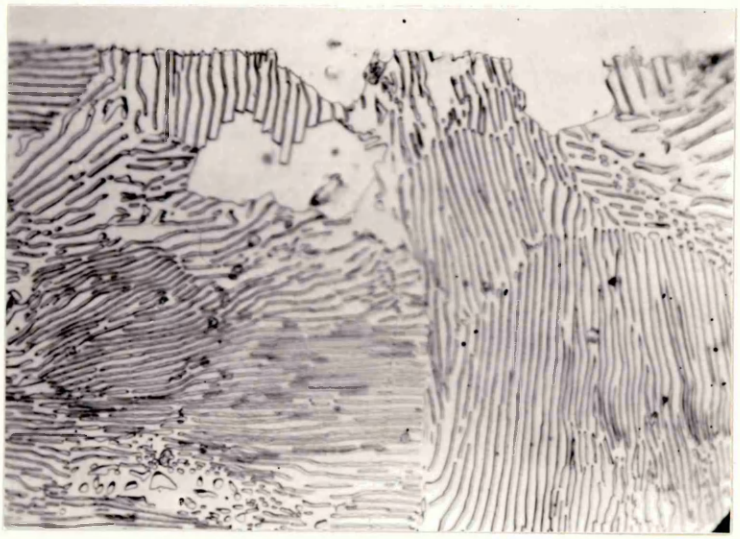

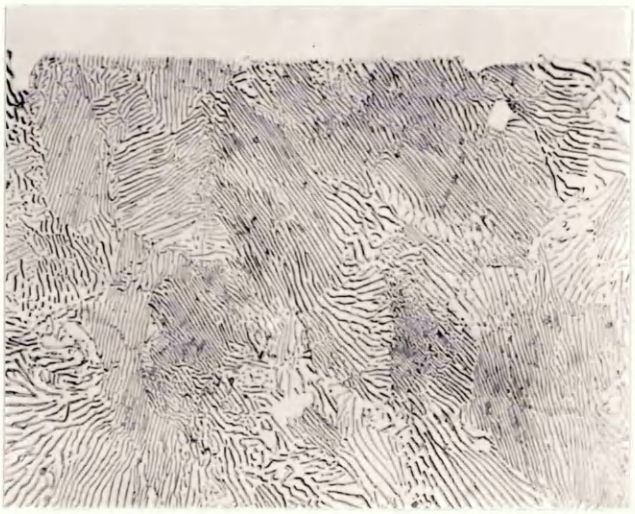

Taper Sections of Specimens showing Fatigue Damage
Taper magnification x 5

Fig. 37 Coarse pearlite fatigued to 10% of life

a. Mag. x 1000

b. Mag. x 1000

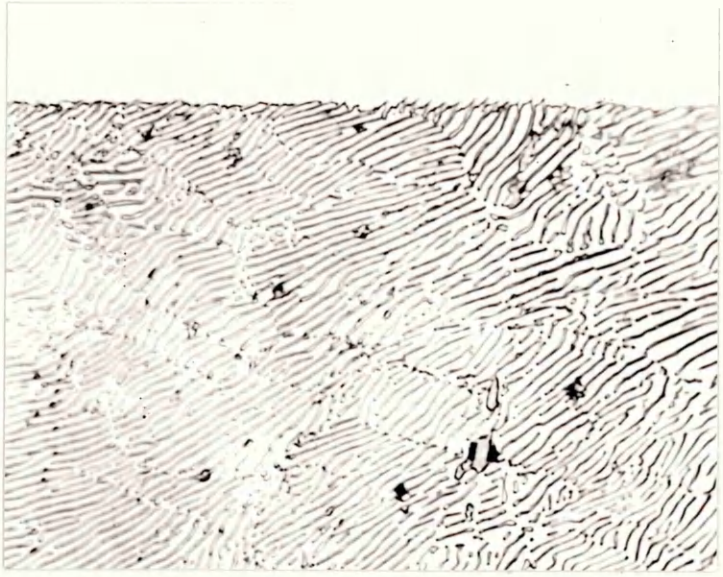

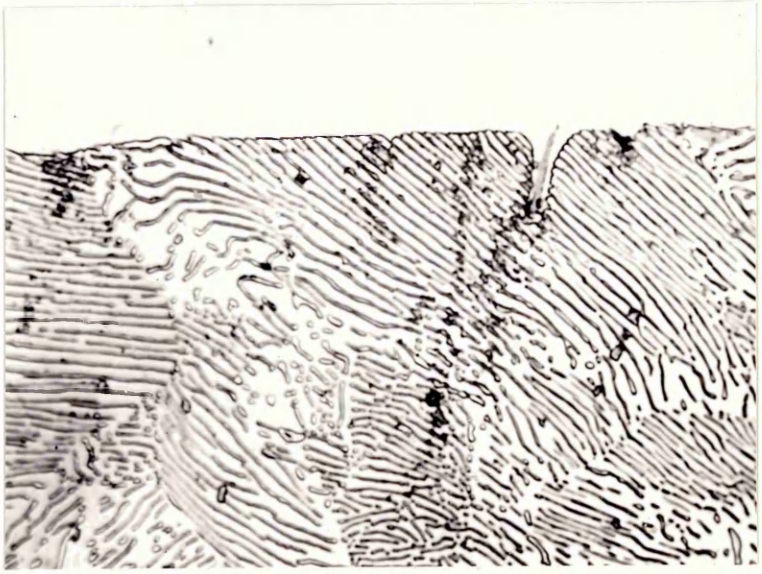

Taper Sections of Spheroidised Carbide Specimens before and after Fatigue Testing.

Taper magnification x 5
Optical magnification x 600

Fig. 38 a. Non-fatigued condition

b. After fatigue testing to 50% of life

Fig. 39 Taper Section of Coarse Pearlite after Fatigue Testing to failure in 2000 cycles.
Taper magnification x 5
Optical magnification x 200

Fig. 40 An Electron Micrograph of Coarse Pearlite after Tensile Fracture
Mag. x 26,000

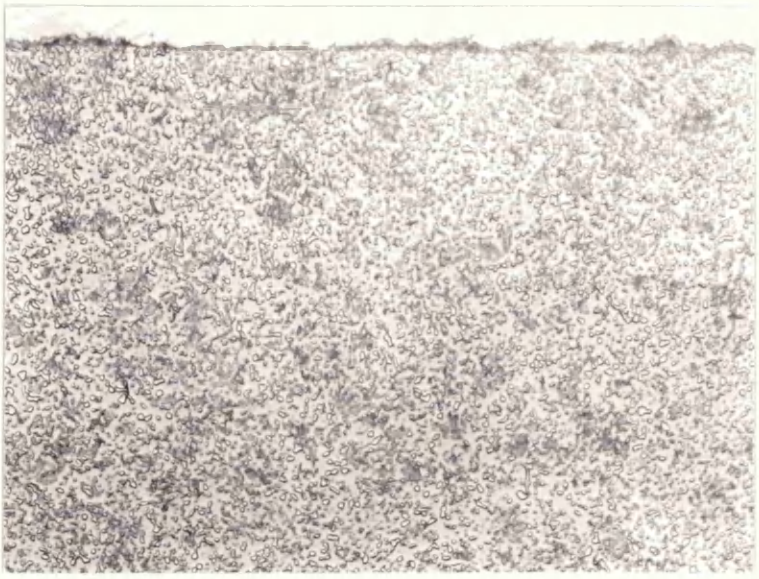

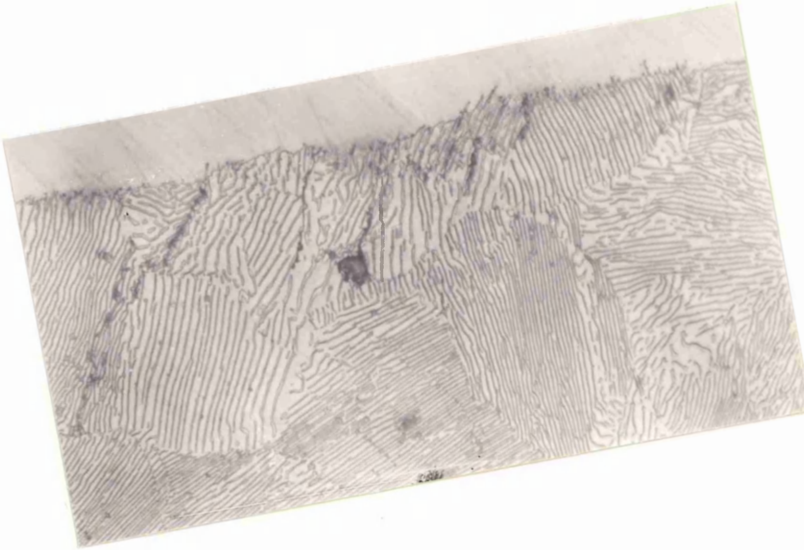

Fig. 41 Electron Micrographs of Coarse Pearlite.

a. Fatigued to 25% of life.
Mag. x 12,000

b. Fatigued to 75% of life.
Mag. x 100,000

c. Not fatigued
Mag. x 30,000


2 17853

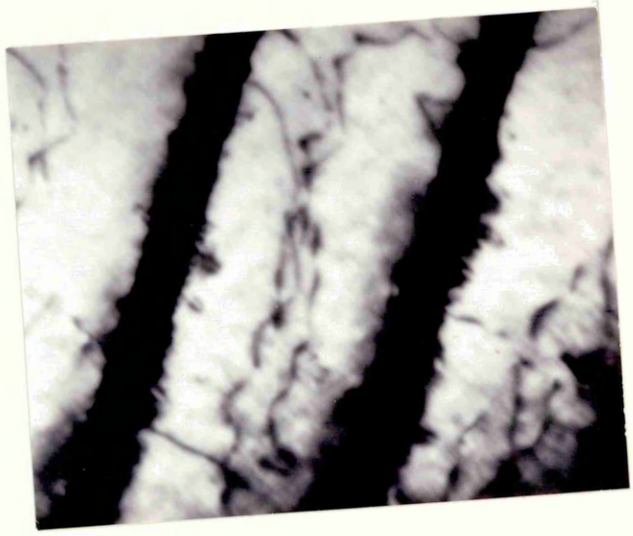

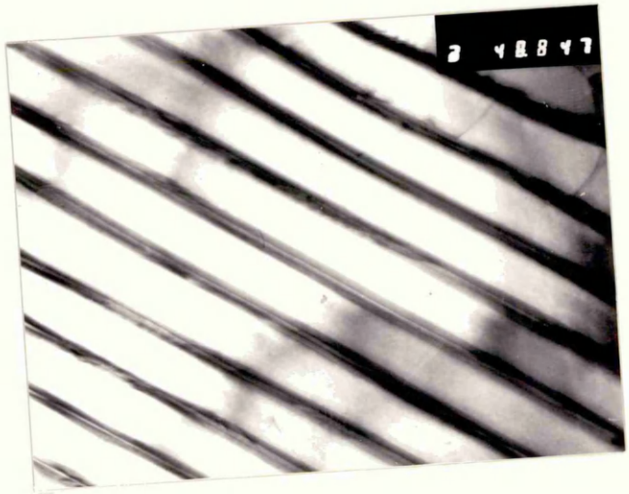
2 48847

Fig. 42 Electron Micrographs of Coarse Pearlite fatigued to 75% of life.

a. Mag. x 60,000

b. Mag. x 100,000

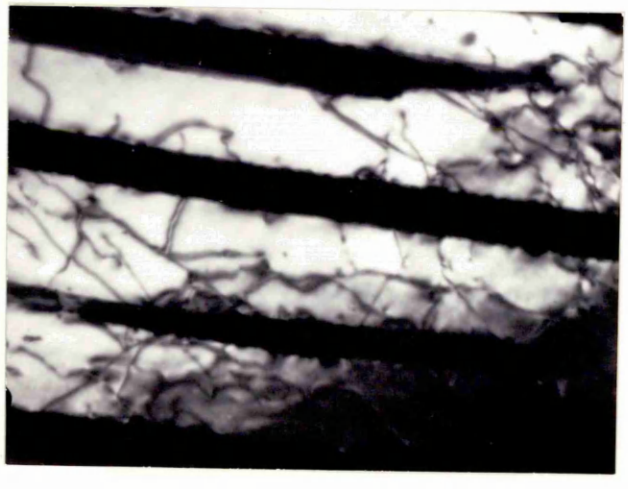

Electron Micrographs of Fine Pearlite

Fig. 43 Fatigued to 75% of life.

a. Mag. x 30,000

b. Mag. x 56,000

Fig. 44 Fatigued to 25% of life.

a. Mag. x 30,000

b. Mag. x 30,000

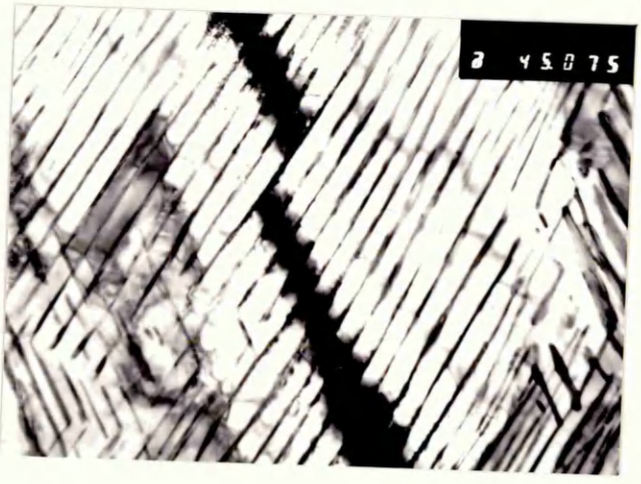

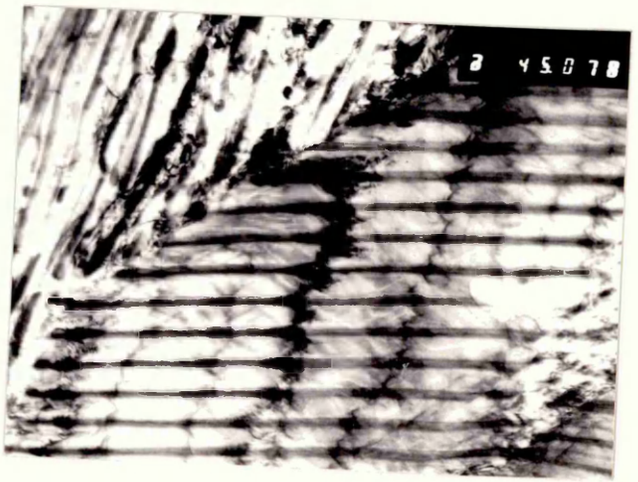

Fig. 45 Electron Micrographs of Fine Pearlite.
Fatigued to 25% of life.

a. Mag. x 30,000

b. Mag. x 30,000

Fig. 46 Electron Micrographs of Spheroidised Carbide.

a. Fatigued to 25% of life.
Mag. x 28,000

b. Fatigued to 75% of life.
Mag. x 56,000

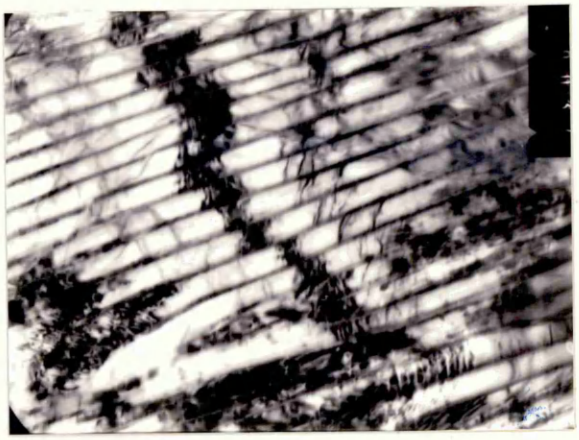

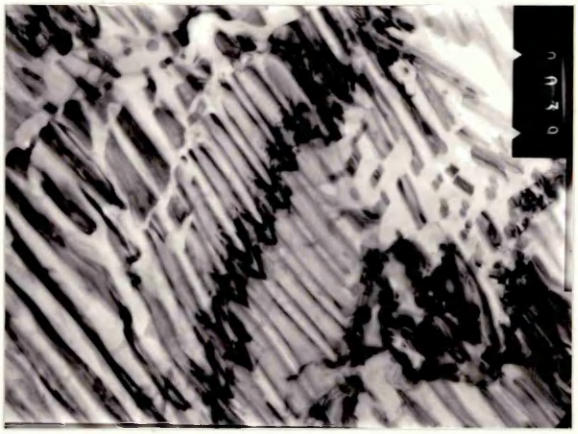

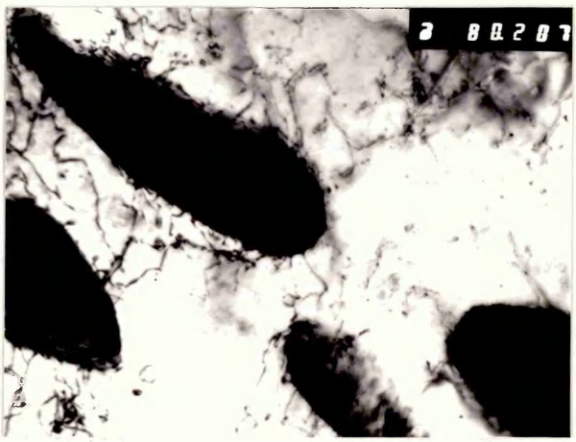

Fig. 47 Scanning Electron Micrograph.
Coarse Pearlite Fatigued to
25% of life.
Mag. x 2000

Principal Stress
Direction

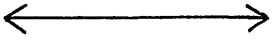

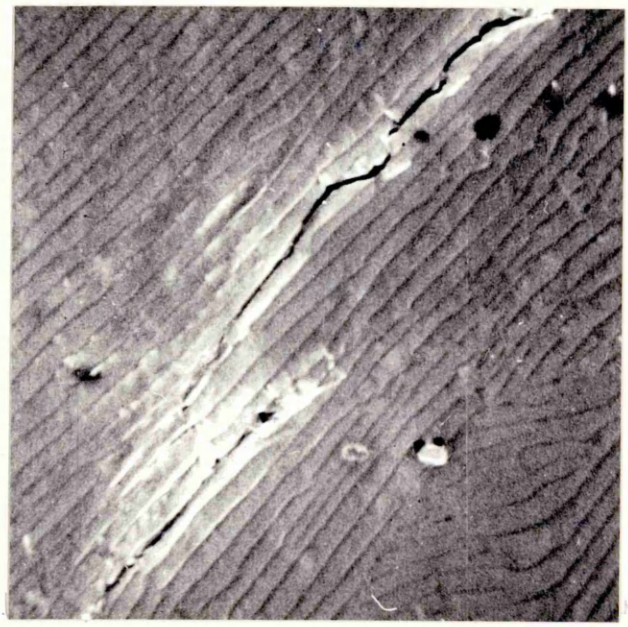

Crack Initiation Sites in Coarse Pearlite
Specimens fatigued to 25% of life then
electro-polished to remove 2 μ metres.
Mag. x 1000

Fig. 48

Fig. 49

Principal Stress
Direction
$\longleftrightarrow$

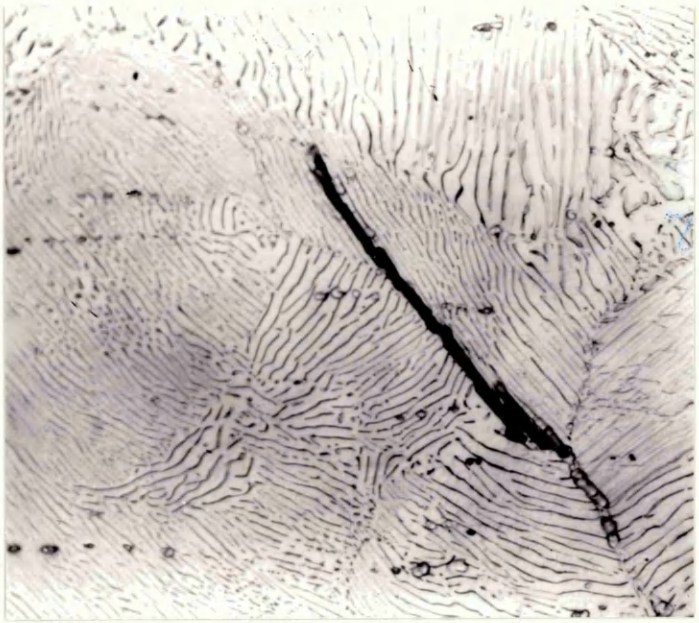

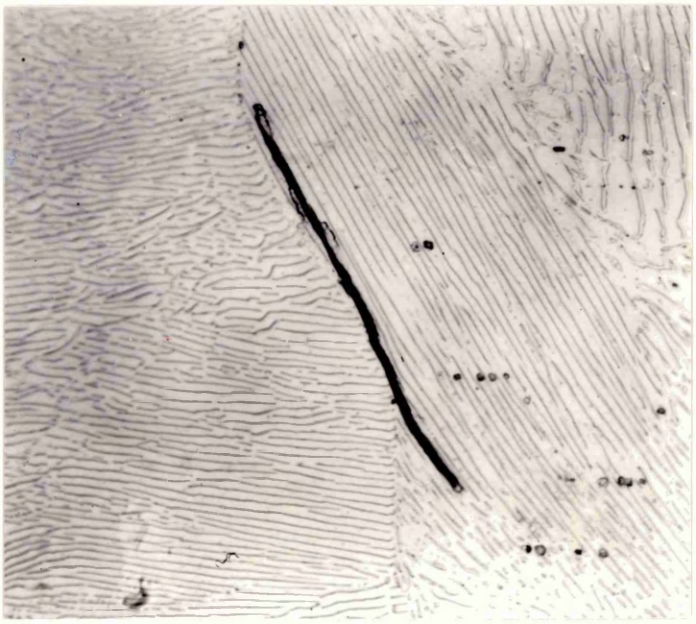

Fig. 50 Crack Initiation Sites in Fine Pearlite.
Fatigued to 75% of life.
Surface replica - Mag. x 15000

Fig. 51 Crack Growth in Coarse Pearlite.
Specimens Fatigued to 50% of life.
Scanning Electron Micrographs.

a. Mag. x 1500

b. Mag. x 1500

Principal Stress
Direction

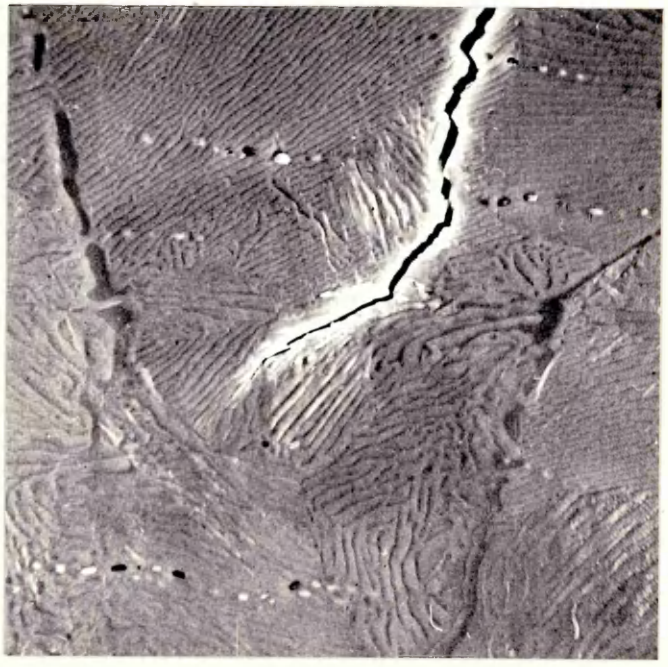

Fig. 52 Crack Growth Development in one area of a Coarse Pearlite during fatigue.

a. Fatigued to 50% of life.
Mag. x 400

b. Same area after fatigue failure.
Mag. x 1000

Principal Stress
Direction

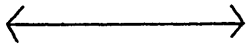

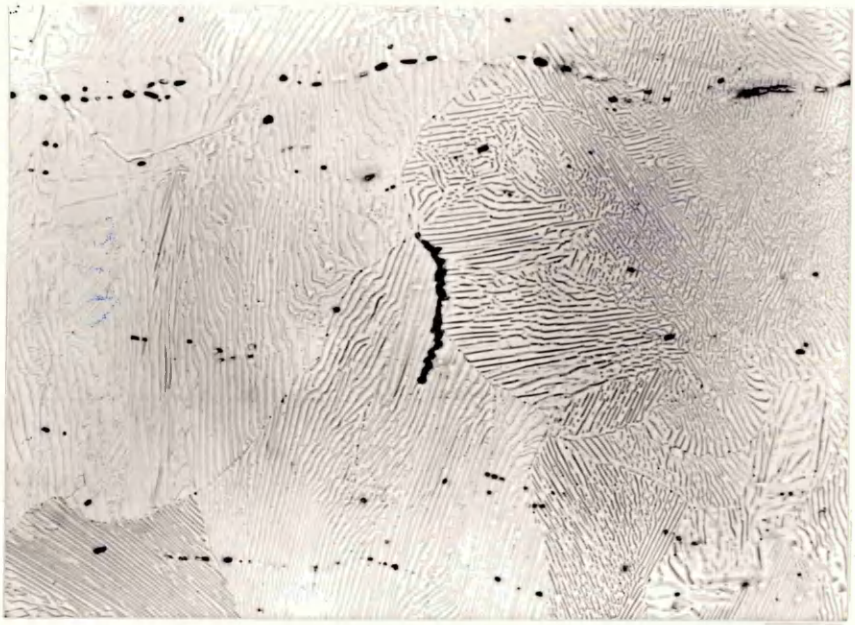

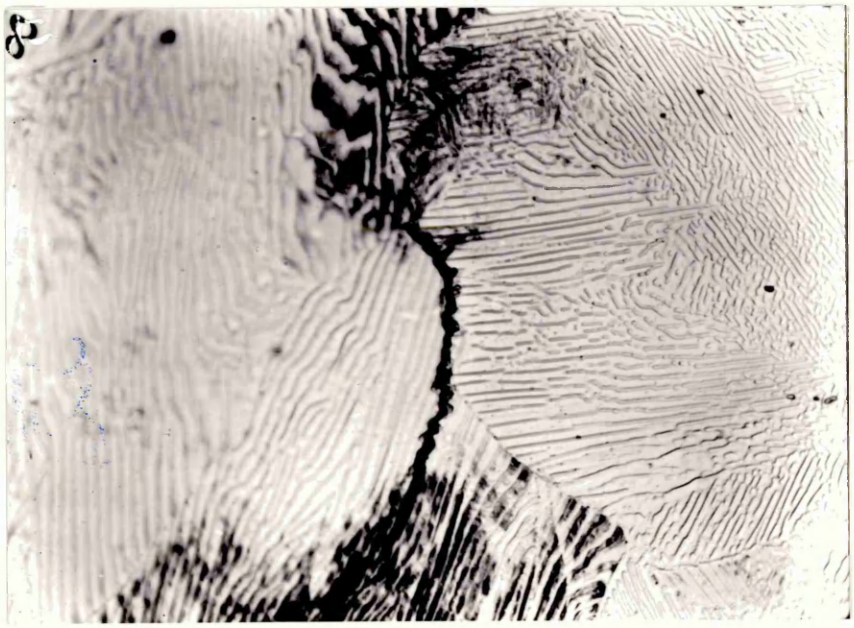

Fig. 53 Crack Growth in Coarse Pearlite during fatigue.
Scanning Electron Micrographs.

a. Mag. x 2500

b. Mag. 1000

Principal Stress Direction

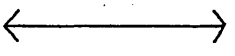

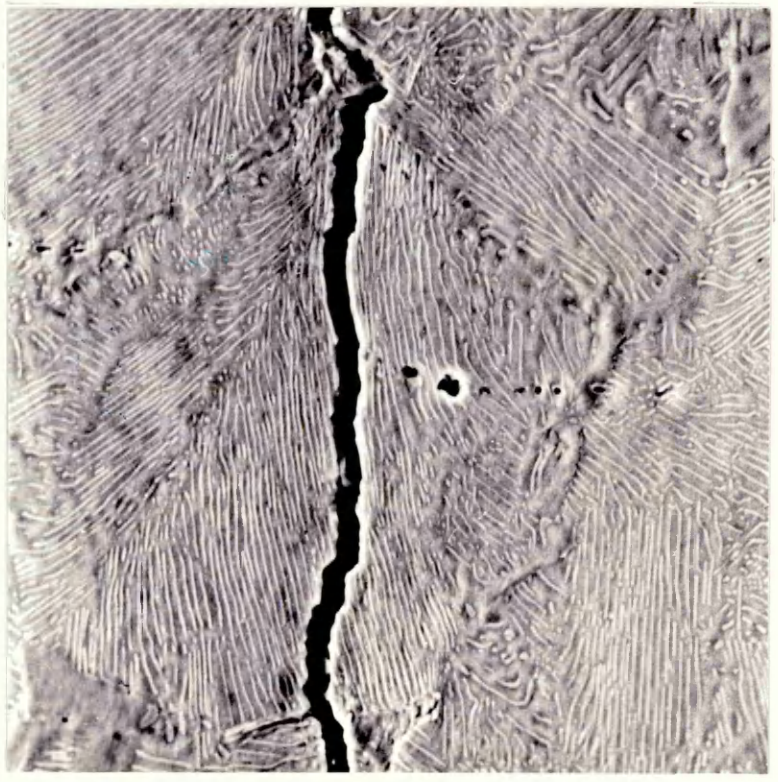

Fatigue Fracture Surfaces in Coarse Pearlite.
Scanning Electron Micrographs.

Fig. 54 Mag. x 600

Fig. 55 Mag. x1500

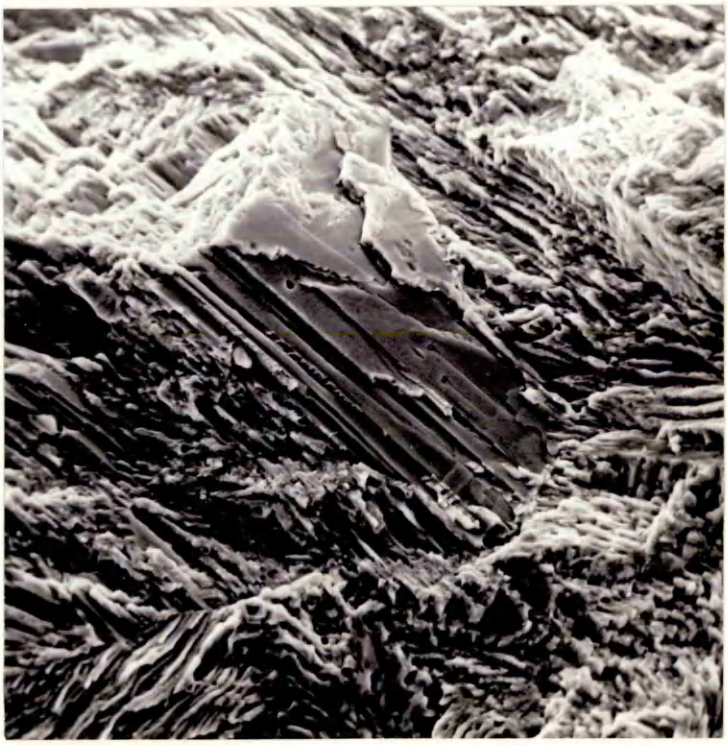

Fatigue Fracture Surface in Coarse Pearlite.

Fig. 56 Mag. x 1000
Scanning Electron Micrograph.

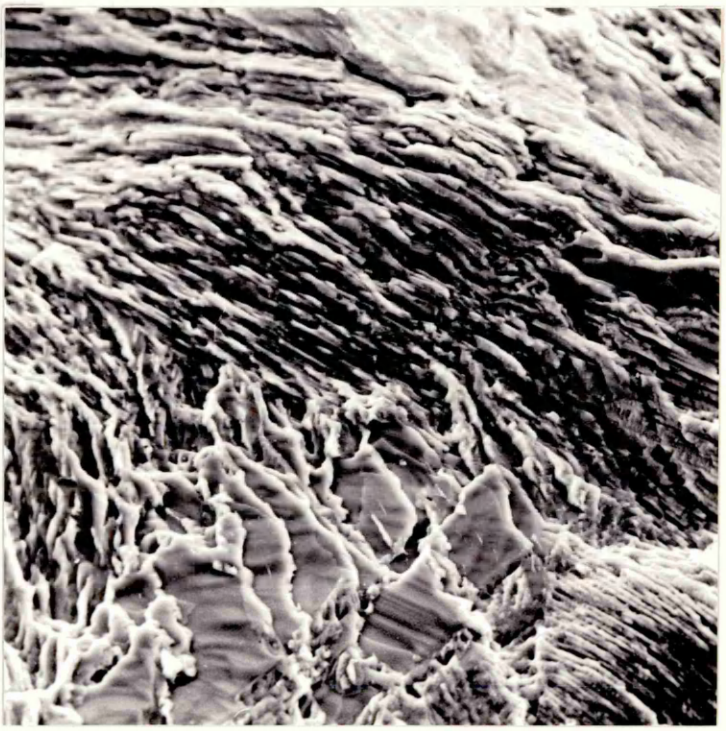

Fig. 57 Crack Growth in Spheroidised Carbide during fatigue (Scanning electron micrographs)

a. Mag. x 10,000

b. Mag. x 20,000

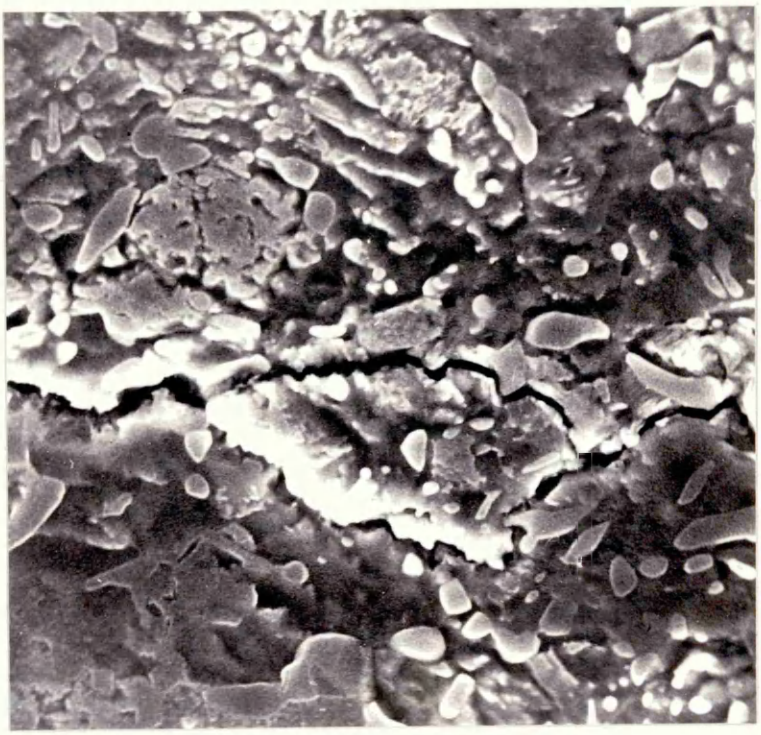

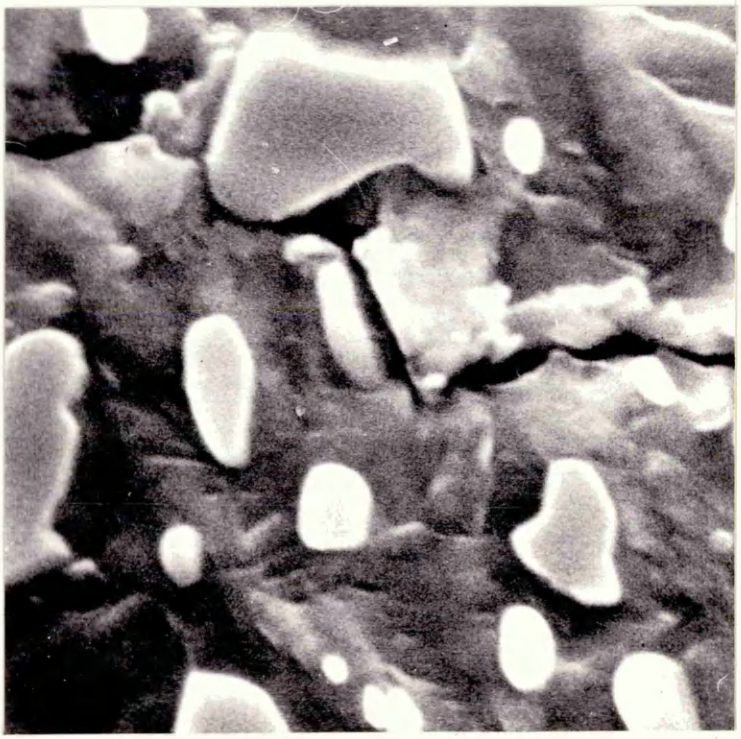

Fatigue Fracture Surface in Spheroidised Carbide

Fig. 58 Scanning Electron micrograph
Mag. x 625

Fig. 59 Single stage replica
Mag. x 5000

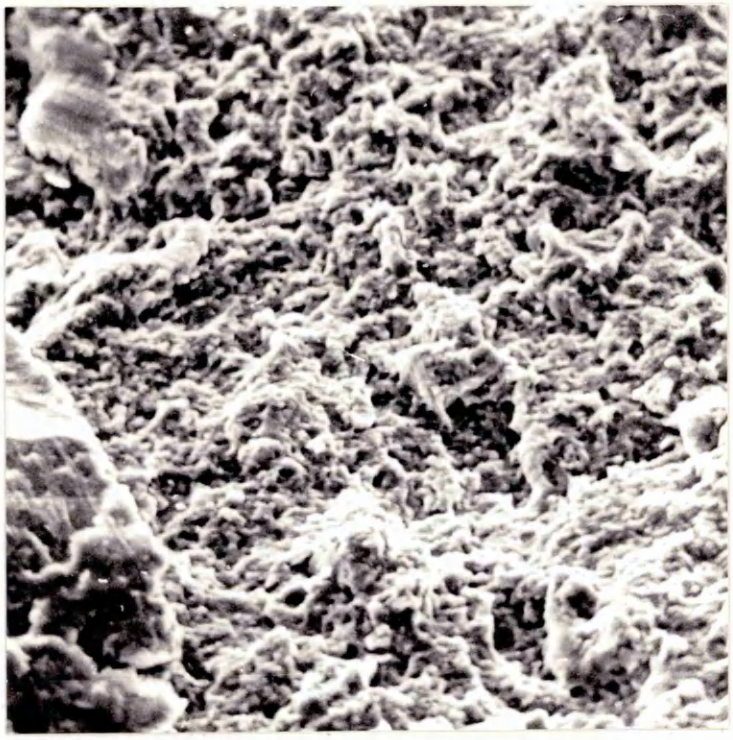

Fatigue Fracture Surface in Fine Pearlite
Scanning Electron Micrographs Mag. x 600

Fig. 60 Note the single initiation site. Specimen stage is tilted at 45° to electron beam.

Fig. 61 Shows one initiation site. Specimen stage is at 0°.

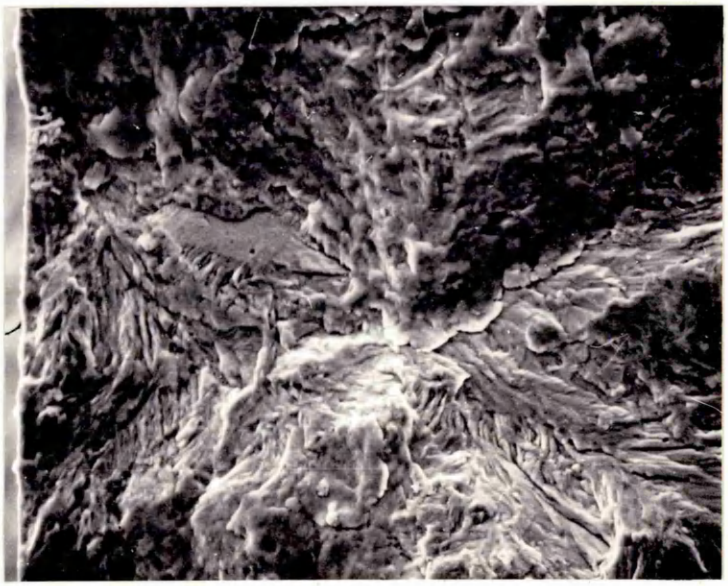

Fatigue Fracture Surface in Fine Pearlite.
Scanning Electron Micrographs

Fig. 62 Mag. x 600
Note the areas of intergranular crack growth.

Specimen stage tilt angle - 45°

Fig. 63 Mag. x 450
Shows more extensive intergranular crack growth.

Specimen stage tilt angle - 45°

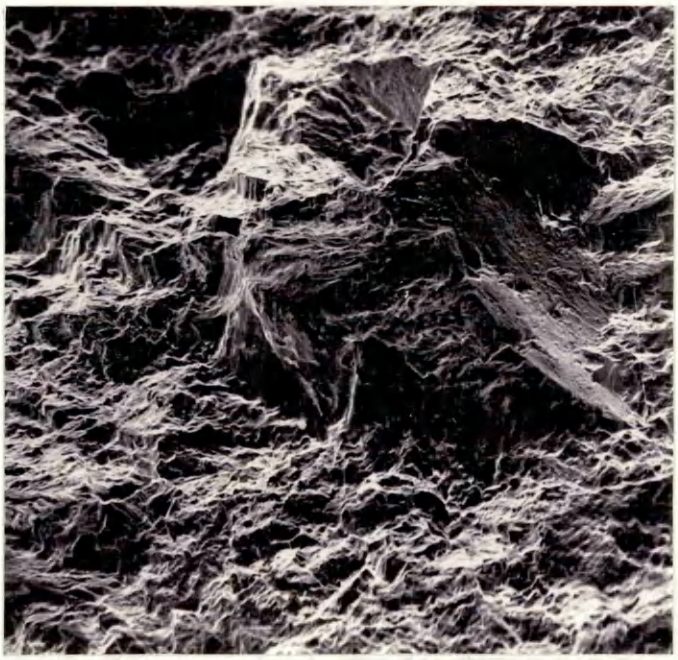

Fatigue Fracture Surface in Fine Pearlite.
Scanning Electron Micrographs

Fig. 64 Mag. x 200
Shows transition between fatigue and rapid fracture zones.

Fig. 65 Mag. x 2000
Shows fatigue fracture across cementite lamellae.

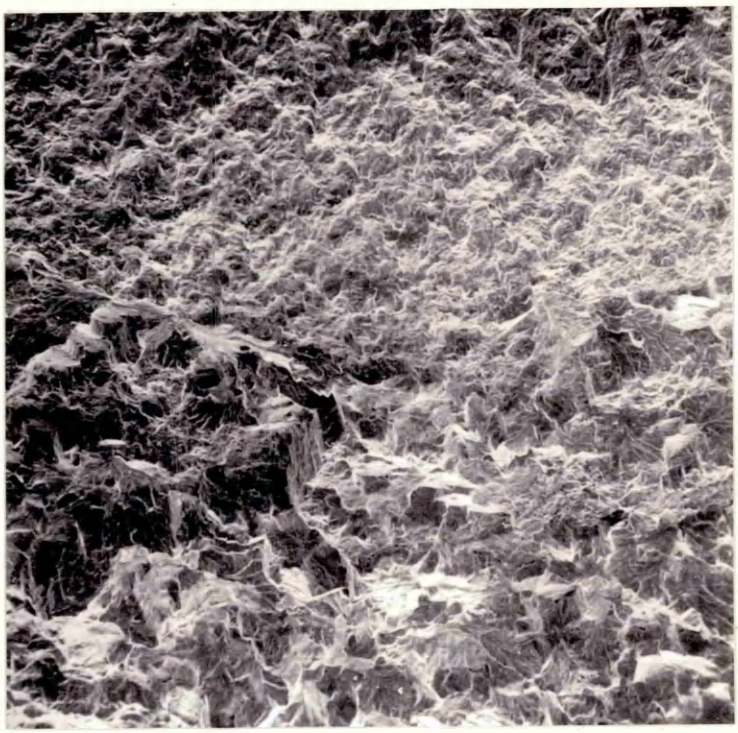

Fig. 66 Fatigue Fracture Surface in Fine Pearlite - Single Stage Replica.

Mag. x 5000